PROCEEDINGS
of the
Third International Conference
on the Ultrasonic Measurement and Imaging
of Tissue Elasticity©

Lake Windermere, Cumbria United Kingdom
October 17-20, 2004

PROCEEDINGS

of the
Third International Conference
on the Ultrasonic Measurement and Imaging
of Tissue Elasticity©

Lake Windermere, Cumbria, UK
October 17–20, 2004

Table of Contents

Welcome

Dear Conference Delegate:

It is a great pleasure to welcome to Cumbria all scientific participants, exhibitors, spouses and other guests of the Third International Conference on the Ultrasonic Measurement and Imaging of Tissue Elasticity©. We are delighted that despite the currently high cost of living in the UK and poor exchange rate for some countries, so many of you have chosen to attend and share your latest findings and discuss the future of this exciting field of research. We hope that our choice of venue, the Low Wood Hotel by Lake Windermere in the Lake District, will provide a peaceful "retreat" for the conference, with an environment and arrangements for both stimulating discussions and pleasurable relaxation. It is also a chance to enjoy some of the British countryside and life outside London or other major cities.

The existence of the Lake District depends on high rainfall. We hope for good weather, but even in the rain, and on occasions even because of the rain, the area is outstandingly beautiful. To help you explore the area, which also has much to offer in terms of history and culture, the Tourists' Information Centre (TIC) is nearby in the town of Ambleside (see the maps in your tourist packet). The TIC will have a booth in the conference exhibition area until 11.00am on Monday 18 October, following a "Tourists' Briefing" in the Low Wood Hotel at 9.00 am and to which all partners of delegates are warmly invited.

Professor Allan Chapman, Scientific Historian at Oxford University and television personality, will extend the "British experience" by presenting our special guest lecture on the life of Robert Hooke, who could be regarded as the ancestral father of our field of research. I am extremely grateful to Professor Chapman for agreeing to present this lecture.

I would also like to thank all members of the groups in Houston and Rochester (their names are mentioned in the Foreword) for their hard work. Together, we have strived to achieve substantial familiarity of arrangements and continuity of style with previous years. This was deliberately extended to items such as the proceedings' book, CD, mug and bag. Some of you have started to collect these things, and we hope that you will be pleased with the thematic continuity this year.

As before, there are no parallel sessions, but the impact of the extraordinarily large number of papers means that timing will be very tight for oral presentations and for refreshment breaks. We respectfully ask presenters to help session chairpersons to keep the conference on time, for fairness to all. However, you will notice that we have developed some innovatively dramatic time-keeping methods, beyond the usual coloured light indicators on the podium. Please forgive the British sense of humour!

For their sterling work in handling local arrangements I would like to thank many staff and students of the Joint Department of Physics at the Institute of Cancer Research, but especially Lesley Brotherston for covering a broad range of issues, Nigel Bush for working with manufacturers, and Gearóid Berry and Louise Coutts, who together dealt with audio-visual matters.

I hope that you will enjoy a walk in the "*fells*" (the local name for the small mountains), but please be careful and make good preparations. The weather and terrain can be dangerously unpredictable. Finally, thank you all for coming. Have a wonderful, beneficial experience and, when the time comes, a safe journey home!

Jeff Bamber
Chair of the Local Organizing Team
17 October 2004

FOREWORD

Dear Conference Delegate:

Welcome to the Third International Conference on the Ultrasonic Measurement and Imaging of Tissue Elasticity©.

The international participation in this Conference is reflected by delegates from some 20 countries. This year marks the first time that we have taken the Conference to Europe. Our 2004 local hosts, Dr. Jeff Bamber and his team at the Institute of Cancer Research in Sutton (UK) have worked tirelessly to assure the success of all the local organizational arrangements.

This year we have experienced a phenomenal growth of some 40% in the number of abstracts submitted to the Conference as compared to last year, bringing the total number of abstracts this year to 103. While we were gratified at this level of participation, it has created some necessary compromises in the Conference program.

Last year's Conference feedback was unanimous in the desire for continuation of the tutorial sessions. We are pleased that Drs. Chris de Korte (NL) and Jan D'hooge (BE) have jointly agreed to present this year's exciting tutorial on cardiovascular elasticity on Monday morning. We are seeing a steady increase in the number of clinical papers presented at the Conference, as well as the participation of more research groups from related disciplines.

We would like to thank all the delegates, the reviewers and the session chairs for their continuing support of the Conference. Special thanks are in order to our enthusiastic support staff. Ms Manette Price (US) of the Conference Secretariat's office has spent much time and effort handling most of the Conference organizational duties; Ms Karen Ophir (US) volunteered to design and create all the Conference artwork and publications. Ms Pam Clark (US) and Ms. Betsy Christianson (US) provided support for the Conference website.

This Conference is conducted under the joint auspices of the University of Rochester Center for Biomedical Ultrasound and the Ultrasonics Laboratory at the University of Texas Medical School at Houston. However, all funding for the Conference is derived from registration fees alone. With your support in abstract submissions and attendance, we hope to continue to organize the conference and improve and expand it in the years to come.

We hope that you will enjoy this year's scientific program as well as the beautiful countryside of the Lake District. We will be looking forward to seeing you again at next year's Conference!

Enjoy your Conference, and we look forward to seeing you at next year's Conference in North America!

J. Ophir and K.J. Parker
Conference Organizers
October 17, 2004

Sponsor

Sunday, October 17   **5:00P – 8:00P**

5:00P – 8:00P		Registration Desk Open	
		Conference Office Open	
6:00P – 8:00P		*Opening Reception*	Gallery Lounge
		Proceedings Book Signing	Gallery Lounge
	Session POS:	Posters	
	Session EEX:	Equipment Exhibit	Gallery Lounge

Monday, October 18   **7:00A – 10:30P**

7:00A – 5:00P		Registration Desk Open	
		Conference Office Open	
8:00A – 5:00P	**Session POS:**	Posters	
8:00A – 5:00P	**Session EEX:**	Equipment Exhibit	Gallery Lounge
9:00A – 9:30A		*Tourists' Briefing*	to be announced
7:45A – 8:00A		Opening Remarks	Lecture Hall
8:00A – 10:00A	**Session TUT:**	Tutorial: Imaging of Cardiovascular Elasticity	Lecture Hall
10:00A – 10:30A		*Coffee Break*	Gallery Lounge
10:30A – 11:30A	**Session MMT:**	Mechanical Measurement Techniques for Tissues	Lecture Hall
11:30A – 12:30P	**Session SIP-1:**	Signal and Image Processing – I	Lecture Hall
12:30P – 1:45P		*Group Lunch*	Restaurant
1:45P – 3:30P	**Session MIP-1:**	Methods for Imaging Elastic Tissue Properties – I	Lecture Hall
3:30P – 4:00P		*Coffee Break*	Gallery Lounge
4:00P – 6:00P	**Session CAA-1:**	Clinical and Animal Applications – I	Lecture Hall
7:30P – 11:00P		*Conference Dinner*, Guest Speaker – Allan Chapman	Zeffirellis

Tuesday, October 19   **7:00A – 9:30P**

7:00A – 5:00P		Registration Desk Open	
		Conference Office Open	
8:00A – 5:00P	**Session POS:**	Posters	
8:00A – 5:00P	**Session EEX:**	Equipment Exhibit	Gallery Lounge
8:00A – 10:00A	**Session FIP-1:**	Forward and Inverse Problems – I	Lecture Hall
10:00A – 10:30A		*Coffee Break*	Gallery Lounge
10:30A – 11:45A	**Session CAA-2:**	Clinical and Animal Applications – II	Lecture Hall
11:45A – 12:30P	**Session MPT:**	Mechanical Properties of Tissues	Lecture Hall
12:30P – 2:00P		*Group Lunch*	Restaurant
2:00P – 3:00P	**Session SIP-2:**	Signal and Image Processing – II	Lecture Hall
3:00P – 3:30P		*Coffee Break*	Gallery Lounge
3:30P – 4:45P	**Session MIP-2:**	Methods for Imaging Elastic Tissue Properties – II	Lecture Hall
4:45P – 7:30P		*No Conference Activities*	
7:30P – 8:45P	**Session AA:**	Alternative Applications	Lecture Hall
8:45P – 9:30P	**Session INS:**	Instrumentation	Lecture Hall

Wednesday, October 20   **7:00A – 4:45P**

7:00A – 4:00P		Registration Desk Open	
		Conference Office Open	
8:00A – 3:45P	**Session POS:**	Posters	
8:00A – 3:45P	**Session EEX:**	Equipment Exhibit	Gallery Lounge
8:00A – 10:00A	**Session CVE:**	Cardiovascular Elasticity	Lecture Hall
10:00A – 10:30A		*Coffee Break*	Gallery Lounge
10:30A – 11:45A	**Session FIP-2:**	Forward and Inverse Problems – II	Lecture Hall
11:45A – 1:00P		*Group Lunch*	Restaurant
1:00P – 2:15P	**Session MIP-3:**	Methods for Imaging Elastic Tissue Properties – III	Lecture Hall
2:15P – 3:00P	**Session CET:**	Complementary Elasticity Imaging Techniques	Lecture Hall
3:00P – 3:30P		*Coffee Break*	Gallery Lounge
3:30P – 4:45P	**Session PTO:**	Phantoms and Test Objects	Lecture Hall

Sunday, October 17   5:00P – 8:00P

5:00P – 8:00P
   Registration Desk Open
   Conference Office Open

Sunday   6:00P – 8:00P
Opening Reception   Gallery Lounge
                                  Proceedings Book Signing   Gallery Lounge
                    Session POS: Posters
                    Session EEX: Equipment Exhibit   Gallery Lounge

Monday, October 18   7:00A – 10:30P

7:00A – 5:00P
   Registration Desk Open
   Conference Office Open
8:00A – 5:00P   **Session POS: Posters**
                    Session EEX: Equipment Exhibit   Gallery Lounge
9:00A – 9:30A   ***Tourists' Briefing***   to be announced

Monday   7:45A – 8:00A
OPENING REMARKS
   J Bamber, J Ophir, KJ Parker   Lecture Hall

Monday   8:00A – 10:00A
Session TUT: Tutorial: Imaging of Cardiovascular Elasticity
Chair: F Duck, UK   Lecture Hall

8:00A – 8:45A
090   CARDIOVASCULAR DEFORMATION IMAGING – PART I: VASCULAR.
      CL de Korte[1], J D'hooge[2].*
      [1]University Medical Center Radboud, Nijmegen, The NETHERLANDS; [2]Catholic University of
      Leuven, Leuven, BELGIUM.
8:45A – 9:00A   Discussion

9:00A – 9:45A
091   CARDIOVASCULAR DEFORMATION IMAGING – PART II: CARDIAC.
      J D'hooge[1], CL de Korte[2].*
      [1]Catholic University of Leuven, Leuven, BELGIUM; [2]University Medical Center Radboud, Nijmegen,
      The NETHERLANDS.

(Session TUT continues on next page)   ** indicates Presenter*

5

9:45A – 10:00A   Discussion

10:00A – 10:30A
    COFFEE BREAK   Gallery Lounge

Monday   10:30A – 11:30A
Session MMT: Mechanical Measurement Techniques for Tissues
Chair: E Mazza, Switzerland   *Co-Chair: S Levinson, USA*   Lecture Hall

10:30A – 10:45A
078 THE EFFECTS OF DEFORMATION ON THE YOUNG'S MODULUS MEASUREMENT BY TWO
    INDENTORS OF DIFFERENT SIZES – A SIMULATION STUDY.
    APC Choi[1], Y Zheng[1]*.
    [1]The Hong Kong Polytechnic University, Hong Kong, CHINA.

10:45A – 11:00A
063 ULTRASOUND CRITICAL–ANGLE REFLECTOMETRY: MEASURING VELOCITIES IN HARD AND
    SOFT ANISOTROPIC TISSUES.
    PP Antich[1], MA Lewis[1]*, E Richer[1], B Smith[1].
    [1]University of Texas Southwestern Medical Center, Dallas, TX, USA.

11:00A – 11:15A
025 A DEVICE FOR THE ASSESSMENT OF NONLINEAR VISCOELASTIC MATERIAL PROPERTIES OF
    SOFT TISSUES *IN VIVO.*
    E Tönük[1]*.
    [1]Middle East Technical University, Ankara, TURKEY.

11:15A – 11:30A
026 ASSESSMENT OF NONLINEAR VISCOELASTIC MATERIAL PROPERTIES OF SOFT TISSUES OF
    RESIDUAL LIMBS OF TRANS TIBIAL AMPUTEES.
    E Tönük[1]*, C Yildiz[2], AS Atesalp[2].
    [1]Middle East Technical University, Ankara, TURKEY; [2]Gülhane Military Medical Academy, Ankara,
    TURKEY.

Monday   11:30A – 12:30P
Session SIP-1: Signal and Image Processing – I
Chair: W Walker, USA   *Co-Chair: R Maurice, Canada*   Lecture Hall

11:30A – 11:45A
057 STRAIN ESTIMATION USING SPECTRAL CROSS–CORRELATION: INITIAL RESULTS USING
    PARAMETRIC METHODS.
    K Hoyt[1,2]*, F Forsberg[2], J Ophir[3].
    [1]Drexel University, Philadelphia, PA, USA; [2]Thomas Jefferson University, Philadelphia, PA, USA;
    [3]The University of Texas Medical School, Houston, TX, USA.

11:45A – 12:00P
053 A NEW TIME DELAY ESTIMATOR FOR TISSUE ELASTICITY IMAGING.
    F Viola[1], WF Walker[1]*.
    [1]University of Virginia, Charlottesville, VA, USA.

12:00P – 12:15P
061 2D STRAIN ESTIMATION ALGORITHM – INITIAL RESULTS.
    E Brusseau[1]*, G Said[1], J Fromageau[1], O Basset[1], D Vray[1].
    [1]CREATIS, Villeurbanne, FRANCE.

* indicates Presenter

12:15P – 12:30P

081   TISSUE STRAIN IMAGING USING A WAVELET-BASED PEAK SEARCH ALGORITHM.
H Eskandari[1]*, SE Salcudean[1].
[1]University of British Columbia, Vancouver, BC, CANADA.

12:30P – 1:45P

GROUP LUNCH   Restaurant

Monday   1:45P – 3:30P
Session MIP-1: Methods for Imaging Elastic Tissue Properties – I
Chair: M Fink, France   *Co-Chair: T Shiina, Japan*   Lecture Hall

1:45P – 2:00P

010   THE SUPERSONIC SHEAR IMAGING TECHNIQUE APPLIED TO NONLINEAR PROPERTIES OF SOFT TISSUES.
S Catheline[1]*, JL Gennisson[1], J Bercoff[1], C Barrière[1] and M Fink[1].
[1]Laboratoire Ondes et Acoustique, E.S.P.C.I., Paris, FRANCE.

2:00P – 2:15P

015   DYNAMICS OF SOFT TISSUE IN RESPONSE TO IMPULSIVE ACOUSTIC RADIATION FORCE WITH CLINICAL APPLICATIONS.
ML Palmeri[1]*, AN Congdon[1], KD Frinkley[1], MS Soo[2], R Bentley[2], KR Nightingale[1].
[1]Duke University, Durham, NC, USA; [2]Duke University Medical Center, Durham, NC, USA.

2:15P – 2:30P

024   VIBRATION SONOELASTOGRAPHIC IMAGING USING A PHASE LOCKING TECHNIQUE.
A Iqbal[1]*, T Frank[1], D McLean[1], A Cuschieri[1].
[1]University of Dundee, Dundee, Scotland, UK.

2:30P – 2:45P

028   VISCOELASTICITY IMAGING BASED ON HYSTERESIS ANALYSIS UNDER QUASI-STATIC DEFORMATION.
N Nitta[1]*, T Shiina[2].
[1]National Institute of Advanced Industrial Science & Technology (AIST), Tsukuba, JAPAN; [2]University of Tsukuba, Tsukuba, JAPAN.

2:45P – 3:00P

030   SHEAR WAVE BEAMFORMING USING THE ACOUSTIC RADIATION FORCE.
J Bercoff[1], M Tanter[1]*, M Fink[1].
[1]Laboratoire Ondes et Acoustique, E.S.P.C.I, Paris, FRANCE.

3:00P – 3:15P

036   VISUALIZTION OF SHEAR WAVE PROPAGATION IN BIOMATERIALS WITH SONOELASTOGRAPHY.
ZC Wu[1]*, KJ Parker[1].
[1]University of Rochester, Rochester, NY, USA.

3:15P – 3:30P

069   A COMPARISON OF METHODS OF SONOELASTOGRAPHY IN MUSCLE.
S Levinson[1]*, ZC Wu[2], KJ Parker[2].
[1,2]University of Rochester, Rochester, NY, USA.

3:30P – 4:00P

COFFEE BREAK   Gallery Lounge

* indicates Presenter

Monday   4:00P – 6:00P
Session CAA-1: Clinical and Animal Applications – I
Chair: WE Svensson, UK   Co-Chair: EE Konofagou, USA   Lecture Hall

4:00P – 4:15P
050   ELASTICITY IMAGING MAY IMPROVE LOCAL PRE–TREATMENT STAGING OF BREAST CANCERS.
WE Svensson[1]*, TJ Hall[3], Y Zhu[4], J Malin[5], A Rattansingh[1], C Lowery[5], S Shousha[2], D Chopra[1].
[1,2]Charing Cross Hospital NHS Trust, London, England, UK; [3]University of Wisconsin–Madison, Madison, WI, USA; [4]University of Kansas Medical Center, Kansas City, KS, USA; [5]Siemens Medical Solutions Ultrasound Group, Issaquah, WA, USA.

4:15P – 4:30P
013   NON–INVASIVE VASCULAR ELASTICITY CAN DETECT VASCULAR DISEASE.
WF Weitzel[1]*, K Kim[1], JM Rubin[1], H Xie[1], X Chen[1], JH Segal[1], JM Sanchez[1], NG Chopra[1], M O'Donnell[1].
[1]University of Michigan, Ann Arbor, MI, USA.

4:30P – 4:45P
014   DIRECT ELASTICITY MEASUREMENT OF INFERIOR VENA CAVA THROMBI IN RATS: CORRELATION WITH ULTRASOUND STRAIN MEASUREMENTS AND THROMBUS AGE.
JM Rubin[1]*, H Xie[1], K Kim[1], SR Aglyamov[2], S Emelianov[2], X Chen[1], WF Weitzel[1], S Wrobleski[1], D Myers[1], T Wakefield[1], M O'Donnell[1].
[1]University of Michigan, Ann Arbor, MI, USA; [2]University of Texas at Austin, Austin, TX, USA.

4:45P – 5:00P
006   APPLICATION OF TRANSIENT ELASTOGRAPHY TO *IN–VIVO* MEASUREMENTS OF LIVER STIFFNESS IN PATIENTS WITH CHRONIC HEPATITIS C.
L Sandrin[1]*, C Fournier[1], V de Lédinghen[2], P Marcellin[3], D Dhumeaux[4], M Beaugrand[5].
[1]Echosens SA, Paris, FRANCE; [2]Haut Lévêque Hospital, Pessac, FRANCE; [3]Beaujon Hospital, Clichy, FRANCE; [4]Henri Mondor Hospital, Créteil, FRANCE; [5]AP-HP, Bondy, FRANCE.

5:00P – 5:15P
011   REAL–TIME MONITORING OF RADIOFREQUENCY ABLATION IN LIVER WITH ACOUSTIC RADIATION FORCE IMPULSE IMAGING.
BJ Fahey[1]*, GE Trahey[1].
[1]Duke University, Durham, NC, USA.

5:15P – 5:30P
016   HIFU PROSTATE CANCER TREATMENT MONITORING BY ELASTOGRAPHY.
L Curiel[1]*, R Souchon[1], O Rouvière[2], A Gelet[2], JY Chapelon[1].
[1]INSERM, Lyon, FRANCE; [2]Hôpital Edouard Herriot, Lyon, FRANCE.

5:30P – 5:45P
034   MECHANICAL BEHAVIOR OF THE HUMAN CERVIX: AN *IN–VIVO* STUDY.
E Mazza[1]*, A Nava[1], M Bauer[2], R Winter[2], GA Holzapfel[3], M Bajka[4].
[1]Swiss Federal Institute of Technology, Zürich, SWITZERLAND; [2]Medical University Graz, Graz, AUSTRIA; [3]Graz University of Technology, Graz, AUSTRIA; [4]University Hospital Zürich, Zürich, SWITZERLAND.

5:45P – 6:00P
071   PROSTATE ELASTOGRAPHY: PRELIMINARY *IN VIVO* RESULTS.
SK Alam[1], EJ Feleppa[1], A Kalisz[1], S Ramchandran[1], RD Ennis[2], FL Lizzi[1], CS Wuu[2], J Ketterling[1].
(EE Konofagou* presenting)
[1]Riverside Research Institute, New York, NY, USA; [2]New York Columbia Presbyterian Medical Center, New York, NY, USA.

First bus to Zeffirellis departs the Low Wood Hotel at 7:00P.

Monday   7:30P – 11:00P
Conference Dinner

7:30P – 10:30P
Proceedings Book Signing
Chair: J Bamber, UK

000   ROBERT HOOKE – ENGLAND'S LEONARDO?
        A Chapman[1]*.
        [1]University of Oxford, Oxford, England, UK.

Musical selections performed by The Patrick Bamber Jazz Band.
The band features Anthony J. Strong (keyboard), Tom Farmer (bass), Oliver Eagan (drums) and Patrick Bamber (saxophone). All members of the band are students working for a Bachelor's of Arts at the Guildhall School of Music and Drama in London (http://www.gsmd.ac.uk/).

First bus to the Low Wood Hotel departs Zeffirellis at 11:00P.

Tuesday, October 19   7:00A – 9:30P

7:00A – 5:00P
        Registration Desk Open
        Conference Office Open
8:00A – 5:00P   **Session POS: Posters**
                Session EEX: Equipment Exhibit   Gallery Lounge

Tuesday   8:00A – 10:00A
Session FIP-1: Forward and Inverse Problems – I
Chair: JA Noble, UK   *Co-Chair: to be announced*   Lecture Hall

8:00A – 8:15A
059   ABSOLUTE MODULUS IMAGING USING ULTRASONIC FREEHAND SCANNING AND PRESSURE
        SENSORY DATA.
        J Jiang[1]*, TJ Hall[1], EL Madsen[1].
        [1]University of Wisconsin–Madison, Madison, WI, USA.

8:15A – 8:30A
046   ELASTICITY RECONSTRUCTION FROM DISPLACEMENT AND CONFIDENCE MEASURES OF
        ULTRASOUND IMAGE SEQUENCES.
        J Li[1]*, JA Noble[1].
        [1]University of Oxford, Oxford, England, UK.

8:30A – 8:45A
047   INVERSE ELASTICITY RECONSTRUCTION BASED ON AN IMAGE SIMILARITY–MEASURE
        APPROACH.
        J Li[1]*, Y Cui[1], JA Noble[1].
        [1]University of Oxford, Oxford, England, UK.

8:45A – 9:00A
068   DIRECT AND INTERATIVE ALGORITHMS FOR INVERSE PROBLEMS IN ELASTOGRAPHY.
        E Park[1]*, AM Maniatty[1].
        [1]Rensselaer Polytechnic Institute, Troy, NY, USA.

9:00A – 9:15A
070   USING ARRIVAL TIMES TO RECOVER SHEAR WAVE SPEED PARAMETERS IN AN ANISOTROPIC
        MEDIUM.
        D Renzi[1]*, J McLaughlin[1].
        [1]Rensselaer Polytechnic Institute, Troy, NY, USA.

* indicates Presenter

9:15A – 9:30A

080 AN INVERSE PROBLEM: LOCALIZATION OF INSERTS BY CORRELATION BETWEEN FINITE ELEMENT MODELS AND ELASTOGRAMS.
P Trompette[1]*, JY Chapelon[1], R Souchon[1], M Rochette[2], G Duffait[2].
[1]INSERM, Lyon, FRANCE; [2]CADOE, Lyon, FRANCE.

9:30A – 9:45A

003 INFLUENCE OF TISSUE VISCOSITY ON WAVE PROPAGATION CHARACTERISTICS IN BOUNDED REGIONS.
JGG Dobbe[1]*, GJ Streekstra[1], J Strackee[1], CA Grimbergen[1].
[1]University of Amsterdam, Amsterdam, The NETHERLANDS.

9:45A – 10:00A

009 PLANE–WAVE DECOMPOSITION FOR AN EXACT RECONSTRUCTION OF TRANSVERSAL ISOTROPIC PROPERTIES IN STEADY–STATE DYNAMIC ELASTOGRAPHY.
R Sinkus[1]*, M Tanter[2], T Xydeas[3], M Fink[2].
[1]Philips Research, Hamburg, GERMANY; [2]Laboratoire Ondes et Acousticque, ESPCI, Paris, FRANCE; [3]University Tuebingen, Tuebingen, GERMANY.

10:00A – 10:30A

COFFEE BREAK   Gallery Lounge

Tuesday   10:30A – 11:45A
Session CAA-2: Clinical and Animal Applications – II
Chair: WF Weitzel, USA   *Co Chair: A Sarvazyan, USA*   Lecture Hall

10:30A – 10:45A

056 A NEW ANIMAL MODEL FOR *IN VIVO* ELASTOGRAPHY.
K Hoyt[1,2]*, F Forsberg[2], CRB Merritt[2], JB Liu[2], TA Krouskop[3], J Ophir[4].
[1]Drexel University, Philadelphia, PA, USA; [2]Thomas Jefferson University, Philadelphia, PA, USA; [3]Baylor College of Medicine, Houston, TX, USA; [4]The University of Texas Medical School, Houston, TX, USA.

10:45A – 11:00A

035 STRAIN PROCESSING OF INTRAOPERATIVE ULTRASOUND IMAGES OF BRAIN TUMOURS.
J Bang[1]*, T Selbekk[1], G Unsgård[2].
[1]SINTEF Health Research, Trondheim, NORWAY; [2]St. Olav's Hospital, Trondheim, NORWAY.

11:00A – 11:15A

060 INTRA–OPERATIVE ULTRASOUND ELASTOGRAPHY AND REGISTERED MAGNETIC RESONANCE IMAGING OF BRAIN TUMOURS; A FEASIBILITY STUDY.
A Chakraborty[1]*, J Bamber[2], G Berry[2], N Bush[2], N Dorward[1].
[1]Royal Free & University College Hospital Medical School, London, England, UK; [2]Institute of Cancer Research, Sutton, Surrey, England, UK.

11:15A – 11:30A

023 PRELIMINARY EVALUATION OF BREAST DISEASE DIAGNOSIS BASED ON REAL–TIME ELASTICITY IMAGING.
T Matsumura[1]*, S Tamano[1], R Shinomura[1], T Mitake[1], M Yamakawa[2], T Shiina[2], A Itoh[3], E Ueno[4].
[1]Hitachi Medical Corporation, Chiba, JAPAN; [2]University of Tsukuba, Tsukuba, JAPAN; [3]Hitachi General Hospital, Ibaraki, JAPAN; [4]University of Tsukuba, Tsukuba, JAPAN.

11:30A – 11:45A

040 NEW ELASTOGRAPHIC ALGORITHM FOR *IN–VIVO* STUDY OF MECHANICAL BEHAVIOR OF SKIN.
Y Mofid[1]*, F Ossant[1,3], C Imberdis[2], F Patat[1].
[1]LUSSI, Tours, FRANCE; [2]LMARC, Besançon, FRANCE; [3]University Hospital, Tours, FRANCE.

Tuesday   11:45A – 12:30P
Session MPT: Mechanical Properties of Tissues
Chair: G Cloutier, Canada   *Co-Chair: R Souchon, France*   Lecture Hall

11:45A – 12:00P
054   ON THE TRANSVERSE ANISOTROPY OF HUMAN AND BOVINE CALCIFIED TISSUES.
JL Katz[1]*, J Kinney[2], P Spencer[1], Y Wang[1], B Fricke[1], M Walker[1], L Friis[3], M Tabib-Azar[4].
[1]University of Missouri–Kansas City, Kansas City, MO, USA; [2]University of California–San Francisco, San Francisco, CA, USA; University of Kansas, Lawrence, KS, USA; [4]Case Western Reserve University, Cleveland, OH, USA.

12:00P – 12:15P
085   ANALYSIS OF BLOOD CLOT FORMATION USING TRANSIENT ELASTOGRAPHY.
JL Gennisson[1]*, S Lerouge[2] and G Cloutier[1].
[1]University of Montréal Hospital, Montréal, Québec, CANADA.

12:15P – 12:30P
101   INTRINSIC LIMITATIONS IN DIFFERENTIAL DIAGNOSTICS BASED ON QUANTITATIVE ELASTOGRAPHY.
A Sarvazyan[1]*.
[1]Artann Laboratories, Lambertville, NJ, USA.

12:30P – 2:00P
          GROUP LUNCH   Restaurant

Tuesday   2:00P – 3:00P
Session SIP-2: Signal and Image Processing – II
Chair: S Emelianov, USA   *Co-Chair: MM Doyley, USA*   Lecture Hall

2:00P – 2:15P
098   TIME DOMAIN CROSS CORRELATION WITH PRIOR ESTIMATES.
R Zahiri-Azar[1]*, SE Salcudean[1].
[1]University of British Columbia, Vancouver, BC, CANADA.

2:15P – 2:30P
019   DIRECT STRAIN MEASUREMENT BASED ON AN AUTOCORRELATION METHOD.
C Sumi[1]*.
[1]Sophia University, Tokyo, JAPAN.

2:30P – 2:45P
083   IMPROVED ELASTOGRAPHIC SIGNAL–TO–NOISE RATIO USING CODED EXCITATION.
R Souchon[1]*, A Pousse[1], JC Béra[1], JY Chapelon[1].
[1]INSERM, Lyon, FRANCE.

2:45P – 3:00P
096   SYSTEMATIC ERROR CAN DOMINATE IMAGE NOISE IN STRAIN MEASUREMENTS.
CX Jia[1], NH Gokhale[1], MS Richards[1], LA Nelson[1], MM Doyley[2], AA Oberai[1], PE Barbone[1]*.
[1]Boston University, Boston, MA, USA; [2]Dartmouth College, Hanover, NH, USA.

3:00P – 3:30P
          COFFEE BREAK   Gallery Lounge

* indicates Presenter

11

Tuesday   3:30P — 4:45P

Session MIP-2: Methods for Imaging Elastic Tissue Properties — II

Chair: KJ Parker, USA   *Co-Chair: N Miller, UK*   Lecture Hall

3:30P – 3:45P
041   A NOVEL HAPTIC SENSOR ACTUATOR SYSTEM FOR PALPATION IMAGING BASED ON ULTRASOUND ELASTOGRAPHY.
W Khaled[1]*, S Reichling[2], OT Bruhns[2], GJ Monkman[3], S Egersdorfer[3], M Baumann[4], H Boese[4], H Freimuth[5], A Tunayar[5], A Lorenz[6], A Pesavento[6] and H Ermert[1].
[1,2]Ruhr-University, Bochum, GERMANY; [3]Fachhochschule Regensburg, Regensburg, GERMANY; [4]Fraunhofer-Institut fuer Silicatforschung ISC, Wuerzburg, GERMANY; [5]Insitut fuer Mikrotechnik, Mainz, GERMANY; [6]LP-IT Innovative Technologies GmbH, Bochum, GERMANY.

3:45P – 4:00P
042   MECHANISM FOR HUMAN DETECTION OF ELASTIC LESIONS IN SIMULATED B–MODE MOVIES DURING PALPATION.
N Miller[1]*, J Bamber[1].
[1]Institute of Cancer Research, Sutton, Surrey, England, UK.

4:00P – 4:15P
100   SHEAR WAVE ELASTICITY IMAGING WITH THE USE OF TIME REVERSAL ACOUSTICS.
A Sarvazyan[1]*, A Sutin[1].
[1]Artann Laboratories, Lambertville, NJ, USA.

4:15P – 4:30P
076   NONCONTACT ULTRASOUND INDENTATION SYSTEM FOR MEASURING TISSUE MATERIAL PROPERTIES USING WATER BEAM.
M Lu[1], Y Zheng[1]*, Q Huang[1].
[1]The Hong Kong Polytechnic University, Hong Kong, CHINA.

4:30P – 4:45P
044   *IN–VITRO* IMAGING OF HIFU–INDUCED LESIONS IN BOVINE LIVERS USING THREE DIMENSIONAL SONOELASTOGRAPHY.
M Zhang[1], LS Taylor[1], DJ Rubens[2], KJ Parker[3]*.
[1,2,3]University of Rochester, Rochester, NY, USA.

4:45P – 7:30P   *No Conference Activities*

Tuesday   7:30P — 8:45P

Session AA: Alternative Applications

Chair: JF Greenleaf, USA   *Co Chair: J D'hooge, Belgium*   Lecture Hall

7:30P – 7:45P
077   SONOMYOGRAPHY ANALYSIS OF THE MORPHOLOGICAL CHANGES OF FOREARM MUSCLES IN ACTION.
Y Zheng[1]*, Xin Chen[1].
[1]The Hong Kong Polytechnic University, Hong Kong, CHINA.

7:45P – 8:00P
021   THERMAL PROPERTIES RECONSTRUCTION TECHNIQUE BASED ON TEMPERATURE MEASUREMENT.
C Sumi[1]*.
[1]Sophia University, Tokyo, JAPAN.

8:00P – 8:15P
099   THERMAL LESION MONITORING USING MINIATURIZED IMAGE–TREAT ARRAYS.
IRS Makin[1], TD Mast[2]*, W Faidi[2], MM Runk[2], PG Barthe[1], MH Slayton[1].
[1]Guided Therapy Systems, Mesa, AZ, USA; [2]Ethicon Endo–Surgery, Cincinnati, OH, USA.

* indicates Presenter

8:15P – 8:30P

086 TISSUE DISPLACEMENT AND STRAIN PATTERNS DURING ACUPUNCTURE FOLLOW CONNECTIVE TISSUE PLANES.
EE Konofagou[1]*, JR Fox[2], HM Langevin[2].
[1]Columbia University, New York, NY, USA; [2]University of Vermont, Burlington, VT, USA.

8:30P – 8:45P

102 COMBINED ULTRASOUND, PHOTOACOUSTIC AND ELASTCITY IMAGING.
S Emelianov[1]*, SR Aglyamov[1], S Mallidi[1], J Shah[1], S Park[1], S Sethuraman[1], A Karpiouk[2], M Motamedi[2], A Oraevsky[3], RD Irving[4], RM Schmitt[4], WG Scott[4].
[1]The University of Texas at Austin, Austin, TX, USA; [2]The University of Texas Medical Branch, Galveston, TX, USA; [3]Fairway Medical Technologies, Houston, TX, USA; [4]WinProbe Corporation, North Palm Beach, FL, USA.

Tuesday   8:45P – 9:30P
Session INS: Instrumentation
Chair: Y Zheng, China   *Co Chair: RM Schmitt, USA*   Lecture Hall

8:45P – 9:00P

062 DEVELOPMENT OF HIGH BANDWIDTH TRANSDUCERS USING INJECTION–MOLDED 1–3 LOW PITCH COMPOSITES: A NUMERICAL STUDY.
RM Schmitt[1]*, WG Scott[1], S Emelianov[2], RD Irving[1].
[1]Winprobe Corporation, North Palm Beach, FL; USA; [2]University of Texas at Austin, Austin, TX, USA.

9:00P – 9:15P

079 DEVELOPMENT OF AN ULTRASOUND RESEARCH PLATFORM.
WG Scott[1]*, RM Schmitt[1], RD Irving[1].
[1]WinProbe Corporation, North Palm Beach, FL, USA.

9:15P – 9:30P

008 AN ACTIVELY SHIELDED ELECTROMAGNETIC TRANSDUCER FOR MR–ELASTOGRAPHY DEDICATED TO MAMMOGRAPHY.
H Hörning[1]*, M Dargatz[2], R Sinkus[2].
[1]Philips Medical Systems, Hamburg, GERMANY; [2]Philips Research, Hamburg, GERMANY.

Wednesday, October 20   7:00A – 4:45P

7:00A – 4:00P
    Registration Desk Open
    Conference Office Open
8:00A – 3:45P   **Session POS: Posters**
                   Session EEX: Equipment Exhibit   Gallery Lounge

Wednesday   8:00A – 10:00A
Session CVE: Cardiovascular Elasticity
Chair: CL de Korte, The Netherlands   *Co Chair: H Kanai, Japan*   Lecture Hall

8:00A – 8:15A

002 TRANSCUTANEOUS MEASUREMENT OF MYOCARDIAL VISCOELASTICITY.
H Kanai[1]*.
[1]Tohoku University, Sendai, JAPAN.

* indicates Presenter

8:15A – 8:30A

004 ADAPTING THE LAGRANGIAN SPECKLE MODEL ESTIMATOR FOR ENDOVASCULAR ELASTOGRAPHY: THEORY AND VALIDATION WITH SIMULATED RADIO–FREQUENCY DATA.
R Maurice[1]*, J Ohayon[2], G Finet[3], G Cloutier[1].
[1]University of Montréal Hospital Research Center, Montréal, Québec, CANADA; [2]Institut A. Bonniot, Lyon, FRANCE; [3]Claude Bernard University, Lyon, FRANCE.

8:30A – 8:45A

017 INVESTIGATION OF "RING RESONANT FREQUENCY" FOR ESTIMATION OF ARTERIAL ELASTICITY.
X Zhang[1], JF Greenleaf[1]*.
[1]Mayo Clinic College of Medicine, Rochester, MN, USA.

8:45A – 9:00A

029 CHARACTERIZATION OF VULNERABLE CORONARY PLAQUE BY STRAIN POWER IMAGE.
T Shiina[1]*, N Nitta[2], M Yamagishi[3].
[1]University of Tsukuba, Tsukuba, JAPAN; [2]National Institute of Advanced Industrial Science and Technology, Tsukuba, JAPAN; [3]National Cardiovascular Center, Osaka, JAPAN.

9:00A – 9:15A

037 CLINICAL EVALUATION OF 3D INTRAVASCULAR ULTRASOUND PALPOGRAPHY FOR VULNERABLE PLAQUE DETECTION.
AFW van der Steen[1,2]*, JA Schaar[1,2], F Mastik[1], CL de Korte[3], PW Serruys[1].
[1]Erasmus MC, Rotterdam, The NETHERLANDS; [2]Interuniversity Cardiology Institute of the Netherlands, Utrecht, The NETHERLANDS; [3]University Medical Centre, Nijmegen, The NETHERLANDS.

9:15A – 9:30A

051 ROBUST ASSESSMENT OF ARTERIAL PLAQUE COMPOSITION *IN VIVO* USING A PARAMETRIC PLAQUE MODEL–BASED YOUNG'S MODULUS RECONSTRUCTION METHOD.
RA Baldewsing[1]*, F Mastik[1], JA Schaar[1,2] and AFW van der Steen[1,2].
[1]Erasmus MC, Rotterdam, The NETHERLANDS; [2]Interuniversity Cardiology Institute of the Netherlands, Utrecht, The NETHERLANDS.

9:30A – 9:45A

067 A NEW METHOD FOR TWO–DIMENSIONAL MYOCARDIAL STRAIN ESTIMATION BY ULTRASOUND: A COMPARISON WITH SONOMICROMETRY *IN VIVO*.
S Langeland[1], J D'hooge[2]*, HA Leather[3], P Claus[1], GR Sutherland[1], PF Wouters[3] and B Bijnens[1].
[1,2,3]Catholic University Leuven, Leuven, BELGIUM.

9:45A – 10:00A

087 TWO–DIMENSIONAL FUNCTIONAL INFORMATION CAN BE USED FOR AUTOMATED LEFT-VENTRICULAR SEGMENTATION.
EE Konofagou[1]* and TC Pulerwitz[2].
[1]Columbia University, New York, NY, USA; [2]Columbia Presbyterian Hospital, New York, NY, USA.

10:00A – 10:30A

    COFFEE BREAK   Gallery Lounge

Wednesday 10:30A – 11:45A
Session FIP-2: Forward and Inverse Problems – II
Chair: PE Barbone, USA   *Co Chair: J McLaughlin, USA*   Lecture Hall

10:30A – 10:45A

020 SIMULATION STUDY OF RECONSTRUCTION OF SHEAR MODULUS, DENSITY, AND POISSON'S RATIO DISTRIBUTIONS.
C Sumi[1]*.
[1]Sophia University, Tokyo, JAPAN.

* indicates Presenter

10:45A – 11:00A

031 INFLUENCE OF VISCOSITY ON SHEAR WAVES INDUCED BY THE ACOUSTIC RADIATION FORCE.
J Bercoff[1], M Tanter[1], M Fink[1]*.
[1]Laboratoire Ondes et Acoustique, E.S.P.C.I, Paris, FRANCE.

11:00A – 11:15A

033 THE INVERSE PROBLEM OF THE SHEAR WAVE PROPAGATION: RECOVERING BOTH SHEAR MODULUS AND VISCOSITY IMAGES FROM SUPERSONIC SHEAR IMAGING DATA.
J Bercoff[1], M Tanter[1]*, M Fink[1].
[1]Laboratoire Ondes et Acoustique, E.S.P.C.I.,Paris, FRANCE.

11:15A – 11:30A

097 ENHANCING THE PERFORMANCE OF MODULUS ELASTOGRAMS.
MM Doyley[1]*, S Srinivasan[2,3], Z Wu[1], BS Garra[4], J Ophir[2,3].
[1]Dartmouth Medical School, Hanover, NH, USA; [2]The University of Texas Medical School, Houston, TX, USA; [3]University of Houston, Houston, TX, USA; [4]University of Vermont College of Medicine-Fletcher Allen Health Care, Burlington, VT, USA.

11:30A – 11:45A

084 TRANSIENT ELASTOGRAPHY: ALGORITHMS AND MODELS.
J McLaughlin[1]*, D Renzi[1], JR Yoon[1], A Glasman[1].
[1]Rensselaer Polytechnic Institute, Troy, NY, USA.

11:45A – 1:00P

GROUP LUNCH   Restaurant

Wednesday   1:00P – 2:15P
Session MIP-3: Methods for Imaging Elastic Tissue Properties – III
Chair: R Sinkus, Germany   *Co Chair: E Brusseau, France*   Lecture Hall

1:00P – 1:15P

094 IMAGING LOCALIZED VISCOELASTIC PROPERTIES USING HARMONIC MOTION IMAGING.
EE Konofagou[1]* and TP Harrigan[2].
[1]Columbia University, New York, NY, USA; [2]Exponent, Inc., Framingham, MA, USA.

1:15P – 1:30P

089 POISSON'S RATIO IMAGING AND POROELASTOGRAPHY IN BIOLOGICAL TISSUES: A FEASIBILITY STUDY.
R Righetti[1,2]*, J Ophir[1,2] and TA Krouskop[1,3].
[1]The University of Texas Medical School, Houston, TX, USA; [2]University of Houston, Houston, TX, USA; [3]Baylor College of Medicine, Houston, TX, USA.

1:30P – 1:45P

088 A METHOD FOR GENERATING PERMEABILITY ELASTOGRAMS USING POROELASTOGRAPHY.
R Righetti[1,2]*, J Ophir[1,2] and TA Krouskop[1,3].
[1]The University of Texas Medical School, Houston, TX, USA; [2]University of Houston, Houston, TX, USA; [3]Baylor College of Medicine, Houston, TX, USA.

1:45P – 2:00P

066 TOWARDS A MODEL–BASED POROELASTIC IMAGING METHOD.
G Berry[1]*, J Bamber[1], N Miller[1].
[1]Institute of Cancer Research, Sutton, Surrey, England, UK.

2:00P – 2:15P

032 MONITORING OF HIFU LESIONS USING SUPERSONIC SHEAR IMAGING: A UNIQUE THERAPY AND IMAGING SYSTEM.
J Bercoff[1], M Pernot[1], M Tanter[1]*, M Fink[1].
Laboratoire Ondes et Acoustique, E.S.P.C.I, Paris, FRANCE.

* indicates Presenter

Wednesday 2:15P — 3:00P
Session CET: Complementary Elasticity Imaging Techniques

Chair: AFW van der Steen, The Netherlands Co Chair: C Sumi, Japan Lecture Hall

2:15P – 2:30P

007 3D *IN–VIVO* LIVER MR–ELASTOGRAPHY.
R Sinkus[1]*, H Hörning[2], L ter Beek[3], M Dargatz[1] and B Van Beers[4].
[1]Philips Research, Hamburg, GERMANY; [2]Philips Medical Systems, Hamburg, GERMANY; [3]Philips Medical Systems, Brussels, BELGIUM; [4]St. Luc, Brussels, BELGIUM.

2:30P – 2:45P

001 DETERMINATION OF ANISOTROPIC ELASTICITIES OF *IN VIVO* SKELETAL MUSCLE USING A GEOMETRIC ANALYSIS OF MR–ELASTOGRAPHY WAVE PATTERNS.
S Papazoglou[1]*, J Braun[2], M Taupitz[1], I Sack[1].
[1]Institute of Radiology–Charité, Berlin, GERMANY; [2]Institute of Biometry and Medical Informatics–Charité, Berlin, GERMANY.

2:45P – 3:00P

065 MEASURING THE MECHANICAL PROPERTIES OF SMALL BIOLOGICAL TISSUES USING MICRO MAGNETIC RESONANCE ELASTOGRAPHY (μMRE).
SF Othman[1]*, H Xu[1], TJ Royston[1,2], RL Magin[1].
[1]University of Illinois at Chicago, Chicago, IL, USA.

3:00P – 3:30P

COFFEE BREAK Gallery Lounge

Wednesday 3:30P — 4:45P
Session PTO: Phantoms and Test Objects

Chair: EL Madsen, USA *Co Chair: to be announced* Lecture Hall

3:30P – 3:45P

064 FAST GENERATION OF 3D SYNTHETIC RF DATA OF NONLINEARLY ELASTIC OBJECTS FOR SPECKLE TRACKING PERFORMANCE EVALUATION.
RQ Erkamp[1]*, PL Carson[1], M O'Donnell[1].
[1]University of Michigan, Ann Arbor, MI, USA.

3:45P – 4:00P

048 TISSUE–MIMICKING SPHERICAL LESION PHANTOMS FOR ELASTOGRAPHY WITH AND WITHOUT ULTRASOUND REFRACTION EFFECTS.
EL Madsen[1]*, G Frank[1], M Hobson[1], H Shi[1], T Varghese[1], J Jiang[1], TJ Hall[1], TA Krouskop[2,3], J Ophir[3], J Weaver[4], MM Doyley[4].
[1]University of Wisconsin–Madison, Madison, WI, USA; [2]Baylor College of Medicine, Houston, TX, USA; [3]The University of Texas Medical School, Houston, TX, USA; [4]Dartmouth College, Hanover, NH, USA.

4:00P – 4:15P

049 TISSUE–MIMICKING ANTHROPOMORPHIC BREAST PHANTOMS FOR ULTRASOUND AND MR ELASTOGRAPHY.
EL Madsen[1]*, G Frank[1], M Hobson[1], H Shi[1], T Varghese[1], J Jiang[1], TJ Hall[1], TA Krouskop[2,3], J Ophir[3], J Weaver[4], MM Doyley[4].
[1]University of Wisconsin–Madison, Madison, WI, USA; [2]Baylor College of Medicine, Houston, TX, USA; [3]The University of Texas Medical School, Houston, TX, USA; [4]Dartmouth College, Hanover, NH, USA.

4:15P – 4:30P

058 DESIGN AND CHARACTERISATION OF A COMPLIANT WALL VASCULAR PHANTOM OF VARYING ELASTICITY FOR ULTRASOUND INVESTIGATION OF ARTERIAL WALL MOTION (AWM).
J Dineley[1], P Hoskins[1]. (TL Poepping* presenting)
[1]University of Edinburgh, Edinburgh, Scotland, UK.

* indicates Presenter

043 DEVELOPMENT OF A NEW TISSUE–EQUIVALENT GEL FOR WALL–LESS FLOW AND WALL MOTION PHANTOMS.
TL Poepping[1]*, PR Hoskins[1], WJ Easson[2].
[1,2]University of Edinburgh, Edinburgh, Scotland, UK.

Sunday, October 17, 6:00P – Wednesday, October 20, 3:45P

Session POS: Posters
Chair: TA Krouskop, USA

005 A STUDY OF VIBRATION CHARACTERISTICS FOR ULTRASONIC ELASTICITY IMAGING.
J Park[1], S Kwon[2] and MK Jeong[2]*.
[1,2]Daejin University, Pocheon, Kyeonggi, KOREA.

012 COMPUTER–BASED VIBRATIONAL VISCOELASTOC MEASUREMENT OF SOFT TISSUES.
EM Timanin[1]*, EV Eremin[1].
[1]Institute of Applied Physics RAS, Nizhny Novgorod, RUSSIA.

018 TWO–DIMENSIONAL ELASTIC MODULUS DISTRIBUTION RECONSTRUCTION BASED ON A MODIFIED THREE–DIMENSIONAL FINITE–ELEMENT MODEL.
M Yamakawa[1]*, T Shiina[1].
[1]University of Tsukuba, Tsukuba, JAPAN.

027 AN ARTERIAL WALL MOTION TEST TOOL TO ASSESS PHILIPS AWM SOFTWARE.
SJ Hammer[1]*, J Dineley[1], WJ Easson[2], PR Hoskins[1].
[1,2]The University of Edinburgh, Edinburgh, Scotland, UK.

038 INTRAVASCULAR ULTRASOUND PALPOGRAPHY FOR DETERMINING THE AGE OF A THROMBUS: AN ANIMAL STUDY *IN VIVO*.
JA Schaar[1,2], F Mastik[1], ED van Deel[1], CJ Slager[1], PW Serruys[1], DJ Duncker[1], AFW van der Steen[1,2]*.
[1]Erasmus MC, Rotterdam, The NETHERLANDS; [2]Interuniversity Cardiology Institute of the Netherlands, Utrecht, The NETHERLANDS.

039 OPTICAL FLOW TISSUE TRACKING USING REAL–TIME 3D ULTRASOUND.
P Jordan[1]*, RD Howe[1], DP Perrin[1].
[1]Harvard University, Cambridge, MA, USA.

045 FEASIBILITY OF SKIN SURFACE ELASTOGRAPHY BY TRACKING SURFACE TOPOGRAPHY.
L Coutts[1]*, J Bamber[1], N Miller[1].
[1]Institute of Cancer Research, Sutton, Surrey, England, UK.

052 DESCRIPTION OF A NEW ITERATIVE ALGORITHM FOR SCALING FACTOR ESTIMATION.
J Fromageau[1], H Liebgott[1], E Brusseau[1]* and P Delachartre[1].
[1]CREATIS, Lyon, FRANCE.

055 GAUSSIAN MODELING OF DISPERSIVE MEDIA: APPLICATION TO CALCIFIED TISSUES.
D Hazony[1], JL Katz[2]*.
[1]Case Western Reserve University, Cleveland, OH, USA; [2]University of Missouri–Kansas City, Kansas City, MO, USA.

072 EXTRACTION OF MODULUS FROM THE OSMOTIC SWELLING OF ARTICULAR CARTILAGE MEASURED USING ULTRASOUND.
H Niu[1], Q Wang[1], Y Zheng[1]*.
[1]The Hong Kong Polytechnic University, Hong Kong, CHINA.

073 OSMOTICALLY–INDUCED SHRINKAGE AND SWELLING BEHAVIOR OF NORMAL BOVINE PATELLAR ARTICULAR CARTILAGE *IN SITU* MONITORED BY ULTRASOUND.
Q Wang[1], Y Zheng[1]*.
[1]The Hong Kong Polytechnic University, Hong Kong, CHINA.

074 EFFECT OF SALINE CONCENTRATION ON SOUND SPEED ON ARTICULAR CARTILAGE.
S Patil[1], Y Zheng[1]*.
[1]The Hong Kong Polytechnic University, Hong Kong, CHINA.

075 SKIN ELASTICITY MEASUREMENT BASED ON A 20 MHZ ULTRASOUND BIOMICROSCOPE.
Y Huang[1], Y Zheng[1]*.
[1]The Hong Kong Polytechnic University, Hong Kong, CHINA.

082 ULTRASONIC MEASUREMENT OF *IN–VIVO* STRAIN OF SURGICALLY REPAIRED ACHILLES TENDON UNDER ISOMETRIC CONTRACTION.
J Chan[1,2], Y Zheng[1]*, KH Ng[3].
[1]The Hong Kong Polytechnic University, Hong Kong, CHINA; [2]Maclehose Medical Rehabilitation Centre, Hong Kong, CHINA; [3]Queen Mary Hospital, Hong Kong, CHINA.

092 EFFECTS OF INTERNAL DISCONTINUITIES ON STRAIN ELASTOGRAMS.
TA Krouskop[1,2]*, R Righetti[2,3], J Ophir[2,3], H Lim[1] and EL Madsen[4].
[1]Baylor College of Medicine, Houston, TX, USA; [2]The University of Texas Medical School, Houston, TX, USA; [3]University of Houston, Houston, TX, USA; [4]University of Wisconsin–Madison, Madison, WI, USA.

093 BIOMECHANICAL PROPERTIES OF CORNEAL TISSUE DETERMINED BY APPLANATION AND THIN SHELL MODEL.
J Liu[1]*, C Roberts[1].
[1]The Ohio State University, Columbus, OH, USA.

095 IMPOSING PHYSICAL CONSTRAINTS TO YIELD ACCURATE AND UNBIASED DISPLACEMENT ESTIMATES.
NH Gokhale[1], MS Richards[1], MM Doyley[2], AA Oberai[1], PE Barbone[1]*.
[1]Boston University, Boston, MA, USA; [2]Dartmouth College, Hanover, NH, USA.

103 ANALYSIS OF 3D LEFT VENTRICULAR WALL MOTION USING TISSUE DOPPLER IMAGING.
AF Kolen[1]*, T Delhaas[1,2], T Arts[2].
[1]University Hospital Maastricht, Maastricht, The NETHERLANDS; [2]Maastricht University, Maastricht, The NETHERLANDS.

Session EEX: Equipment Exhibit
Chair: N Bush, UK   Gallery Lounge

Hitachi Medical Corporation.
Kashiwa, JAPAN.

Medison Corporation.
Seoul, KOREA.

Precision Acoustics, LTD.
Dorchester, Dorset, England, UK.

AUTHOR INDEX

ABSTRACTS

Third International Conference
on the Ultrasonic Measurement and Imaging
of Tissue Elasticity©

Lake Windermere, Cumbria, UK
October 17–20, 2004

Guest Lecture

000   **ROBERT HOOKE – ENGLAND'S LEONARDO?**

Allan Chapman[1]*.
[1]Modern History Faculty, Wadham College, University of Oxford, Broad Street, Oxford, OX1 3BD, England, UK.

Although he is perhaps most widely known to participants of this international conference for "Hooke's law" (of elasticity), Dr Robert Hooke was in fact one of the leading creators of modern science. For while he did not invent the experimental method, he did more than any other single individual to develop it and show that it worked, and could help transform not only our knowledge of nature but also our technological capacity. Lying at the heart of all of Hooke's work was what, in 1665, he referred to as "Artificial Organs" or instruments. These devices, such as the telescope, microscope, air pumps and barometer, were invented or developed by him and enabled him, and mankind, to inquire into whole classes of hither to unimaginable phenomena. They also created new, objective standards in physical research, which made scientific knowledge communal and not subjective.

Robert Hooke's interests covered every branch of physical science, as it was then understood; from attempts to measure the distance of the stars, to establishing what happens when blood passes through the lungs. In addition to being an experimental scientist of genius and a medical doctor, he was a successful architect, designer, and a draughtsman of brilliance. He was, indeed, "England's Leonardo!"
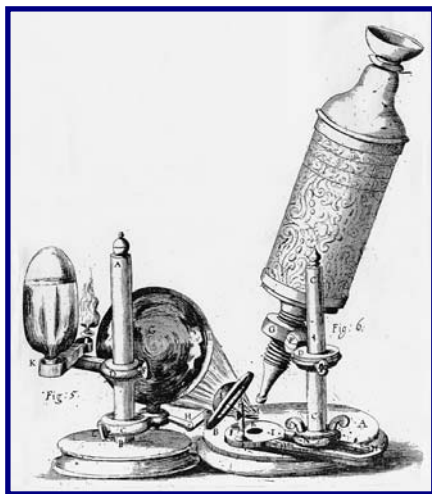
Robert Hooke's Microscope, from his book
Micrographia (1665)
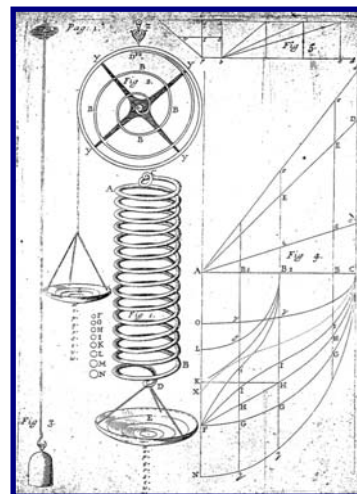
"Of Spring" (1678)

Dr Allan Chapman is currently Historian of Science and Medicine and a member the Faculty of Modern History at Oxford University. He has published 10 books as well as his research, and he lectures extensively on the history of science in England and abroad. In January 1994, he gave the Royal Society's triennial Wilkins Lecture in the History of Science, on Edmond Halley. Although his principle research areas lie in the histories of astronomy and medicine, he is particularly interested in the biographies and careers of scientists. He is an authority on the life of Robert Hooke, and his new book on Hooke, entitled "England's Leonardo", will be published by the Institute of Physics towards the end 2004.

* indicates Presenter

090   **CARDIOVASCULAR DEFORMATION IMAGING – PART I: VASCULAR.**

C.L. de Korte[1]*, J. D'hooge[2].
[1]Clinical Physics Laboratory, Dept. of Pediatrics, University Medical Center Radboud, Nijmegen, The NETHERLANDS; [2]Depts. of Electrical Engineering, Cardiology and Physics, Catholic University of Leuven, Leuven, BELGIUM.

Elastography is a technique that enables assessment of the mechanical (i.e. elastic) properties of tissue by imaging the tissue strain given a certain tissue stress (i.e. load). Strictly speaking, elastography uses a user dependent mechanical load (as described in the original patent from 1990), but also natural sources that were first considered an error source are nowadays considered useful. In vascular medicine, this technique is typically used for characterisation of plaques.

In (intra-)vascular applications, strain imaging is used for plaque characterization and identification of the rupture prone plaque. The pulsatile blood pressure is primarily used as the force for deforming the tissue. A non-invasive application is the carotid artery. Using a commercial scanner, 200 frames per second were acquired. RF based techniques were applied to calculate the strain in the carotid plaques. This technique was validated *in vitro* and is nowadays used by several groups around the world.

Invasively, the focus is on coronary arteries. In this application, an intravascular catheter is positioned at the cross-section of interest and data is acquired in the diastolic phase of the heart cycle. In this phase, decorrelation due to catheter motion in minimal. Also, the use of a compliant balloon is described. With this technique, catheter motion is prevented at the expense of possible injury of the vessel wall. Intravascular elastography is validated using phantom and *in vitro* experiments. *In vitro* experiments as performed by various groups using different types of catheters demonstrated a highly significant correlation between strain value and plaque type. Furthermore, a high correlation between a high strain spot and the typical morphology of a vulnerable plaque was found. The technique was also validated *in vivo* using a Yucatan animal model.

Recently, this technique was extended to 3D. With this technique called 3D palpography, the strain at the lumen vessel wall boundary for a full coronary artery is determined. Evaluation in rabbits and patients revealed a high reproducibility. Studies in different patient populations revealed a high correlation between the number of high strain spots and clinical manifestation as well as blood serum markers for rupture prone plaques.

In conclusion, vascular deformation imaging offers a unique tool to assess the composition and vulnerability of a lesion.

091   **CARDIOVASCULAR DEFORMATION IMAGING – PART II: CARDIAC.**
J. D'hooge[1]*, C.L. de Korte[2].
[1]Depts. of Electrical Engineering, Cardiology and Physics, Catholic University of Leuven, Leuven, BELGIUM; [2]Clinical Physics Laboratory, Dept. of Pediatrics, University Medical Center Radboud, Nijmegen, The NETHERLANDS.

Unlike for vascular applications, tissue deformation of the heart muscle (i.e. the myocardium) is not only the result of a passive load on the cardiac tissue but is also the result of an active muscle contraction. The heart should thus not be treated as a passively deforming elastic body such as e.g. vascular tissue but should rather be seen as an actively deforming elastic body. In fact, as the function of the heart is to eject blood through actively contracting and thereby changing the shape of the ventricular cavity, it is extremely important clinically to assess the active contraction force regionally developed. Indeed, it is the regional myocardial force development that will determine the regional contribution to the ejection of blood. It is therefore clinically referred to as 'regional myocardial function'.

At present, a direct non-invasive measurement of regional force development is not feasible. However, if passive loading of the myocardial segment under investigation is considered negligible with respect to the active force development, then regional force development can be approximated by assessing regional myocardial deformation, i.e. strain.

Several approaches have been proposed in the literature in order to measure instantaneous tissue strain by ultrasound (cf. elastography). Normalization of the instantaneous deformation to time gives a measure of the regional rate of deformation, i.e. strain rate. Integration of the strain rate curve over the cardiac cycle results in the total (cumulative) tissue strain. Cardiac strain and strain rate have been shown to provide complementary clinical information.

The applicability of ultrasonic deformation imaging (better known as 'strain and strain rate imaging') in cardiology has been studied extensively. Different methodologies towards ultrasound based strain (rate) estimation have been developed and validated by prototyping on simulated ultrasound data sets and subsequently testing these methodologies in gel phantoms and animals using modified ultrasound scanners. These methodologies have been validated extensively in the *in-vivo* setting and their clinical use has been evaluated in a wide range of pathologies.

One of the major pitfalls of the current implementation of the technique is its angle dependency. Indeed, as only tissue motion along the ultrasound line can be detected using conventional motion estimation techniques, only the deformation along the image line can be assessed. Recently however, new algorithms have been proposed that solve this problem by measuring all in-plane deformation components. These methodologies have recently been validated in the *in-vivo* setting.

Finally, as cardiac tissue deformation is intrinsically influenced by passive loading conditions (and not only by regional contractile force) mechanical models of the heart have been used in combination with the ultrasound deformation data in order to measure regional contractile force more accurately, i.e. independent of the passive loading conditions. Interesting results have recently been presented in the literature.

In conclusion, ultrasound strain and strain rate imaging allow for a non-invasive assessment of regional myocardial function. As this remains an important goal in clinical cardiology, these techniques are thus expected to have an important impact on clinical echocardiography.

078   THE EFFECTS OF DEFORMATION ON THE YOUNG'S MODULUS MEASUREMENT BY TWO INDENTORS OF DIFFERENT SIZES – A SIMULATION STUDY.

Alex Pong Chi Choi[1], Yongping Zheng[1]*.
[1]Rehabilitation Engineering Centre, The Hong Kong Polytechnic University, Hong Kong, CHINA.

Indentation has been commonly used in the measurement of the mechanical properties of the biological tissue, such as articular cartilage and skin together with subcutaneous tissues. In 1972, Hayes et al. [1] developed a solution for an indentation of the cartilage tissue by using flat-ended cylindrical rigid indenter. From the indentation, the Young's modulus (E) can be determined by the following equation:

$$E = \frac{(1 - v^2)}{2a\kappa(v, a/h)} \cdot \frac{P}{w}$$

where E is the Young's modulus, P is the indentation force, v is the Poisson's ratio, w is the indentation depth, a is the radius of the indenter, h is the original thickness of the tissue, k is a scaling factor which depends on the aspect ratio (a/h) and Poisson's ratios (v). In 1997, Zhang et al. [2] considered the effects of large deformation and derived a new set of kappa values by using finite element analysis. Using the above equation, we need to assume the Poisson's ratio or to measure the Poisson's ratio using other methods. Jin and Lewis [3] proposed a new method that determines the Poisson's ratio from two indentations using two indenters with different diameters.

$$\frac{P_1}{w_1} \bigg/ \frac{P_2}{w_2} = \frac{2Ea_1k(a_1/h, w/h, v)/(1 - v^2)}{2Ea_2k(a_2/h, w/h, v)/(1 - v^2)}$$

Two indentations were carried out on the same materials by using two different size indenters. The Poisson's ratio will be the only unknown in the above equation and can be solved by the non-linear relationships between kappa to kappa ratios with respect to different radius of indenters. In this study, we looked into the effects of large deformation on the Young's modulus measurement by using the above method in finite element analysis and calculated the Young's modulus by using the kappa value with and without consideration of large deformation effects.

Using finite element simulation, the axisymmetric indentations with different sized indenters were used to perform the indentation on the linear-elastic tissue. ABAQUS finite element software (Version 6.4, Hibbitt, Karlsson & Sorensen, Inc, US) was used in this study. We inputted the parameters of Young's modulus and Poisson's ratio, then the indentation force and indentation depth were calculated by the simulation. The soft tissue was assumed to be homogenous and isotropic. The Young's modulus was fixed at 60 kPa which was similar to the soft tissues [4] and the Poisson's ratio was fixed at 0.45.

Table 1 shows the results of the Young's modulus obtained with and without consideration of the deformation effects. When the indentation depth w is 0.01% of the original thickness h, the results of the Young's modulus without considering the deformation effects is 61.24 kPa (percentage error = +2.08%) and the Young's modulus with considering the deformation effects is 63.21 kPa (percentage error = +5.35%). For the indentation depth w is 15% of the original thickness h, the results of the Young's modulus without considering of deformation effects is 67.51 kPa (percentage error = +12.52%) and the Young's modulus with considering of deformation effects is 61.64 kPa (percentage error = + 2.73%).

From the results, we found that the difference of the Young's modulus calculated from the small deformation (0.01%) is not obvious. However, when the deformations become larger, the effects of the deformation on the Young's modulus become obvious. In summary, we can obtain the Young's modulus and Poisson's ratio simultaneously by conducting two indentation tests with finite deformations using two different diameters. This new method for measurement of the material properties is very useful in the biomechanical characterization of various tissues.

Table 1: The comparison of the Young's modulus with and without consideration of the effects of large deformation

Effects of large deformation	With consideration		Without consideration	
Deformation	E (kPa)	% error	E (kPa)	% error
0.01%	63.21	+ 5.35%	61.25	+ 2.08%
0.10%	61.72	+ 2.86%	65.47	+ 9.12%
0.15%	61.64	+ 2.73%	67.51	+ 12.52%

References:
[1] Hayes WC, et al., Biomech. 5, 541-551 (1972);
[2] Zhang M, et al., Med Eng Phys 19: 512-517 (1997);
[3] Jin H and Lewis L, Proc of 2003 Summer Bioengr Conference. Sonesta Beach Resort, Florida.
[4] Zheng YP and Mak AFT. IEEE Trans Biomed Eng 43: 912-918, 1996.

* indicates Presenter

063 ULTRASOUND CRITICAL–ANGLE REFLECTOMETRY: MEASURING VELOCITIES IN HARD AND SOFT ANISOTROPIC TISSUES.

Peter P. Antich[1], Matthew A. Lewis[1]*, Edmond Richer[1], Billy Smith[1].
[1]University of Texas Southwestern Medical Center, Dallas, TX, USA.

Ultrasound Critical-Angle Reflectometry (UCR) is a relatively recent method that had been introduced to measure both bone elasticity and its anisotropy [1, 2]. Changes in the micro-architecture and relative constituents of bone lead to altered mechanical and functional properties that may or may not be symptomatic and cannot be directly measured by either bone mineral densitometry (BMD) or ultrasound broadband attenuation and quantitative ultrasound techniques (BUA/QUS). In the complex interaction between a finite ultrasonic beam and a material, the reflected acoustic field is modulated by the material properties with a dependence on angle of incidence and relation to material principle axes. The ability of UCR to sample the complete material elasticity matrix is unique when compared to other methods for bone quality assessment. We present developments in our latest clinical UCR system (see Figure 1 below) based on several new technologies, including large aperture, focused transducers for simultaneous insonification at multiple angles of incidence, and multi-element receiver arrays with full waveform sampling. Although recent work has focused on measurements in the calcaneus [3], UCR is applicable at many anatomical locations, and we believe the technique has applications beyond calcified tissues.

Unlike previous systems that utilized water baths, this UCR device uses a liquid-filled ultrasonic head for acoustic coupling to tissues. In order to apply the UCR technique to soft tissues, we present a revised method by which the normal coupling liquid (deionized water) is replaced by oils and alcohols of lower index of refraction. By increasing the velocity differential between the coupling liquid and the tissue, the reflection spectrum can be shifted to smaller angles of incidence, where precision is greater and reflected power is increased. We describe *in vitro* experiments for a variety of soft tissue samples and phantoms. Particularly of interest is the ability of UCR to detect anisotropy in highly ordered tissues such as rat tail tendon.

Figure 1: Third generation clinical UCR system.

References:
[1] Antich PP and Mehta SM: Ultrasound critical-angle reflectometry (UCR): a new modality for functional elastometric imaging. Physics in Medicine and Biology, 42:1763-1777, 1997.
[2] Mehta SM and Antich PP: Measurement of shear-wave velocity by ultrasound critical-angle reflectomerty (UCR). Ultrasound in Medicine and Biology, 23(7):1123-1126, 1997.
[3] Richer E, Lewis M, Odvina CV, Vasquez MA, Pak CYC, Antich PP: Impaired Bone Quality in Bisphosphonate (BISPHOS) Treatment and Renal Transplantation by Ultrasound Critical Angle Reflectometry (UCR). Journal of Bone and Mineral Research, 18(2 Supplment): SU111, S207, 2003.

025 **A DEVICE FOR THE ASSESSMENT OF NONLINEAR VISCOELASTIC MATERIAL PROPERTIES OF SOFT TISSUES *IN VIVO*.**

Ergin Tönük[1]*.
[1]Middle East Technical University, TR-06531, Ankara, TURKEY.

A mechanical device to assess the nonlinear elastic and viscoelastic material properties of soft tissues *in vivo* is presented. The device is composed of three major components, a portable computer, a control box and a probe. The portable computer has the software that controls the experimental protocols and collects raw data. It communicates with the control box through the USB connection. The control box houses the power supplies (±15VDC for the load cell, and 12VDC for data acquisition system and step motor), step motor driver card and data acquisition system. It has a 220VAC power connection and has cable connection to the probe. The probe is driven by a step motor which has a displacement resolution of 0.05 mm. The probe has a replaceable tip with different geometries (currently cylindrical with flat tip and spherical) to indent soft tissue and a load cell to measure the soft tissue reaction force to indentation. The single-cable connections between these main units and compact architecture of the system make it suitable for the clinical environment.

The experimental protocols currently available on the soft tissue testing system include cyclic loading and unloading of soft tissue, force-relaxation, and creep experiments. In cyclic loading and unloading tests the soft tissue can be indented to a desired level with a desired velocity in desired number of cycles. This test is mainly used to observe the nonlinear elastic properties of soft tissue, the difference in force-displacement characteristics of soft tissue in loading and unloading, and the preconditioning effects (Figure 1). In force-relaxation tests, the soft tissue can be indented to the desired level with the desired velocity and stopped. The decrease in soft tissue reaction force (force-relaxation) is observed for a desired interval of time. This test is mainly used to observe the viscoelastic properties of soft tissues like amount of relaxation, relaxation time constants and number of terms in Prony series approximation of the observed mechanical response (Figure 2). In creep tests, the soft tissue can be indented to the desired level of soft tissue reaction force with the desired velocity. When the target force is reached, the system starts a proportional closed loop control algorithm that tries to keep the soft tissue reaction force at the desired level. The step motor moves back or forth with a velocity proportional to the difference between the measured and the target soft tissue reaction force or stops. This test is mainly used to observe the viscoelastic properties of soft tissues like the amount of creep, creep time constants and number of terms in Prony series approximation of the observed mechanical response (Figure 3).

The soft tissue test system presented can be used *in vivo* in order to assess the bulk mechanical properties of soft tissues. The device may help further our understanding of the soft tissue mechanical behavior. The device can be used to assess the mechanical properties of soft tissues which are externally accessible on the body. Currently the system has three different experimental test protocols, cyclic loading, force-relaxation and creep. Depending on future needs, modification on experimental protocols or addition of new protocols is possible.
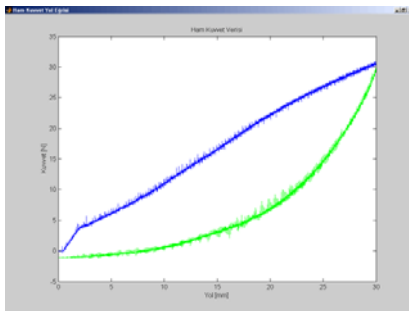

Figure 1: Force-displacement of a viscoelastic dummy during cyclic testing (upper curve loading, lower curve unloading)
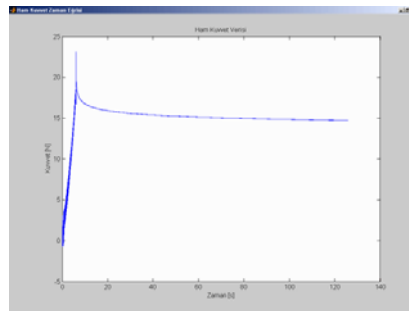
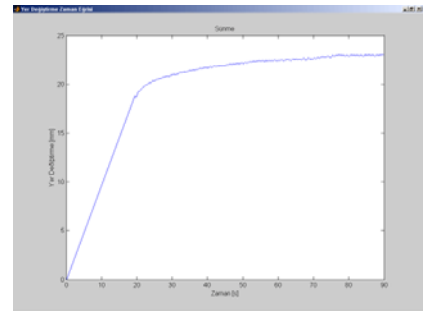Figure 2: Force-relaxation response of a viscoelastic dummy

Figure 3: Creep response of a viscoelastic dummy

026 **ASSESSMENT OF NONLINEAR VISCOELASTIC MATERIAL PROPERTIES OF SOFT TISSUES OF RESIDUAL LIMBS OF TRANS TIBIAL AMPUTEES.**

Ergin Tönük[1]*, Cemil Yildiz[2], A. Sabri Atesalp[2].
[1]Middle East Technical University, TR-06531, Ankara, TURKEY; [2]Gülhane Military Medical Academy, TR-06018, Ankara, TURKEY.

The individuals with trans tibial amputation are generally rehabilitated by a patellar tendon bearing (PTB) prosthesis. For the individual design of the PTB prosthetic socket, the soft tissue material properties are subjectively evaluated by a qualified prosthetist. To assess the material properties objectively and to obtain a soft tissue material model that can be used for finite element analysis of residual limb-prosthetic socket mechanical interface there is ongoing research on *in vivo* soft tissue tests and test protocols.

Soft tissue experiments were performed on the residual limbs of 6 individuals using the soft tissue test device developed [1]. The soft tissue experiment protocols were cyclic tests with 1, 2, 4, and 8 mm/s indentation rate, all with 10 cycles, force-relaxation, and creep tests. The test locations include patellar tendon, medial and lateral aspects and popliteal regions. The experiments reveal that bulk soft tissue (i.e. skin, fat, muscle etc.) of a residual limb has a considerable nonlinear and fading history behavior in addition to preconditioning.

The raw experimental data contained the following forms of noise:
1. The step motor does not move smoothly but in steps which contaminate the reaction force of soft tissue with the inertia force of the tip.
2. For most test locations, the pulse is seen together with the soft tissue reaction force.
3. Change in activation level of muscles (especially during long lasting experiments like force-relaxation and creep) changed the soft tissue reaction force considerably.

Although the first two items can be filtered out by using appropriate filters, for the last item, precautions during experiments would be necessary.

The soft tissue experiments performed on individuals with trans tibial amputation would be useful in following ways. It would help understanding the mechanical response of bulk soft tissues to indentation. The proposed mechanical models for soft tissues would be checked against experimental data. Finite element models of residual limb and prosthetic socket using realistic material models for soft tissues would help understanding the details of the prosthetic socket biomechanics and might help improving prosthetic socket design.

Reference:
[1] Tönük, E. "A device for the assessment of the nonlinear viscoelastic material properties of soft tissues *in vivo*", Third International Conference on the Ultrasonic Measurement and Imaging of Tissue Elasticity, Lake Windermere, Cumbria, United Kingdom, October 17-20, 2004

057 **STRAIN ESTIMATION USING SPECTRAL CROSS–CORRELATION: INITIAL RESULTS USING PARAMETRIC METHODS.**

K Hoyt[1,2]*, F Forsberg[2], J Ophir[3].
[1]Drexel University, Philadelphia, PA, USA; [2]Thomas Jefferson University, Philadelphia, PA, USA; [3]The University of Texas Medical School, Houston, TX, USA.

It has been shown, that strain estimation using spectral cross-correlation (between pre- and postcompressed power spectra) is less precise than its RF cross-correlation counterpart, but far more robust against decorrelation processes such as axial jitter [1, 2]. This strain estimator technique may be particularly useful in noisy environments, e.g. when using a freehand elastography setup or performing intravascular elastography. In this study, we revisit the incoherent strain estimation method and investigate the feasibility of using parametric spectral estimators in place of the DFT-based, or periodogram, approach which is known to exhibit high spectral variance (erratic behavior). In general, parametric methods have the potential to provide more accurate spectral estimates, and, consequently, strain estimates, than their nonparametric counterparts.

Monte-Carlo simulations were developed in MATLAB where spectral strain estimates were obtained over 20 independent realizations of the pre- and postcompressed RF echo signals. Specifically, the simulation allowed for evaluation of strain estimators against several common decorrelation processes, e.g. electronic noise, large applied strain, axial jitter and lateral scatterer motion, which were superimposed directly into the postcompressed RF echo sequences. Strain estimator performance was quantified in terms of the experimental strain filter (SF) [3], strain estimation standard deviation, and the correlation coefficient (as computed from the cross-correlation between congruent pre- and postcompressed data sequences).

Initial simulations compared the RF cross-correlation and the periodogram strain estimators for robustness against axial jitter and lateral scatterer motion. For the latter, the postcompressed window was shifted and sized in order to allow analysis of congruent data segments. Additionally, the following parametric autoregressive (AR) spectral estimators: Yule-Walker, modified Covariance Least Squares (LS), and the Burg methods, and autoregressive moving average (ARMA) spectral estimators: modified Yule-Walker and 2-stage LS methods, were implemented and evaluated as strain. Model orders and data window lengths for the above were chosen to maximize the elastographic signal-to-noise ration (SNR_E) and then compared to that of the periodogram. Strain estimator robustness was investigated against decorrelation for the selected model order.

Overall, the periodogram-based strain estimator outperformed the RF cross-correlation technique in terms of SNR_E (lower SD) and SF dynamic range when evaluating robustness to axial jitter and lateral scatterer motion. Though the spectral strain estimators were susceptible to axial jitter, this was shown to be minimized when frequency smoothing was implemented albeit with a significant reduction in SNR_E (factor of 10). Additionally, the Yule-Walker yielded the best performance for the AR spectral estimators with a maximum SNR_E of 13 compared to a SNR_E of 20 obtained using the unsmoothed periodogram-based strain estimator. Additionally, the SD deviation associated with each estimator was nearly identical, but the correlation coefficient associated with AR method was noticeably higher for larger applied strains. Under decorrelation conditions, both strain estimators exhibited comparable performances. The ARMA-based strain estimators failed to perform as well as any of the AR-based methods.

In conclusion, the potential of strain estimation using spectral cross-correlation was demonstrated. In direct comparison, strain estimation using the Yule-Walker parametric-based method outperformed that of the frequency smoothed periodogram method.

References:
[1] Konofagou E, Varghese T, Ophir J, et al. Power spectral strain estimators in elastography. Ultrasound Med Biol 1999; 25:1115-1129.
[2] Varghese T, Konofagou E, Ophir J, et al. Direct strain estimation in elastography using spectral cross-correlation. Ultrasound Med Biol 2000; 26:1525-1537.
[3] Varghese T, Ophir J. A theoretical framework for performance characterization of elastography: The strain filter. IEEE Trans Ultrason Ferroel Freq Cont 1997; 44(1):164-172.

* indicates Presenter

053   A NEW TIME DELAY ESTIMATOR FOR TISSUE ELASTICITY IMAGING.

Francesco Viola[1], William F. Walker[1]*.
University of Virginia, Charlottesville, VA, 22908, USA.

Time delay estimation (TDE) is a fundamental signal-processing step in many application fields, including tissue elasticity imaging. Accurate time delay estimation is an essential prerequisite for accurate reconstruction of mechanical properties.

Echo decorrelation is usually considered the main source of TDE error in tissue elasticity estimation. Such decorrelation is introduced primarily by out of plane motion and compressive deformation (or axial strain). In addition to these well recognized sources of error, we believe that current estimators suffer from significant error due to accumulation of bias. Together these factors conspire to degrade the ability to characterize tissue mechanical properties.

We present a new time delay estimator that directly determines continuous time delay estimates from sampled data with a high degree of accuracy and at a reasonable computational cost. The technique forms a spline-based piecewise continuous representation of the reference signal and then solves for the minimum of the sum squared error between the reference and the delayed signals to determine their relative time delay. The mathematical formulation of the proposed tracking algorithm makes it particularly well suited for application in tissue elasticity estimation, since it can easily include companding, or axial signal stretching. Unlike existing estimators, companding introduces little additional computational cost in our method.

We have performed simulations and ultrasound experiments to test the performance of this algorithm and compare it to currently accepted delay estimators implementing a variety of sub-sample interpolation methods. Simulation results show that this algorithm significantly outperforms other algorithms in terms of jitter and bias over a broad range of conditions. For a 5 MHz, 50% bandwidth signal sampled at 40 MHz with a sub-sample delay of 0.3 samples, the bias of the proposed method is over 300 times smaller than that for the normalized correlation with grid slopes interpolation, and over 80 times better than that for normalized correlation implementing cosine fitting interpolation. We also present simulation results depicting the performance of our estimator compared to other "well known" time delay estimators using a synthetic tissue elasticity model. Finally, we compare our algorithm to established methods for radiation force based tissue elasticity estimation. These results suggest that the biases of conventional methods may have a significant detrimental effect in this application.

061 **2D STRAIN ESTIMATION ALGORITHM – INITIAL RESULTS.**
E. Brusseau[1]*, G. Said[1], J. Fromageau[1], O. Basset[1], D. Vray[1].
[1]CREATIS UMR CNRS 5515, INSERM U630, Bât. Blaise Pascal, 7 avenue Jean Capelle; 69621 Villeurbanne, FRANCE.

Background: Strain estimation techniques used in elastography are mainly one dimensional. However, when subjected to any load, whatever the direction, soft biological media deform in the three dimensions. Accurately estimating the strain in only one dimension thus requires taking into account the 3D motion of the tissue induced by the deformation.

Because acquired ultrasound data are mainly 2D images, we propose to begin in this study with a 2D numerical processing model for the local strain estimation.

Methods: The principle consists, for each 2D RF ultrasound footprint selected in the image before deformation, in searching the corresponding deformed 2D footprint in the image after deformation and in estimating the strain locally. In the axial direction, the 2D footprint is supposed to be time-shifted and scaled, the time-shift being induced by the previous axial deformations. Because the lateral resolution is much lower than that in the axial direction, only shifts will be considered to occur in the lateral direction.

The procedure works as follows: first, while displacing regularly the 2D window of study in the image before deformation, the window, in the image after deformation, is adaptively displaced according to the previously estimated axial scaling factors and lateral displacements. Then the current axial scaling factor (α) and lateral displacement (τ) are estimated. They are searched as the arguments that maximize the correlation $f(\alpha,\tau)$ between the initial footprint and the deformed footprint axially scaled and laterally shifted. In practical terms, this is achieved by minimizing the functional $-f(\alpha,\tau)$ by an optimization strategy (gradient descent).

Results: In order to assess the performance of the algorithm, the latter was used to process simulated data. One numerical phantom consists of a cube within which a spherical inclusion is embedded. The Young's modulus of the inclusion has been set to 100 kPa while that of the surrounding medium has been fixed to 50 kPa. Poisson's ratio is equal to 0.45 through the whole phantom. The deformation of the medium was performed with finite element modeling and RF ultrasound images of the medium before and after deformation were generated with the FIELD II software.

Initial results demonstrate the good performance of our algorithm. Indeed, axial deformations as well in the inclusion, as in the surrounding tissue have been accurately estimated, exhibiting very clearly the areas of stress concentration. Moreover, the strain profile through the inclusion shows sharp boundaries. Finally, the lateral displacement field is smooth and of significant magnitude, demonstrating the need of taking into account the lateral displacement to more accurately estimate the axial strain distribution.

Conclusions: The developed algorithm has provided encouraging initial results with numerical phantoms. Future work tends toward the assessment of the algorithm with physical phantoms and biological tissues.

081 **TISSUE STRAIN IMAGING USING A WAVELET-BASED PEAK SEARCH ALGORITHM.**

Hani Eskandari[1]*, S.E. Salcudean[1].
[1]Department of Electrical and Computer Engineering, University of British Columbia, Vancouver, BC, CANADA.

A new method is devised to estimate the motion and relative local compressions between two different ultrasound RF signals under different compression states. The underlying idea is that the displacement of the peaks in a recorded RF signal can be assigned to the displacement of the medium. Therefore, the peaks of both pre- and post-compression signals can be detected, and by estimating the relative motions between them, the strain of the medium can be calculated.

The algorithm uses a dyadic wavelet transform method to locate the positions of the peaks in the RF signals. The mother wavelet which is used has the capability of smoothing the signals, and the resulting continuous wavelet transform will be the derivative of the smoothed version of the original signal. After the peaks have been found, each two peaks in the pre- and post-compression signals are assigned to each other. So, starting from the beginning of the signals, the motion of the peaks is tracked, and for each peak in the original signal, the expected location of its match in the compressed signal is estimated and then a peak is located in that neighborhood. Using sub-pixel approximation, the position of the peaks and also the displacements can be calculated with better precision.

The method has been tested on simulation and phantom data and successfully reconstructed images under practical values of steady state and also dynamic compressions. By using the simulated RF signals, the real local displacements in the medium are known. Hence, utilizing the ratio of the standard deviation over the mean value of the strain in a specific constant-strain region, a criterion for error can be defined. Comparisons have been made between the proposed method and the Time-Domain Estimation (TD) and Adaptive Stretching (AS) algorithms.

The results show that compared to the TD method, the new approach is far more accurate, having lower errors and is able to estimate the motions accurately up to about 3% strain. On the other hand, in comparison to the AS method, the proposed algorithm is much less time consuming and at the same time shows some improvements in the results using the above criterion for error. Comparing the speed of these three methods for a signal using 100 blocks with 60% overlap for TD and AS, resulted that the new method is 3 times slower than TD but 7 to 50 times faster than AS, depending on whether the focus is on speed or accuracy in the AS method. However, the dynamic range of the compression states under which the AS method works properly is wider than that of the peak search algorithm. Another advantage of the new method is that it has better resolution compared to any other motion estimation techniques for Ultrasound RF signals, i.e. the accuracy is no less than the distances between the peaks. Moreover, since there are no data windows used in the present procedure, there is no such trade-off between the window length and resolution as we have in TD and AS methods.

Having a good estimation of motion in simulation and phantom studies, plus being time efficient to an extent that is suitable for elastography, the peak search method can be viewed as a good tool to be utilized in real-time strain imaging and elastography systems. Implementing wavelet transforms of signals with a simple convolution and using the product of the FFT's of RF signals to speed up the process, even the frame-rates that are needed for dynamic elastography are achievable in this case.

References:
[1] M. A. Lubinski, S. Y. Emelianov and M. O'Donnell, "Speckle Tracking Methods for Ultrasonic Elasticity Imaging Using Short-Time Correlation," in *IEEE Trans. On Ultras. Ferro. And Freq. Control*, vol. 46, no. 1, pp. 82-96, Jan. 1999.
[2] S. K. Alam, J. Ophir and E. E. Konofagou, "An Adaptive Strain Estimator for Elastography," in *IEEE Trans. On Ultras. Ferro. And Freq. Control*, vol. 45, no. 2, pp. 461-472, March 1998.

010   **THE SUPERSONIC SHEAR IMAGING TECHNIQUE APPLIED TO NONLINEAR PROPERTIES OF SOFT TISSUES.**

Stefan Catheline[1]*, Jean-Luc Gennisson[1], Jeremy Bercoff[1], Christophe Barrière[1] and Mathias Fink[1].
[1]Paris 7 University, Laboratoire Ondes et Acoustique, E.S.P.C.I., 10 rue Vauquelin 75231 Paris cedex 05, FRANCE.

The ultrafast scanner has shown to be a powerful tool to detect shear wave propagation within soft tissues in transient elastography experiments. More recently, it was also used to generate shear waves due to the acoustic radiation pressure. This technique, the so called supersonic shear imaging, can easily be implemented in an acoustoelasticity experiment. Thus, the association of static elastography with dynamic elastography, can reveal the nonlinear properties of soft materials. More over, using a new theoretical approach of the strain energy in soft solid [Hamilton, Ilinsky and Zabolotskaya, J. Acoust. Soc. Am., 114, 2436 (2003)], it is shown that the acoustoelasticity experiment can be greatly simplified. Instead of measuring shear wave speed for three different polarizations in order to completely determine the nonlinearity of standard solids, one is sufficient in soft solids to characterize the nonlinear shear elasticity.

015   **DYNAMICS OF SOFT TISSUE IN RESPONSE TO IMPULSIVE ACOUSTIC RADIATION FORCE WITH CLINICAL APPLICATIONS.**

Mark L. Palmeri[1]*, Amy N. Congdon[1], Kristin D. Frinkley[1], Mary Scott Soo[2], Rex Bentley[2], Kathryn R. Nightingale[1].
[1]Duke University, Durham, NC USA; [2]Duke University Medical Center, Durham, NC USA.

Background: Acoustic Radiation Force Impulse (ARFI) imaging utilizes brief, high-intensity, focused acoustic pulses to generate radiation force in tissue. Conventional, correlation-based ultrasound methods are used to track the resulting tissue displacements and generate images of maximum displacement, time to peak displacement, and tissue recovery time. These images elucidate soft tissue material properties and structure.

Methods: Finite Element Method (FEM) models of ARFI excitation were developed that simulate the mechanical and thermal response of soft tissue to ARFI excitations. Gelatin-based, tissue-mimicking phantoms with stiff, spherical inclusions were fabricated to validate the mechanical FEM models, while thermocouple experiments were performed in porcine muscle to validate the thermal FEM models. *In vivo* ARFI imaging of breast masses prior to needle biopsy, using a multiple focal zone configuration (4 focal depths, with 50 lateral locations per focal depth), were performed using a Siemens Antares scanner and a VF10-5 linear array. Data was acquired in real-time, and matched B-mode and ARFI displacement images were generated for each lesion. *Ex vivo* studies of gastrointestinal organs from surgical pathology specimens and cadavers, including stomach, esophagus, colon, and rectum, were performed using a Siemens Elegra scanner with a 75L40 linear array.

Results: The dynamic mechanical FEM models demonstrate that displacement magnitude, time to peak displacement, and tissue recovery time are inversely proportional to tissue elasticity. The dynamic tissue response is also a function of acoustic radiation force distribution; when tissues have increased ultrasonic absorption, greater volumes of tissue are excited and increased inertial effects (e.g., increased time to peak displacement) are observed in ARFI images. The dynamic response of stiffer inclusions to ARFI imaging in the FEM models was validated in phantom studies, with the lesions taking longer to reach their peak displacements due to inertial effects. Simulation and phantoms studies demonstrated that using multiple, tightly-focused radiation force excitations in both axial and lateral dimensions improve image contrast for spherical inclusions with stiffer elastic moduli. Thermal FEM models and thermocouple measurements demonstrate that soft tissue heating is below 2°C in current ARFI imaging applications, while transducer heating is below 1°C.

In *in vivo* breast studies, structures in B-mode directly correlate with corresponding ARFI images, with similar spatial resolution in both modalities. Malignant breast masses exhibit increased contrast and margin definition in ARFI displacement images over matched B-mode images, with several malignant lesions having larger diameters in the ARFI images than in the B-mode images. Rings of uniform recovery time also have been observed in ARFI images of malignant lesions. Fibroadenomas and cysts exhibit less contrast in ARFI images than in B-mode images.

ARFI displacement images illustrate mechanical contrast between different layers of gastrointestinal tissue. In an ulcerated adenocarcinoma at the gastro-esophageal junction, status-post neoadjuvant chemotherapy and radiation treatment, ARFI displacement images show clear delineation between stiffer fibrotic scar tissue and normal layers of surrounding organs, both in lateral extent and depth of penetration.

Conclusions: Mechanical and thermal FEM models of ARFI imaging in soft tissue, with the presence of stiff, spherical inclusions, were developed and validated using tissue-mimicking phantoms. ARFI imaging, as currently implemented, generates safe amounts of tissue heating, although thermal safety must be evaluated when developing new ARFI beam sequences. *In vivo* breast studies demonstrated that ARFI images provide both different and complementary information with matched B-mode images. Differences in ARFI image displacement contrast and tissue dynamics were identified as potential differentiating features between benign and malignant breast lesions. *Ex vivo* studies in gastrointestinal organs indicate that ARFI imaging has the potential to assess lateral extent and degree of invasion of stiff inclusions in layers of bowel wall, aiding in ultrasonic staging of colorectal cancers.

024 **VIBRATION SONOELASTOGRAPHIC IMAGING USING A PHASE LOCKING TECHNIQUE.**

Asif Iqbal[1]*, Tim Frank[1], Donald McLean[1], Alfred Cuschieri[1].
[1]Surgery Technology Group, Department of Surgery & Molecular Oncology, Ninewells Hospital & Medical School, University of Dundee, Dundee, DD1 9SY, Scotland, UK.

Aim: Ultrasound sonoelastographic images can be difficult to interpret due to an indeterminate phase relationship between the exciting signal and the ultrasound frame rate. A system was developed to control this phase relationship and produce pairs of frames at selected instants within each excitation cycle. This allows a direct visual approach to maximising the information available from the sonoelastographic imaging process.

Methods: The system triggers the ultrasound scanner, via the ECG trigger input, using two interleaved pulse trains. The combined trigger rate of these trains is set just below the maximum frame rate for the scanner set at the desired operating parameters. In addition, the trigger pulses are phase locked to the excitation signal with independently adjustable delays. This technique was demonstrated using phantoms constructed to mimic breast tissue with included hard lesions that were formulated to be indistinguishable from the background material in B-mode images.

Results: The technique allowed the phases to be adjusted dynamically to maximise the variation between alternate frames. It was also useful for investigating the motion field in the target material. As well as providing direct visualisation, the system was used for selecting images for further processing in the form of frame to frame correlation studies to reveal the small non-uniformities that could correspond to stiffness variations.

Conclusion: The relative simple phase control technique can improve the interpretation of sonoelastographic imaging.

028   VISCOELASTICITY IMAGING BASED ON HYSTERESIS ANALYSIS UNDER QUASI-STATIC DEFORMATION.

Naotaka Nitta[1]*, Tsuyoshi Shiina[2].
[1]Institute for Human Science and Biomedical Engineering, National Institute of Advanced Industrial Science & Technology (AIST), 1-2-1 Namiki, Tsukuba, Ibaraki 305-8564, JAPAN; [2]Institute of Information Sciences and Electronics, University of Tsukuba, 1-1-1 Tennoudai, Tsukuba, Ibaraki 305-8573, JAPAN.

While present ultrasonic tissue elasticity imaging is based mainly on measurements of strain and elastic modulus, the inherent viscoelasticity of soft tissue cannot be evaluated. Viscoelasticity of soft tissue is one of the noticeable properties for clinical diagnosis and has the potential of providing different information from elastic evaluation. Therefore, viscoelasticity assessment and imaging under applied quasi-static deformation is useful as an extention of real-time elasticity imaging. Typical viscoelastic analysis of soft tissue provides the elastic and viscous constants by selecting an appropriate viscoelastic model such as Voigt model. However, this means that inconsistent constants are obtained according to each model selection. On the other hand, several phenomena such as hysteresis, creep and stress relaxation are observed in a viscoelastic body. Therefore, parameterization of these phenomena holds potential for assessing viscoelasticity of soft tissue, instead of using a model.

In this paper, we focus on the hysteresis phenomenon and define the hysteresis parameter (HP) as the ratio of the loop area to the strain energy in the loading process [1]. We also create HP images by measuring the HP distribution using an ultrasound-based method. The local hysteresis loop in soft tissue is generalized by applying cyclic quasi-static loading and unloading with an ultrasonic probe on the body surface.

Knowledge of the internal stress is required in order to obtain the hysteresis loop precisely. The internal stress-strain curves, however, are estimated based on the pressure measured on the surface, and the HP distribution is mapped. In order to confirm the usefulness of this method, two experiments were performed. First, the potential of HP for characterizing tissue was investigated by a direct mechanical test using porcine thigh muscle and kidney. Second, the ultrasound-based method for mapping HP distribution was evaluated through *in vitro* experiments on porcine kidney.

Results from a direct mechanical test on porcine thigh muscle before and after formalin immersion showed that the HP value for the post-immersed muscle decreased to about 46% of the value obtained prior to immerssion (Figure 1), which revealed the ability to distinguish tissue components. Results from the HP mapping experiment and the mechanical test for porcine kidney showed that the ultrasound-based method was valid for mapping the HP distribution. Moreover, the pattern displayed in the HP image (Figure 2(c)) was different from that in the conventional images, that is, B-mode and strain images (Figure 2(a) and (b)). These results imply that HP imaging can provide different types of diagnostic information from conventional imaging.

Reference: [1] N. Nitta *et al.* : Proc. of IEEE Ultrasonics Symp., 1606-1609, 2003.
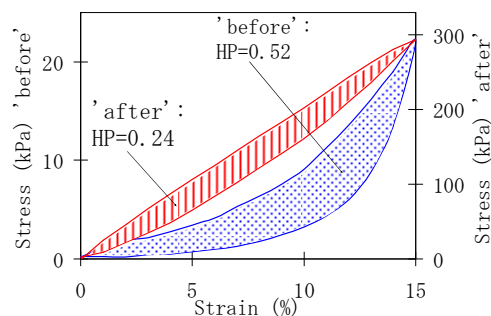
Figure1: Hysteresis loop of porcine muscle

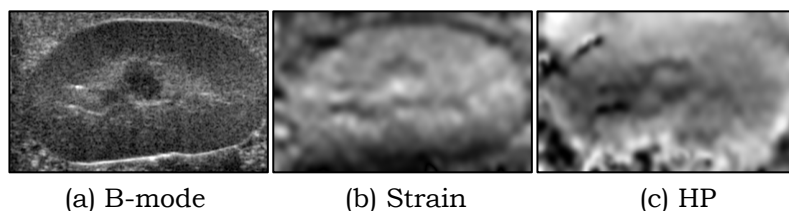(a) B-mode   (b) Strain   (c) HP
Figure 2: Results of *in vitro* experiment for porcine kidney

030   **SHEAR WAVE BEAMFORMING USING THE ACOUSTIC RADIATION FORCE.**
Jeremy Bercoff[1], Mickael Tanter[1]*, Mathias Fink[1].
[1]Laboratoire Ondes et Acoustique, E.S.P.C.I, C.N.R.S. (UMR 7587), Paris, FRANCE.

Using ultrasound focused beams, mechanical sources radiating low-frequency shear waves can be generated inside the body. Such waves propagate inside tissues at a few m/s and are sensitive to the mechanical properties of soft tissues. The ultrafast scanner developed at our laboratory (5000 images/s) is able to generate shear sources and image, in real time, the propagation of the resulting shear waves. Pushing and imaging sequences can be interleaved as desired. This great versatility enables various strategies concerning the pushing sequence. In particular, the supersonic regime, which consists of moving the shear source at a speed higher than shear wave speed, has been introduced in previous works. In this work, a detailed vectorial analysis of the supersonic regime is presented using a 3D Green's function formalism. By varying the speed and the trajectory of the shear source, conical waves of different angles, curved waves, or focused waves can be generated. Furthermore, changing the amplitude of the pushing sequences allows the temporal modulation of the resulting shear waves, leading to a complete control of the spatio-temporal shape of the shear wave. These palpation strategies are carefully studied using numerical simulations and tested on tissue-mimicking phantoms. *In vivo* experiments on breast are also conducted.

036 **VISUALIZTION OF SHEAR WAVE PROPAGATION IN BIOMATERIALS WITH SONOELASTOGRAPHY.**

Zhe C. Wu[1]*, Kevin J. Parker[1].
[1]University of Rochester, Rochester, NY, USA.

Sonoelastography is an ultrasonic technique which estimates local peak vibration amplitude of low amplitude low frequency vibration by analyzing the ultrasound echo spectrum.

Previously, we have reported that sonoelastography is applied to visualize shear wave interference patterns when multiple coherent shear wave sources are present. Moreover, if two shear wave sources with a slight frequency difference are applied simultaneously, the interference patterns appear in the form of a crawling wave, which approximately represents the shear wave propagation in the medium.

In this abstract we propose a novel approach which utilizes only one shear wave source, yet is capable of visualizing the exact shear wave propagation where no approximation is introduced.

In this approach, one shear wave source propagates shear waves into the medium at the frequency w. An ultrasound probe is held above the surface of the medium. The ultrasound probe is vibrated by a vibrator at the frequency w-dw, where dw is much smaller than w. The ultrasound probe is carefully positioned so that there is always a gel filled gap between the probe and the surface of the phantom to make sure the vibration of the probe does not propagate into the phantom (Figure 1).

The total field estimated by the ultrasound scanner is the shear wave propagation relative to the probe vibration:

$$A*exp[2*pi*i\ (f(x) + wt)] - B*exp\ [2*pi*i\ (w-dw)*t] \quad\quad \text{Equation (1)}$$

The amplitude of which is:

$$Sqrt\{ A^2+B^2-2A*B*cos[2*pi*\ (\ f(x)\ +dw*t\ )\ \} \quad\quad \text{Equation (2)}$$

where f(x) is an arbitrary function of spatial variables and A and B are constants.

Apart from a DC shift and an amplitude change, Equation (2) is an exact representation of the shear wave field, only at a different frequency and thus different velocity, which can be visualized by sonoelastography.

The advantage of the approach is that it does not assume any particular type of wave propagation (such as plane wave assumption). This is because the probe vibration is completely temporal dependent and does not interfere with the spatial variation of the shear wave propagation. In addition, this approach requires only one shear wave source, which is more practical in future applications. According to Equation (2), it is advantageous to set A=B to utilize the full dynamic range of the sonoelastography estimator. However, this approach holds for any A, B greater than zero.

Experiments are performed on a homogeneous and a heterogeneous phantom, respectively. One frame of the shear wave propagation video in heterogeneous phantom is depicted in Figure 2. The videos in the format of avi files are available to download at:

http://www.ece.rochester.edu/~wuzhe/research/holo.html

This method provides many of the advantages of MRE, but with the additional advantages of real time visualization of the vibration fields.
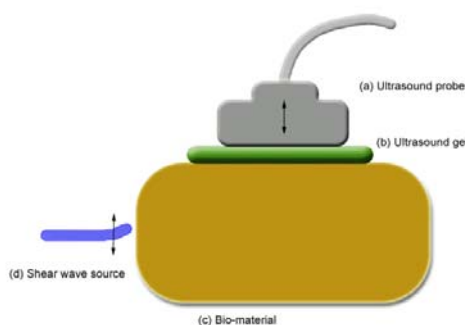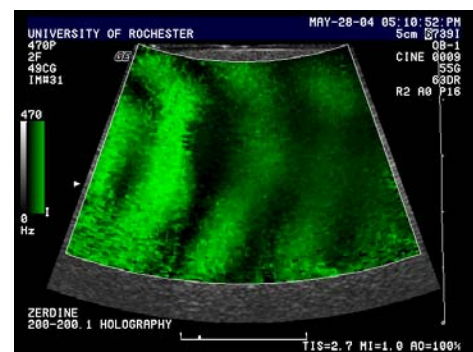

Figure 1

Figure 2

069   A COMPARISON OF METHODS OF SONOELASTOGRAPHY IN MUSCLE.

S Levinson[1]*, ZC Wu[2], KJ Parker[2].

[1]Department of Physical Medicine and Rehabilitation, [2]Department of Electrical and Computer Engineering, University of Rochester, Rochester, NY, USA.

We have had an interest in the imaging of skeletal muscle elasticity that in some of our cases spans more than two decades. The utility of biomechanical analysis of muscle is well-known, however sonoelastography of muscle has in many ways lagged behind the imaging of tissue inhomogeneities and tumor detection. There are many potential reasons for this, but chief among them would seem to be the increased difficulty of imaging a material whose elasticity is changing dynamically. We have explored three different approaches to sonoelastic myography (SMG), all of them based on vibration propagation. The first of these is simple wave propagation in which the phase gradient is used to calculate the speed of sound, from which elasticity can be inferred. This is the simplest approach, however, it is very sensitive to imperfect boundary conditions and guided modes of wave propagation are common. Still, a direct relationship between speed of vibration propagation and muscle tension has been demonstrated during active contraction of the human quadriceps muscle group.

The second approach, dynamic compression, involves the imposition of a plane strain state by applying a vibration along the entire length of the muscle. Young's modulus of elasticity is reconstructed from the induced internal vibrations imaged in cross-section using an iterative forward finite element solution of Navier's equation. This approach to SMG has the advantage of not being dependent on the particular solution of the wave equation, and it is less prone to boundary value problems except when a boundary falls within the region of interest, at which point the reconstruction algorithm becomes unstable. Because the muscles are imaged in cross-section, muscle anisotropy is not a factor, although speckle decorrelation from elevational motion is problematic at higher contraction velocities. The most significant problem with dynamic compression is that a relatively large region of interest is required for elastic modulus reconstruction, resulting in spatial resolutions on the order of a centimeter (1 cm). From the standpoint of quantitative analysis, however, this has been the most promising approach explored thus far and high degrees of correlation between elasticity and measured muscle tension have been observed.

The newest approach to be investigated is the interference technique in which two vibrations of slightly different frequencies are propagated into a muscle in opposite directions, as shown in Figure 1. Amplitude sonoelastography is used to directly image the resulting interference bands, resulting in an image that can be visualized without the need for any type of reconstruction algorithm. Elasticity can be calculated from the spacing of the interference bands using a similar approach to that of the simple wave propagation method. In an alternative approach, the ultrasound transducer itself serves as the second vibrator, as shown in Figure 2. A representative interference SMG is shown in Figure 3. One tremendous potential advantage of the interference technique is that the use of two differing vibration frequencies makes it possible, at least in theory, to compensate for guided modes of propagation. Boundary effects, however, may still be a problem, and we are currently looking into this issue using layered soft tissue phantoms and simulations. Anisotropy may also be an issue if propagation is in a direction parallel to the muscle fibers. Still, the relative simplicity of this method compared to other methods makes it well worth exploring.
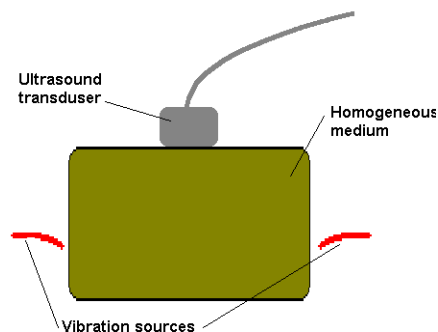

Figure 1: Interference sonoelastography for muscle imaging using 2 shear wave vibration sources.
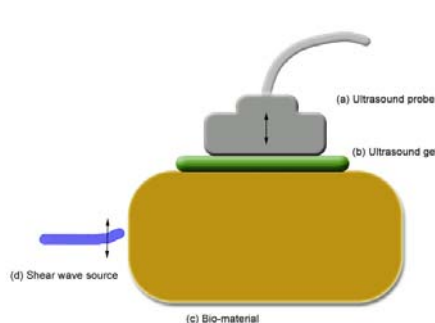

Figure 2: Interference sonoelastography for muscle imaging using a single shear wave vibration source and a vibrating ultrasound transducer
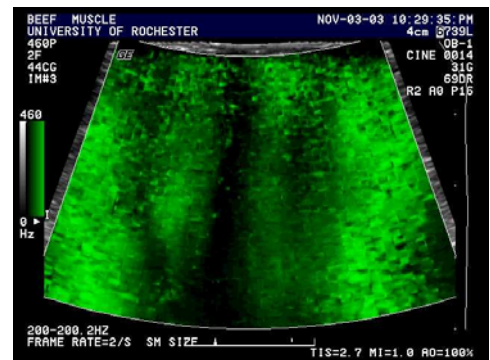

Figure 3: Interference sonoelastograms of a beef muscle specimen. Fringe spacing is indicative of muscle elasticity.

050 **ELASTICITY IMAGING MAY IMPROVE LOCAL PRE–TREATMENT STAGING OF BREAST CANCERS.**

WE Svensson[1]*, TJ Hall[3], Y Zhu[4], J Malin[5], A Rattansingh[1], C Lowery[5], S Shousha[2], D Chopra[1].
Departments of [1]Radiology and [2]Pathology, Charing Cross Hospital, Imperial College School of Medicine, London, England, UK; [3]Medical Physics Dept, University of Wisconsin–Madison, Madison WI, USA; [4]Radiology, University of Kansas Medical Center, Kansas City, KS, USA; [5]Siemens Medical Systems, Ultrasound Group, Issaquah, WA, USA.

Aim: Though breast ultrasound has good sensitivity for the detection of cancerous breast masses, it tends to underestimate extent of disease when used for local tumour staging. Initial results of breast ultrasound elasticity have shown that the area of stiffness is larger than the area of B-mode abnormality which can be used to aid diagnosis. This study shows that the dimensions of stiffness have the potential to provide a better estimation of tumour size than the B-mode image thus improving local tumour staging.

Methods: Data have been used from a breast ultrasound elasticity study set up to prove the utility of breast elasticity ultrasound in the differentiation of benign and malignant pathology. The pathological dimensions of cancers included in the study have been compared with the diameters of B-mode imaging measurements of the tumours and diameters recorded on single plane images of elasticity images. Greatest diameters were compared for each method of measurement.

Results: Forty-eight (48) cancers were reviewed. In ten (10) cases, the maximum B-mode and pathology diameters were larger than the elasticity image frame and the elasticity diameter was the largest achievable filling the image frame. In seventeen (17) cases, the maximum elasticity diameter was larger than the maximum B-mode diameter; six were slightly larger than the maximum pathology diameter. In one (1) case, the maximum diameter was the same for all.

In eighteen (18) of twenty (20) cases, the paired B-mode image diameters were smaller than the elasticity image diameters. In these cases, the maximum elasticity diameter was less than the maximum B-mode and pathology diameters probably because the elasticity images were not obtained in the plane of maximum B-mode/pathology diameters. In two (2) cases, the paired B-mode image diameters were slightly smaller than the elasticity image diameters.

Conclusion: When combined with B-mode imaging, elasticity imaging appears to provide more accurate measurement dimensions of extent of breast cancers than does B-mode on its own. This has important relevance for tumour staging in patients who are suitable for breast conservation surgery or pre surgical chemotherapy.

013   NON–INVASIVE VASCULAR ELASTICITY CAN DETECT VASCULAR DISEASE.

William F. Weitzel[1]*, Kang Kim[1], Jonathan M. Rubin[1], Hua Xie[1], Xunchang Chen[1], Jonathan H. Segal[1], Joseph M Sanchez[1], Nita G. Chopra[1], Matthew O'Donnell[1].
[1]University of Michigan, Ann Arbor, MI, 48109, USA.

Arterial compliance has been related to the presence of cardiovascular disease, peripheral vascular disease, diabetes, renal failure, and aging. Vascular elasticity imaging offers the potential to directly measure intramural arterial wall deformations under conditions that can characterize the complex and non-linear mechanical properties of arteries.

We evaluated a novel method of applying elasticity imaging to assess the mechanical properties of the vascular wall of the brachial artery *in vivo* for 10 subjects, 5 with and 5 without a clinical history of renal failure and vascular disease. The method involves applying ultrasound strain imaging while applying external pressure to equalize the transmural arterial pressure, eliciting the non-linear mechanical properties of the vessel wall. We imaged the brachial arteries and processed the data off line using a correlation-based, phase-sensitive, 2-dimensional speckle-tracking algorithm to calculate the strain and strain rate from the internal displacement of the inner 0.2 millimeters of the artery wall.

Peak percent strain measurements for healthy controls increased from (5.7 +/- 2.8 S.D.) under physiologic conditions to (32.9 +/- 10.2 S.D.) as result of pressure equalization. For diseased subjects strains increased from (2.2 +/- 0.5 S.D.) to (4.9 +/- 1.8 S.D.). The strain rate computed from the accumulated displacements for healthy controls increased from (0.5 Hz +/- 0.3 S.D.) under physiologic conditions to (4.2 Hz +/- 1.2 S.D.) as result of pressure equalization. For diseased subjects strain rates increased from (0.2 Hz +/- 0.1 S.D.) to (0.5 Hz +/- 0.2 S.D.). We further performed an elastic modulus reconstruction for these *in vitro* strain measurements to estimate Young's modulus of the undistended arterial wall. The undistended arterial elastic moduli differed by an order of magnitude between healthy subjects (20.1 kPa +/- 3.7 S.D) and those with vascular disease (181.1 kPa +/- 25.2 S.D.).

These results suggest elasticity imaging may be able to directly measure intramural wall strain allowing for robust, non-invasive characterization of vascular stiffness over a wide dynamic range.
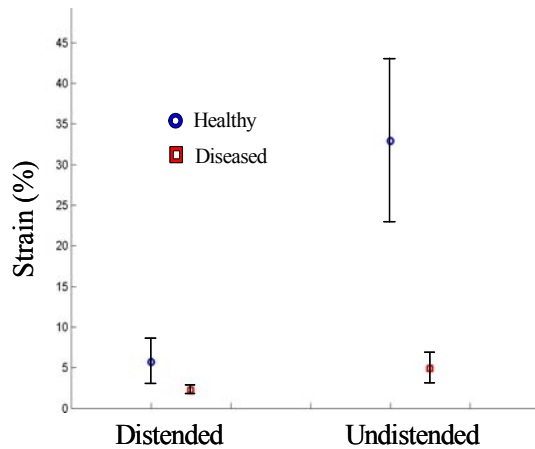
Figure 1: Strain
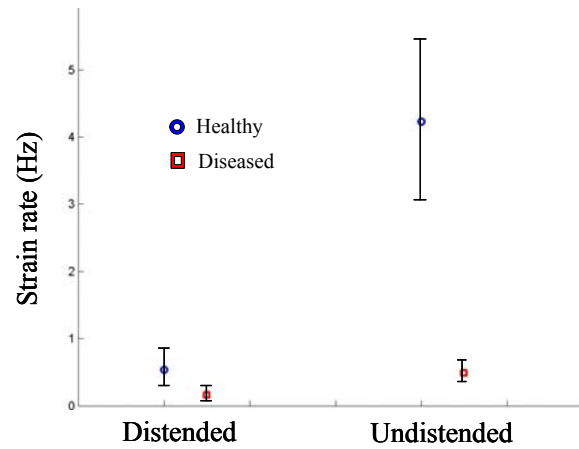
Figure 2: Strain Rate

Strain (Figure 1) and strain rate (Figure 2) comparisons of mean and standard deviations under physiologic pressure (distended) and after pressure equalization (undistended). When the mean arterial pressure is lowered, the arterial pulse pressure can create much larger strain and strain rate (right side of each graph). The elastic nonlinearity of the arterial wall measured under "undistended" conditions shows the dramatic difference in elastic properties of the vessel wall between healthy subjects and those who have a history of vascular disease. Each data point and error bar represents the mean value and standard deviation of each study group of 5 subjects.

014 **ELASTICITY MEASUREMENTS OF INFERIOR VENA CAVA THROMBI IN RATS: CORRELATION WITH ULTRASOUND STRAIN MEASUREMENTS AND THROMBUS AGE.**
JM Rubin[1]*, H Xie[1], K Kim[1], SR Aglyamov[2], S Emelianov[2], X Chen[1], WF Weitzel[1], S Wrobleski[1], D Myers[1], T Wakefield[1], M O'Donnell[1].
[1]University of Michigan, Ann Arbor, MI, USA; [2]University of Texas at Austin, Austin, TX, USA.

Purpose: To correlate the hardness and age of rat inferior vena caval (IVC) thrombi based on strain estimates using ultrasound elasticity imaging with direct measurements of the Young's moduli of *ex-vivo* thrombi.

Materials and Methods: Fourteen 300 gram Sprague-Dawley rats, twelve of which developed thrombi, had their IVCs ligated just below the renal arteries to produce thrombi in the distal portions of the vessel. The rats were subsequently all scanned starting at day 3 post-ligation for up to a week post-ligation. Scanning was performed using a 12 MHz linear array scanhead on a Siemens Elegra (Siemens Ultrasound, Issaquah, WA) ultrasound scanner during continuous, constrained external deformation of each thrombus using the ultrasound scanhead. Strain estimates for the deformation of each thrombus were based on a 2D phase-sensitive speckle tracking algorithm. The strains in the thrombi were normalized to the average strain in the abdomen based on the motion of the spine. On days 3, 6, and 10, at least 4 rats were sacrificed, and their IVC thrombi were removed. The thrombi were then directly deformed *ex-vivo* with a device specially designed to estimate Young's moduli in thrombi (Artann Laboratories, Lambertville, NJ). The device has a piston which applies an external force under computer control on the thrombus, which is resting on an electronic balance.

Results: The hardness ratios of the thrombi based normalized ultrasound strain estimates for days 3, 6, and 10 were 1:2.13:5.84, whereas the Young's modulus estimate ratios were 1:2.34:4.49. The average estimates for Young's moduli for the sampled days were 8.94 ± 3.84 kPa, 21.0 ± 5.10 kPa, and 40.1 ± 9.64 kPa respectively. Estimates of thrombus age with strain over the entire 7 day span demonstrated a precision of ±0.8 days.

Conclusions: It is well accepted that thrombi harden as they age, and earlier research, as well as this study, have shown that ultrasound elasticity imaging can estimate clot hardness accurately enough to estimate the age of rat IVC thrombi to less than a day on average. This study further demonstrates that ultrasound strain estimates of thrombi in rat IVCs correspond extremely well with actual Young's modulus measurements of the same thrombi. Thus, it is reasonable to believe that ultrasound elasticity truly estimates clot hardness and can be expected to lead to a sensitive method for aging deep venous thrombi.

006 APPLICATION OF TRANSIENT ELASTOGRAPHY TO *IN–VIVO* MEASUREMENTS OF LIVER STIFFNESS IN PATIENTS WITH CHRONIC HEPATITIS C.

Laurent Sandrin[1]*, Céline Fournier[1], Victor de Lédinghen[2], Patrick Marcellin[3], Daniel Dhumeaux[4], Michel Beaugrand[5].

[1]Echosens SA, Paris, FRANCE; [2]Haut Lévêque Hospital, Pessac, FRANCE; [3]Beaujon Hospital, Clichy, FRANCE; [4]Henri Mondor Hospital, Créteil, FRANCE; [5]AP-HP, Bondy, FRANCE.

A non-invasive medical device (Fibroscan®) based on one-dimensional transient elastography has been designed to measure liver stiffness. It relies on an ultrasonic transducer (3.5 MHz) mounted on the axis of a vibrator. A low-frequency (50 Hz) and mild amplitude vibration is applied on the skin surface to induce shear waves while the transducer is used in pulsed echo mode to acquire RF lines. Liver stiffness is directly related to shear wave velocity that is derived from the evolution of the tissue strains as a function of time and depth.

Nowadays liver fibrosis is the main reliable predictor of the progression of chronic hepatitis C and is assessed by liver biopsy in order to determine therapy in these patients. However, liver biopsy is an invasive procedure with poor patient acceptance and with respective morbidity and mortality rates of 3% and 0.3%. We investigated the use of liver stiffness measurement in the evaluation of liver fibrosis in patients with chronic hepatitis C.

323 patients with chronic hepatitis C were prospectively enrolled in a multicentre study. Patients underwent liver biopsy and liver stiffness measurements with Fibroscan®. Liver fibrosis stages (F0: no fibrosis, F1: portal fibrosis, F2: few septa, F3: many septa, F4: cirrhosis) were assessed independently on biopsy specimens by 2 pathologists. Efficiency of liver stiffness measurements and optimal cut-off values for fibrosis stage assessment were determined by a receiver-operating characteristics (ROC) curve analysis and cross-validated by the jack-knife method.

Liver stiffness measurements were well correlated with METAVIR fibrosis stage (Kendall correlation coefficient: 0.55, $p < 0.0001$). Diagnosis performances were estimated using the area under ROC curves for the detection of patients requiring treatment ($F \geq 2$) and the screening of patients with cirrhosis ($F = 4$). Area under ROC curves were 0.79 for $F \geq 2$ and 0.97 for $F = 4$. Optimal stiffness cut-off values of 8.7 and 14.5 kPa showed $F \geq 2$ and $F = 4$ with 55 and 84 % sensitivity and 84 and 94 % specificity, respectively.

The non-invasive, rapid and painless assessment of liver stiffness using one-dimensional transient elastography may be used to detect significant fibrosis or cirrhosis in patients with chronic hepatitis C.

011 **REAL–TIME MONITORING OF RADIOFREQUENCY ABLATION IN LIVER WITH ACOUSTIC RADIATION FORCE IMPULSE IMAGING.**

Brian J. Fahey[1]*, Gregg E. Trahey[1].
[1]Duke University, Durham, NC, USA.

The vast majority of patients with liver cancer are not candidates for liver resection, typically due to either the anatomical distribution of the disease or an insufficient hepatic reserve. Radiofrequency ablation (RFA) techniques have thus become an accepted alternative to resection for treatment of both primary and metastatic liver cancers at many institutions. When possible, sonographic methods are typically utilized to guide RFA procedures. If the target mass is not visualized well with ultrasound, CT or CT-based fluoroscopy methods may also be used. Although these methods perform well in aiding ablation electrode placement, they are deficient in real-time monitoring of the growth of the ablated region of tissue during the procedure. The pre-set algorithms used by many ablation systems to control procedures have been demonstrated to create thermal lesions of inconsistent size *in vivo*, and thus an imaging system capable of visualizing RFA lesion development would be an invaluable tool to physicians in determining if the entire cancerous region of tissue has been treated.

Several research groups have investigated novel methods for monitoring RFA treatments *in vivo* with varying degrees of success. These methods include open-magnet MR, elastography, and gray-scale harmonic sonography techniques. Each of these imaging methods have shown improvements relative to B-mode ultrasound and CT-fluoroscopy in imaging ablation sites, but each also has its inherent disadvantages. Perhaps the most significant deficiency of each of these methods is the current inability to monitor RFA lesion growth and development in real-time.

We have developed a method of monitoring thermal lesion growth in real-time during ablation procedures using Acoustic Radiation Force Impulse (ARFI) imaging. ARFI imaging uses short duration (10-300 microsecond) pulses of ultrasound to displace tissue and conventional ultrasonic methods to track the displacements. Previous work in our laboratory [Fahey 2004 a,b] has demonstrated the feasibility of using ARFI imaging to monitor RFA. Adapting this technique to be used at realistic depths (6-12 cm) presents unique challenges in generating sufficient radiation forces to measurably displace these tissues and in characterizing these small (0-3 microns) displacements with low PRF tracking pulses. We have optimized beam sequences and focal configurations in order to achieve RFA monitoring in clinically-realistic circumstances.

RFA experiments have been performed on *ex vivo* bovine livers in a windowed water tank. ARFI images were acquired at one-minute intervals throughout the twelve minute ablation procedure and displayed in real-time on a monitor adjacent to the ultrasound machine. The thermal lesion was displaced less (0 - 1 microns) than adjacent healthy tissue (1.5 – 3 microns), and is visualized well in ARFI images. In addition, ARFI imaging was able to visualize lesion development as it grew larger through time. ARFI images of liver and kidneys of healthy human volunteers will also be presented. Furthermore, plans for upcoming human trials taking place at Duke University Medical Center – both to monitor lesion development in real-time during RFA surgery as well as to evaluate the induced lesion size when patients return for post-procedure follow-up examinations – will be discussed.

References:
[a] Fahey, Brian J., et al. "Acoustic Radiation Force Impulse Imaging of Thermally- and Chemically-Induced Lesions in Soft Tissues: Preliminary *Ex Vivo* Results". Ultrasound in Medicine and Biology 30(3): 321-328, 2004.
[b] Fahey, Brian J., et al. "Acoustic Radiation Force Impulse Imaging of Myocardial Radiofrequency Ablation: Initial *In Vivo* Results". IEEE Transactions on Ultrasonics, Ferroelectronics, and Frequency Control, in review, 2004.

* indicates Presenter

016   HIFU PROSTATE CANCER TREATMENT MONITORING BY ELASTOGRAPHY.

Laura Curiel[1]*, Rémi Souchon[1], Olivier Rouvière[2], Albert Gelet[2], Jean-Yves Chapelon[1].
[1]INSERM U556, Lyon, FRANCE; [2]Hôpital Edouard Herriot, Lyon, FRANCE.

High Intensity Focused Ultrasound (HIFU) provides an efficient alternative for the treatment of localized prostate cancer [1]. Elastography was shown to be able to depict HIFU-induced lesions *in vivo* and may provide an inexpensive alternative for patient follow-up. The objective of the present study was to evaluate the reliability of elastography to predict the thermal lesion extension.

HIFU treatment was performed with the Ablatherm™ machine. The treatment probe was mechanically associated to an imaging probe and covered by a balloon filled with a coupling liquid. After the treatment, multi-compression elastograms were acquired from consecutive RF frames and calculated using a standard cross-correlation algorithm. The imaging probe operated at 5.5 MHz with a return-trip fractional bandwidth of 40%, and performed 8 fps. RF data were acquired during the compression of the prostate by injection of 40-ml coupling liquid.

20 patients were included in the study. In the minutes following the HIFU treatment, elastograms were acquired every 4.4 mm from the base of the prostate to the apex. Four to five days later, gadolinium-enhanced T1-weigthed TSE MRI was performed using the same inter-slice spacing. Two readers were asked to outline the lesion for each elastogram and MRI image. The lesion volume was calculated as the surface within the outline multiplied by the slice width. The reader was also asked to qualify each elastogram as good (score 3), medium (score 2) or illegible (score 1). Images were presented to readers under different codes to avoid association between MR and elastogram images. If the average score for a patient was lower than 2.5 the global elastogram quality was considered too low and the image series was excluded.

Figure 1 shows the volume measured from elastograms vs. MRI measured volume. The correlation coefficient between both series was 0.64 (p = 0.002). The perfect equality curve, shown as a dotted line, illustrates that the volume in elastography was generally underestimated. This may be explained by prostatic edema (visible in MRI) that developed in the days following the treatment. No significant difference was observed between the two readers (Tables 1 and 2). Seven patients were excluded because of low-quality elastograms associated with deficient balloon expansion due to anatomic limitations and/or contact with the therapy probe.

Although a statistically significant trend was found between elastographic and MRI measurements, the dispersion was too large to predict MRI measurements from the elastograms in a single individual. The acquisition system, which in its current form is known to be sub-optimal in terms of frame rate and bandwidth, needs to be improved for the technique to eventually find clinical application.
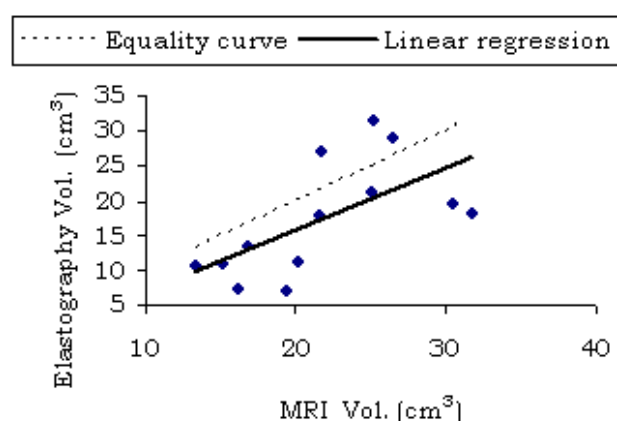

Figure 1:

	Elastogram	MRI
Average (cm³)	1.16	-0.31
St dev. (cm³)	3.26	0.72
t	1.59	1.93
p [19 d.o.f.]	0.13	0.07

Table 1. Difference between readers for measured volumes (20 patients)

Score	1	2	3
R1	64	64	109
R2	73	71	93
χ^2	2.22		
p [4 d.o.f.]	0.69		

Table 2. Number of elastograms vs. score for two readers (R1, R2). The χ^2 test shows no significant difference

Tables 1 & 2:

Reference:
[1] J.Y. Chapelon et al., "Treatment of localized prostate cancer with transrectal high intensity focused ultrasound", Europ J Ultras 1999, 9, 31-38.

---

* indicates Presenter

034   **MECHANICAL BEHAVIOR OF THE HUMAN CERVIX: AN *IN–VIVO* STUDY.**

Edoardo Mazza[1]*, Alessandro Nava[1], Margit Bauer[2], Raimund Winter[2], Gerhard A. Holzapfel[3], Michael Bajka[4].
[1]Department of Mechanical Engineering, Swiss Federal Institute of Technology, 8092 Zürich, SWITZERLAND; [2]Department of Obstetrics and Gynecology, Medical University Graz, 8036 Graz, AUSTRIA; [3]Computational Biomechanics, Graz University of Technology, 8010 Graz, AUSTRIA; [4]Department of Gynecology, University Hospital Zürich, 8091 Zürich, SWITZERLAND.

In the first part of the talk, the tissue aspiration device for *in-vivo* mechanical testing of human organs is presented (Figure 1). The experiments are performed during open surgery under sterile conditions. The technique is based upon the pipette aspiration procedure. The device consists of a tube in which the internal pressure can be controlled according to a desired pressure law. The experiment is performed by (i) gently pushing the tube against the tissue to ensure a good initial contact, (ii) creating a (time variable) vacuum inside the tube so that the tissue is sucked in through the aspiration hole (diameter of 10 mm). A digital camera records the tissue deformation and a pressure sensor measures the applied pressure. A control system guarantees the repeatability of the same loading conditions for all the experiments performed and, therefore, allows a direct comparison of the results obtained in different tests.

From the analysis of the experimental data a hyperelastic viscoplastic constitutive model is determined through iterative finite element calculations. The mechanical behavior is directly related to the tissue's microstructure and depends on the health condition of the tissue. Alterations of the mechanical behavior due to pathologies (for example a tumor or, in the case of a uterus, pre-natal diseases) are detectable so that the device can be applied for diagnostic purposes.

The second part of the talk presents the results of a clinical application. We performed tissue aspiration experiments on human cervices before and after hysterectomy in order to evaluate the reproducibility of the measurements and the applicability in clinical practice. A series of *in-vivo* experiments were performed before vaginal hysterectomy as well as *ex-vivo* one hour after organ extraction (Figure 2). Preconditioning was observed *ex-vivo* and to a lesser extent *in-vivo*. Comparison of the data from *in-vivo* and *ex-vivo* experiments reveals differences in the mechanical response to multi cycle experiments. Statistical data analysis is used for determining the sensitivity of the experimental procedure for detecting changes in the mechanical response of the cervix.

Future perspective: application of the aspiration test on cervices of pregnant women to establish the mechanical properties of normal cervical tissue at different gestational ages. The main purpose will be to determine mechanical parameters defining pathologic conditions, such as preterm cervical softening. In particular, the detection of early cervical changes leading to preterm labor is still an unsolved problem of crucial clinical importance.
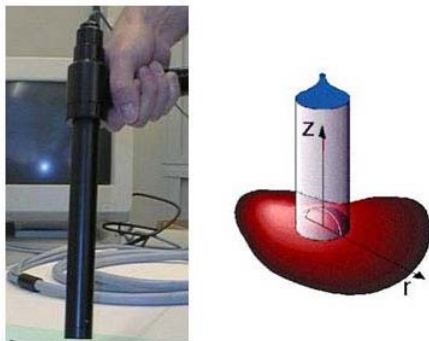

Figure 1: Tissue aspiration device

Figure 2: *Ex-vivo* testing of the human cervix

071 PROSTATE ELASTOGRAPHY: PRELIMINARY *IN VIVO* RESULTS†.

S. Kaisar Alam[1]*, Ernest J. Feleppa[1], Andrew Kalisz[1], Sarayu Ramchandran[1], Ronald D. Ennis[2], Frederic L. Lizzi[1], Cheng-Shie Wuu[2], Jeffrey Ketterling[1].
[1]Riverside Research Institute, New York, NY, USA; [2]New York Columbia Presbyterian Medical Center, New York, NY, USA.

In this paper, we report preliminary results from our investigation of *in vivo* prostate elastography. For the male population in the US, prostate cancer is the most commonly detected cancer, is the second most common lethal cancer and is the leading cancer-killer of men over age 50. Fewer than 50% of all prostate cancers are typically visible in any current clinical imaging modality. Tumors tend to be stiffer than surrounding tissue; thus, physicians routinely use palpation to feel them manually during digital rectal exams. However, manual palpation is of limited use for deep lesions or when elasticity differences are small; it does not provide quantitative information, and its utility depends on physician skill and experience. Thus, elastography, an imaging method based on tissue stiffness, may be potentially very useful in visualizing prostate cancers. Elastography displays a map of strain due to externally applied compression; stiffer regions generally exhibit lower strain in elastograms. Thus, elastography seems ideal for imaging prostate cancer, and already has shown promise in the detection and identification breast cancers.

In our study, digital radio-frequency (RF) ultrasound echo data were acquired from prostate-cancer patients undergoing brachytherapy. We acquired RF data before seed-implantation in some cases, and after implantation in the other cases. Seed placement was guided by a transrectal ultrasound (TRUS) probe, held in a seed-guidance template. In this mechanical fixture, the probe can be moved in XYZ directions and tilted. The mechanical fixture contains detents, enabling the TRUS probe to be introduced into or withdrawn from the rectum in 5-mm steps. We used two approaches to apply compression. In the first approach, the transducer face contacted with the rectal wall, and we applied a compression force to the immediately adjacent prostate using lateral movement and tilt motion to press the TRUS probe against the gland. In the second approach, we used a water-filled (acoustic) coupling balloon to compress the prostate. Increasing the water volume inside the balloon distended it, which applied a compressive force to the rectal wall and deformed the prostate. Scans were in transverse planes, approximately perpendicularly oriented with respect to the urethra. In each scan plane, we acquired RF data from thirteen scans at the scanner frame rate as the deformation force on the rectal wall was continuously increased. We computed strain using RF cross-correlation analysis (1D or 2D) in conjunction with least-squares fitting of the estimated displacement. We are also currently exploring the utility of advanced signal processing methods such as adaptive stretching and non-rigid motion estimation for processing these data.

The compression method based on fixture displacement produced nice (low-noise) elastograms despite a small compression area that caused strain dissipation with depth—dissipation did not prevent applying compression over the entire gland. Balloon-based compression also produced low-noise elastograms that beautifully displayed the prostate architecture and emphasized stiff areas. Initial results demonstrate that most prostate cancers are visible in prostate elastograms, and cancer detectability is significantly higher with prostate elastography compared to conventional B-mode TRUS imaging. Thus, elastography may be very useful in the detection and evaluation of prostate cancers that are occult in conventional imaging modalities.

059   **ABSOLUTE MODULUS IMAGING USING ULTRASONIC FREEHAND SCANNING AND PRESSURE SENSORY DATA.**

Jingfeng Jiang[1]*, Timothy J. Hall[1], Ernest L. Madsen[1].
[1]Department of Medical Physics, University of Wisconsin–Madison, Madison, WI, USA.

The onset of many diseases is accompanied by changes in tissue macrostructure and microstructure that often result in an increase in stiffness. Ultrasonic modulus imaging (UMI), derived from relative displacement of echo signal sources between two echo fields, has the potential for detecting and characterizing tumors. More importantly, the elastic moduli can also be absolute measures of inherent tissue properties that are otherwise unavailable during the pathological evolution of tumors. However, there are several problems that prevent UMI from reaching its full potential. Firstly, many previous methods are only capable of showing the 'relative' modulus distribution. This limitation results in little advantage in UMI over ultrasonic strain imaging which can be performed in real-time and provides the very similar information. Furthermore, many existing UMI methods require complete knowledge of either natural or essential boundary conditions. Obviously, this is a difficult requirement for ultrasonic freehand scanning. An additional challenge limiting the use of ultrasonic freehand scanning is that the natural coordinate system is referenced to the contact surface of the transducer, which is actually mobile, but a fixed coordinate with respect to the reaction force of deformation is needed to simplify the inverse solution.

The objective of this study was to develop a practical method for Young's modulus reconstruction using ultrasonic freehand scanning. The challenges mentioned above may be met by modifying the Kallel-Bertrand (K-B) method (IEEE Trans. on Med. Imag., Vol. 15, pp. 299–313) as follows. First, the original (K-B) formulation was recast in the presence of the acquiring surface pressures using a pressure sensor array mounted on the compression plate. As a result, the absolute modulus can be reconstructed, instead of the relative modulus distribution. However, a simple example demonstrates that the reconstructed Young's modulus distribution may not be unique when only displacement boundary conditions are used. Secondly, a forward finite element analysis program (ANSYS Inc., Pittsburg, PA) was used to systematically convert the surface pressure acquired from the integrated pressure sensor array on the top of the deformed object into the reaction forces on the bottom of the region of interest (ROI) where the displacements were known from a 'speckle tracking' algorithm. Speckle tracking was also used to establish the boundary conditions around the ROI. Then, the estimated displacements within the ROI and the converted reaction forces were utilized to iteratively reconstruct the Young's modulus distribution.

The proposed method is tested with data acquired (Siemens Antares with Ultrasound Research Interface software) from several tissue-mimicking phantoms with hard spherical or cylindrical inclusions embedded within soft backgrounds. The reconstructed modulus distributions match well with the known modulus distributions in phantoms. However, the size of inclusions is usually 10–20% overestimated. The performance of this approach and its limitations will be discussed and compared with other approaches.

046 **ELASTICITY RECONSTRUCTION FROM DISPLACEMENT AND CONFIDENCE MEASURES OF ULTRASOUND IMAGE SEQUENCES.**
Junbo Li[1]*, J. Alison Noble[1].
[1]Department of Engineering Science, University of Oxford, Parks Road, Oxford, OX1 3PJ, England, UK.

Modern ultrasound elasticity imaging techniques provide new opportunities for detection and diagnosis of cancers in the breast, prostate, coronary artery and other sites by assessing the elastic characteristics of soft tissue. Most of these techniques can be classified into the direct or inverse approaches. The inversion elasticity imaging approaches have been widely investigated because of their robustness, while the noisiness of displacement estimates in solving the ill-posed inverse problem has become an impediment to restrict its diagnostic effectiveness, especially for ultrasound images with limited spatial and contrast resolution.

In a recent paper [3], we developed a multi-frame elasticity reconstruction approach that we showed led to a more robust reconstruction solution on simulated data (displacements). In the current paper, we have extended the approach to work on real displacement data. Specifically, a 3-D freehand ultrasound imaging system is employed to deform tissue with certain contact forces at the same time as imaging. A feature-based contrast enhancement approach is applied to the image sequence to enhance the quality of the noisy ultrasound images [1]. Inter-frame displacement distributions over consecutive B-mode images are calculated using Singh's region-based block matching method [2]. Confidence measures of displacement estimation are employed as weighting factors in the objective function solution of the inverse problem. Averaged strain image of the acquired sequence is used as *a priori* knowledge of the tissue relative stiffness distribution to constrain the inverse solution. A finite-element based inverse split-and-merge strategy is applied for elasticity reconstruction [3].

In simulated experiments, the L_2-error between the target and reconstructed Young's modulus is found to be less than 1% for a single inclusion model even with a 5% noise level. Experimental results on a gelatin phantom are also presented. Although multi-frame processing is computationally intensive, the presented method shows promise to give significantly higher accuracy for elasticity imaging than previously reported work. The results are based on a B-mode image sequence. Improvements are expected by using RF data which is the subject of current work.
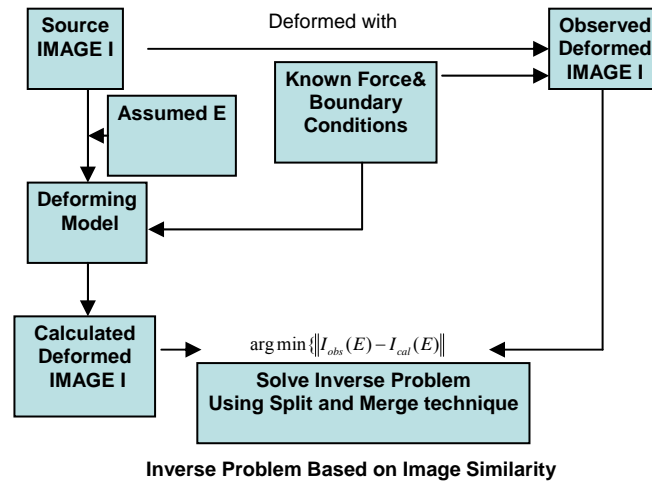
References:
[1] D. Boukerroui, J. A. Noble, M. C. Robini, and J .M. Brady, " Enhancement of Contrast Regions in Sub-Optimal Ultrasound Images with Application to Echocardiography ; Ultrasound in Med. & Biol., vol. 27, pp. 1583-1594, 2001.
[2] A. Singh and P. Allen, "Image-Flow Computation: An estimation - Theoretic Framework and Unified Perspective", CVGIP: IU, vol. 56, no. 2, pp 152-177, 1992.
[3] J. Li, J. A. Noble, L. Han and M. Burcher, "Inversion Elasticity Reconstruction of Soft Tissue Using Split-and-Merge Strategy from Strain Map of Ultrasound Image Sequence", Proc. of the IEEE International Ultrasonics Symposium, Hawaii, USA, 2003.

INVERSE ELASTICITY RECONSTRUCTION BASED ON AN IMAGE SIMILARITY–MEASURE APPROACH.

Junbo Li[1]*, Yaoyao Cui[1], J. Alison Noble[1].
[1]Department of Engineering Science, University of Oxford, Parks Road, Oxford, OX1 3PJ, England, UK.

The commonly used inverse approaches to elasticity imaging compute the elasticity parameters by minimization of the sum of squared differences between measured and calculated DISPLACEMENTS over the entire tissue [1]. However, solving the inverse problem is sensitive to noise. This has been a major factor in limiting the advancement of ultrasound elasticity imaging from laboratory to real clinical use. Recently, a novel approach to elastography was introduced by Miga [2] that attempts to relate the inverse reconstruction problem to the problem of non-rigid image registration. Miga [2] poses the elasticity problem as a minimization of a functional of the square of an image similarity residual involving the Jacobian of the similarity measure with respect to the material distribution E. The approach we have developed is related to this but poses the optimization in a more natural and computationally efficient way.

In this preliminary study, we pose the inverse elasticity problem as a global optimization involving a SIMILARITY MEASURE of ultrasound images. Ultrasound images are acquired before and after deformation. Assuming small deformations, a forward model that simulates the deformation process is defined. An estimated deformation image (deformation transform of the pre-compressed image) is obtained from the forward model with known boundary conditions and pre-set elasticity distribution, which is the optimization variable of the inverse problem. The inverse problem is defined as minimization of the similarities (cross-correlation coefficients in our study) of the observed and calculated deformed image at every block centered at the observing pixels. An iterative split-and-merge approach [3] is employed to solve the problem based on the local mismatch of the calculated and deformed source image.

By converting the displacement-based inverse problem into a similarity-based one, the optimal elasticity distribution is the one that finds the calculated deformed image with the best registration result with the observed deformation image. An obvious advantage of the proposed method is that no displacement calculation is needed. The displacement calculation is actually embodied implicitly in the optimization. Thus there is no displacement measurement error introduced in the solution. The main error sources relate to the validity of the deformation model and accuracy of the observed image itself. Simulation experiments of the method using ultrasound images simulated by Field II package are presented.

$$\arg\min\{\|I_{obs}(E) - I_{cal}(E)\|\}$$

Inverse Problem Based on Image Similarity

References:
[1] F. Kallel and M. Bertrand, "Tissue elasticity reconstruction using linear perturbation method", IEEE Trans. Medical Imaging, vol 15, no. 3, pp. 299-313, 1996.
[2] M. I. Miga, "A new approach to elastography using mutual information and finite element", Phy. Med. Biol., vol. 48, pp. 467-480, 2003.
[3] J. Li, J. A. Noble, L. Han and M. Burcher, "Inversion Elasticity Reconstruction of Soft Tissue Using Split-and-Merge Strategy from Strain Map of Ultrasound Image Sequence", Proc. of the IEEE International Ultrasonics Symposium, Hawaii, USA, 2003.

068   **DIRECT AND ITERATIVE ALGORITHMS FOR INVERSE PROBLEMS IN ELASTOGRAPHY.**

Eunyoung Park[1]*, Antoinette M. Maniatty[1].
[1]Rensselaer Polytechnic Institute, 110 8th Street, Troy, NY, USA.

In elastography, the mechanical response of tissue, for example the displacement field, to a disturbance, such as a pressure or vibration, is recorded. The relationship between the mechanical response and the disturbance is defined by the equations of motion and the constitutive behavior of the tissue. The constitutive behavior, i.e. the relationship between deformation and stress, is closely related to the underlying structure and pathological changes in the tissue. Thus, imaging properties associated with the constitutive behavior are very informative. In this work, the tissue constitutive behavior is approximated as nearly incompressible, isotropic, elastic, and the parameter of interest is the shear modulus, which characterizes the tissue's resistance to shape change.

In the usual forward elasticity problem, the governing partial differential equations consisting of the equations of motion, kinematic relations, and elastic constitutive equation are solved for the displacement field given the boundary conditions and elastic property data. Conversely, elastography can be considered as an inverse problem, since it involves determining the elastic property distribution given the displacement field data. In this work, the finite element method is used to reconstruct the shear modulus field using the full governing equations of elasticity. Two algorithms are explored; one is a direct inversion algorithm and the other is an iterative one. In the direct method, the algorithm is developed to detect the shear modulus field which minimizes the residual of the equation of motion. In the iterative method, the difference between the measured and the calculated displacement is minimized to characterize the shear modulus field. The strengths and weaknesses of each method are explored.

USING ARRIVAL TIMES TO RECOVER SHEAR WAVE SPEED PARAMETERS IN AN ANISOTROPIC MEDIUM.

D Renzi[1]*, J McLaughlin[1].
[1]Rensselaer Polytechnic Institute, 110 8th Street, Troy, NY, USA.

In an isotropic medium, one technique for shear wave speed recovery in transient elastography is level set based inversion of arrival times. Using this technique, one first finds the arrival times of a shear wave using a cross-correlation technique, and then determines the shear wave speed by using level sets of the arrival times to solve the inverse eikonal equation. In many kinds of tissue, especially tissue with fibers like muscle, the wave speed depends quite heavily on direction. In this case, an anisotropic model would be more appropriate. The method described above can only determine the speed orthogonal to the wave front. We will present results on a related technique that uses multiple transient elastography experiments to determine all the parameters that govern the directionally dependant shear wave speed.

080 AN INVERSE PROBLEM: LOCALIZATION OF INSERTS BY CORRELATION BETWEEN FINITE ELEMENT MODELS AND ELASTOGRAMS.

P Trompette[1]*, JY Chapelon[1], R Souchon[1], M Rochette[2], G Duffait[2].
[1]INSERM, U556, Lyon, FRANCE; [2]CADOE, Lyon, FRANCE.

The experimental data are a collection of elastograms which have been obtained from a phantom made of a hollow gelatine cylinder stressed by pressure, in which several stiffness inserts have been introduced. The pressure is applied using a balloon and is not uniformly distributed, and the displacements of the inner cylinder surface are taken as boundary condition (fixed displacements).

In this first attempt the elasticity problem is assumed to be in a plane, which means that the identification of the soft and hard parts take place in the plane of the elastogram only.

The numerical procedure can be divided into several steps which are summarized as follows:

1) At the first iteration, the cylinder is assumed to be homogeneous, and the elasticity problem is solved by the FEM using an adequately refined mesh.
2) The objective function is the sum of the squared difference between the directional experimental and finite element nodal displacements. This function is calculated at each step, and its gradients are obtained by an adjoint state method; the design variables are the shear moduli $G^{(e)}$ of each finite element.
3) The gradient values allow a selection of the finite element candidates to a $G^{(e)}$ value change. In the previous selection auxiliary information originating from the spatial shear energy density distribution and from possible singularities (boundary conditions) are taken in account.
4) A surrogate model is determined using, in the design space, high order derivative calculations and limited intervals of G variations in finite element groups.
5) A genetic algorithm is applied to minimize the objective function in the limited design space defined in Step 4. We update the model with the new G coefficients. The convergence of the inverse problem is controlled by objective function evolution.

The algorithm then returns to Step 2 until convergence is obtained.

This inverse problem procedure takes advantage of very efficient techniques: adjoint and direct derivation, surrogate models using high order derivation and genetic algorithms.

* indicates Presenter

003 **INFLUENCE OF TISSUE VISCOSITY ON WAVE PROPAGATION CHARACTERISTICS IN BOUNDED REGIONS.**

Johannes G.G. Dobbe [1]*, Geert J. Streekstra[1], Jan Strackee[1], Cornelis A. Grimbergen[1].
[1]Academic Medical Center, University of Amsterdam, Meibergdreef 9, Amsterdam, The NETHERLANDS.

Introduction: In elastography, tissue is usually excited harmonically by a low-frequency actuator at the tissue boundary. Imaging techniques, such as motion sensitizing ultrasound or MRI, are used to measure the displacement field of the mechanical wave that propagates through the tissue as a result of the excitation. One can reconstruct tissue mechanical parameters from the displacement field. In many studies, researchers model tissue as being purely elastic. Evaluation of techniques that reconstruct tissue mechanical properties is often performed using gel phantoms, which are mainly elastic and hardly feature viscous properties. Recent studies, however, acknowledge the importance of including the viscoelastic component for accurate description of the wave propagation in tissue. To gain insight into the influence of tissue viscosity on shear wave characteristics, we analyzed wave propagation in a one-dimensional Kelvin-Voigt model.

Methods: We derived an analytical model for wave propagation in a bar of length L that is excited harmonically at one end while fixed at the other end. Wave characteristics such as damping coefficient, location-dependent amplitude and the shear wave settling time following activation of the actuator are expressed in terms of viscoelastic parameters (G' and G''), medium geometry (length L), angular excitation frequency (ω) and density (ρ). With this model, we compare wave characteristics in a gel phantom (near elastic) with those in a pig kidney (viscoelastic) using parameters obtained from the literature.

Results: It appears that all of the investigated wave characteristics (damping, amplitude and settling time) depend on ω, L and viscosity (η). The amplitude on its own is not a reliable measure of tissue elasticity since it highly depends on the combination of G', G'', ρ, L, ω, and measurement location (x) as well. Damping of a shear wave is relatively low in the gel phantom while viscous damping is relatively high in pig kidney. Interferences with reflected waves – that may result in amplification of the wave amplitude – will therefore be observed in gel phantoms while viscous damping reduces this effect in real tissue like pig kidney.

Initiation of the actuator causes a transient effect of the shear wave that contains low-frequency components. These low frequencies experience a reduced viscous damping compared to the actual excitation frequency. This introduces a disturbance of the displacement field that may last for many seconds in gel phantoms and up to tenths of seconds in pig kidney.

Conclusions: Viscous damping may be low in gel phantoms but is relatively high in tissue such as pig kidney. Elastography systems may therefore perform quite differently when measuring gel phantoms compared to measuring tissue samples. Wave amplitude poorly represents tissue elasticity since it depends on viscosity, geometry, location and frequency as well. The shear wave settling time that is the result of initiating excitation may be quite high in gel material and must be taken into account before acquiring the displacement field in elastography.
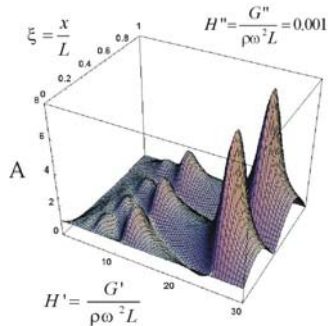

Figure 1: Location (x/L) -dependent amplitude (A) vs. dimensionless elastic (H') and viscous (H'') parameters for near elastic media. G' and G'': complex shear modulus, L: medium length, x: location, ω: angular frequency, ρ: density.
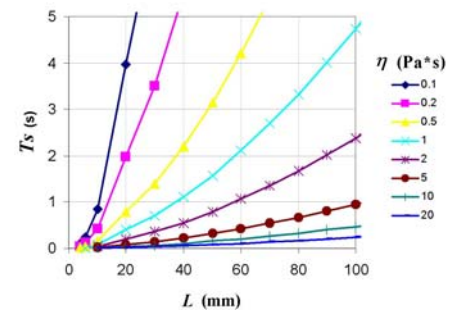

Figure 2: Shear wave settling time Ts at different viscosities calculated halfway a viscoelastic bar of length L with a shear wave elasticity of 10 kPa at an excitation frequency of 100 Hz.

009 **PLANE–WAVE DECOMPOSITION FOR AN EXACT RECONSTRUCTION OF TRANSVERSAL ISOTROPIC PROPERTIES IN STEADY–STATE DYNAMIC ELASTOGRAPHY.**

Ralph Sinkus[1]*, Mickael Tanter[2], Tanja Xydeas[3] and Mathias Fink[2].

[1]Philips Research, Hamburg, GERMANY; [2]Laboratoire Ondes et Acousticque, ESPCI, Paris, FRANCE; [3]University Tuebingen, Radiology, Tuebingen, GERMANY.

One of the main current aims of Elastography is to improve specificity in the differential diagnosis between benign and malignant tumors. The measurement of potential anisotropic viscoelastic properties of a tumor might provide additional insight in the tumor pathology. Assessment of anisotropic properties (here transversally isotropic) in steady-state is limited by the fact, that each location inside the object experiences waves from all directions with different weights. This leads to a bias, because exact reconstruction is only feasible for shear waves propagating orthogonally with respect to the local direction of the fiber, while shear waves propagating parallel to the fiber direction do not "feel" the anisotropy. We present a technique overcoming this limitation and thereby providing the capability of reconstructing unbiased transversally isotropic elastic properties in steady-state Elastography.

MRI (as well as US) allows assessing the 3D complex-valued displacement field $\vec{u}(\vec{x},t) = \vec{A}\cos(\omega t + \vec{\varphi})$ in steady-state dynamic Elastography [1]. Thus, reconstruction of viscoelastic properties turns into a local inversion of the partial differential equation (PDE) describing the propagation of the mechanical wave in the medium. Certainly, boundary effects influence the local properties of the displacement field, but inversion remains a local operation. *In-vivo* measurements require a longitudinal mode of mechanical excitation to efficiently transport the energy into the entire organ (for instance the breast or the liver). Mode conversion at heterogeneities and boundaries leads to the presence of shear waves, which are the source of information for reconstructing viscoelastic properties. Contributions of the compressional wave within the measured displacement field are removed via the so-called Helmholtz-Hodge decomposition, which utilizes the fact that the shear wave is divergence-free, while the compressional wave is curl-free [2]. Assuming compressional isotropy, the underlying PDE reads as follows:

$$-\rho\omega^2\vec{u}^T = \mu_\perp\nabla^2\vec{u}^T + \tau\begin{pmatrix} \partial_z^2 u_x^T + \partial_{xz}^2 u_z^T \\ \partial_z^2 u_y^T + \partial_{yz}^2 u_z^T \\ \nabla^2 u_z^T \end{pmatrix} + i\varsigma\omega\nabla^2\vec{u}^T, \qquad \text{Equation (1)}$$

with $\vec{u}^T$ the transversal component of the displacement vector, $\mu_\perp$ the shear modulus orthogonal to the local direction of the fiber, τ the anisotropy with $\mu_\parallel = \mu_\perp + \tau$ ($\mu_\parallel$ the shear modulus parallel to the fiber and $\tau \geq 0$) and ς the shear viscosity. Given $\vec{u}^T$, the values for $\mu_\perp, \tau$ and ς can be found analytically by minimizing the quadratic error between left-hand and right-hand side of Equation (1) at two different points in time (preferably $t = 0$ and $t = \pi/(2\omega)$). The direction of the fiber can be found by rotating $\vec{u}^T$ locally (and its spatial derivatives) and exhaustive minimum search of the quadratic error as a function of the two Euler angles (Θ, Φ), which determine the rotation. It is obvious from Equation (1), that a plane wave propagating in z-direction is not capable of differentiating $\mu_\perp$ and $\mu_\parallel$ (mind, that for this particular case $u_z^T = 0$). In such a case, reconstruction yields $\mu_\perp^{recon} = \mu_\perp + \tau$ and $\tau^{recon} = 0$. The longitudinal mode of excitation ensures that all modes are excited inside a "chaotic" cavity, which the breast can certainly be considered to be [3]. Therefore, the displacement field $\vec{u}^T$ is Fourier-transformed locally, filtered in Fourier-domain to select the plane-wave contribution of a specific direction $\hat{n}$, back-transformed and fed into the reconstruction. This yields a set of viscoelastic parameters for a certain selected direction of propagation $\hat{n}$, i.e. $\mu_\perp^{recon,\hat{n}}, \tau^{recon,\hat{n}}, \varsigma^{recon,\hat{n}}$ and $\Theta^{recon,\hat{n}}, \Phi^{recon,\hat{n}}$. All directions $\hat{n}$ are now tested consecutively. The "correct" set of parameters is identified as the one with minimal shear modulus $\mu_\perp^{recon,\hat{n}}$ and maximum anisotropy $\tau^{recon,\hat{n}}$. Results are presented for simulations, phantoms, beef muscle, *in-vivo* breast cancer as well as *in-vivo* benign breast lesions. The reconstructed parameters from breast lesions are related to that information obtained from contrast-enhanced breast MR-Mammography utilizing Gadolinium.

References:
[1] Sinkus et. al, Physics Medicine Biology **45** (2), 1649-1664 (2000)
[2] L.D. Landau and E.M. Lifschitz, Theory of Elasticity, Butterworth-Heinemann (1986)
[3] C. Draeger and M. Fink, J. Acoust. Soc. Am. **105** (2), Pt. 1, 611-617 (1999)

* indicates Presenter

056   A NEW ANIMAL MODEL FOR *IN VIVO* ELASTOGRAPHY.

K Hoyt[1,2]*, F Forsberg[2], CRB Merritt[2], JB Liu[2], TA Krouskop[3], J Ophir[4].
[1]Drexel University, Philadelphia, PA, USA; [2]Thomas Jefferson University, Philadelphia, PA, USA; [3]Baylor College of Medicine, Houston, TX, USA; [4]The University of Texas Medical School, Houston, TX, USA.

The main purpose of this study was to evaluate ethanol for inducing stiff isoechoic lesions *in vivo* and to investigate corresponding elastograms and gross pathology for lesion reproducibility. Stiff hepatic lesions were created in 7 swine by ethanol injection (0.33-2.0 ml) at depths of 10 to 25 mm. A modified HDI 1000 scanner (Philips Medical Systems, Bothell, WA, USA) with a 7.5 MHz linear array was used (either in automated or freehand mode), directly on the surgically exposed surface of the liver with respiration suspended. Axial displacements were obtained using the cross-correlation between pre- and post-compressed RF echo sequences. Elastograms were generated as the gradient of the displacement estimates for each A-Line. Multiple regression was performed against swine, ethanol dose, induced lesion depth, and acquisition technique. Additionally, linear regression was used for varying doses at constant depth (and vice versa). Automated and freehand results were compared with t-tests. Elastographic lesion sizes were compared to corresponding gross pathology.

The elastograms characterized lesions as being areas harder than the surrounding soft hepatic tissue while being invisible in the corresponding sonogram (Fig. 1). Elastographic lesion sizes and the corresponding injected ethanol dose used to induce the lesions correlated (p = 0.029) when analyzed using linear regression analysis. Additionally, lesion depth was shown to be not statistically significant ($p > 0.10$) when regressed against elastographic lesion size. An analysis of elastographic and gross pathology lesion sizes indicated no correlation (p = 0.973). Subsequently, lesion types were sorted by size and regression lines were computed from quasi-linear regions of the corresponding run charts. Trend lines indicate a 4-to-3 size relationship between the selected elastographic and pathological lesion sizes. To investigate this observation further, modulus measurements from thin pathological samples (stiff lesions and surrounding soft tissue) were obtained using a nanoindenter (Testworks Inc, Nashville, TN, USA). The resultant modulus images were correlated to elastographic images. Experimental results from these comparisons are currently ongoing and results will be presented.

In conclusion, ethanol induced lesions are reproducible across subjects. These swine studies validate the feasibility of using ethanol lesions for *in vivo* elastographic testing.
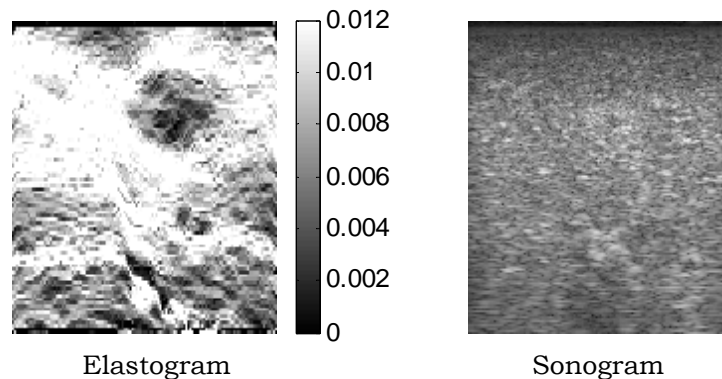

Elastogram   Sonogram

Figure 1: *In vivo* elastogram (left) and sonogram (right) of an induced hepatic lesion (1.0 mL ethanol dose injected at a depth of 12 mm). Dark regions in the elastogram indicate stiff tissue as compared to the soft background.

* indicates Presenter

035 **STRAIN PROCESSING OF INTRAOPERATIVE ULTRASOUND IMAGES OF BRAIN TUMOURS.**

Jon Bang[1]*, Tormod Selbekk[1], Geirmund Unsgård[2].
[1]SINTEF Health Research, Trondheim, NORWAY; [2]St. Olav's Hospital, Dept. of Neurosurgery, Trondheim, NORWAY.

Background:
Conventional B-mode ultrasound (US) imaging is established in brain surgery, and may discriminate solid tumours from normal brain tissue. The purpose of this work was to investigate whether strain processing of US radio-frequency (RF) data can provide additional information that might be useful to the surgeon.

Method:
We acquired RF data with a flat-linear-array (FLA) probe during surgery of a low-grade astrocytoma and a metastasis. This was done before start of the resection. The probe was held in a fixed position while collecting image sequences over 1.5-2 cardiac cycles. These sequences were transferred to a computer for off-line processing by a prototype program. We used a phase-sensitive cross-correlation technique to calculate the radial displacements between consecutive US frames. From these displacements, we obtained the local radial strain by differentiation. We also tested several post-processing options, which were implemented for the purpose of enhanced tumour detection and visualization.

Results:
The results show that the strain varies periodically during the acquisition time, in excellent correspondence with the simultaneously acquired ECG signal. Movements induced by moving the probe manually, however, typically gave radial displacements that were too large or too rapid for proper processing. Contours derived from the strain images show reasonable correspondence with the tissue structures apparent in the B-mode images (Figure 1).

Conclusions:
We conclude that strain imaging of brain tumours is feasible, and that the inherent blood pulsation of the brain arteries provides the necessary movement of the brain parenchyma for successful strain calculation. By differentiating between regions with different elastic properties, the strain processing may help delineating the tumour boundaries. Our ultimate goal is to develop the technique into an intraoperative imaging modality.

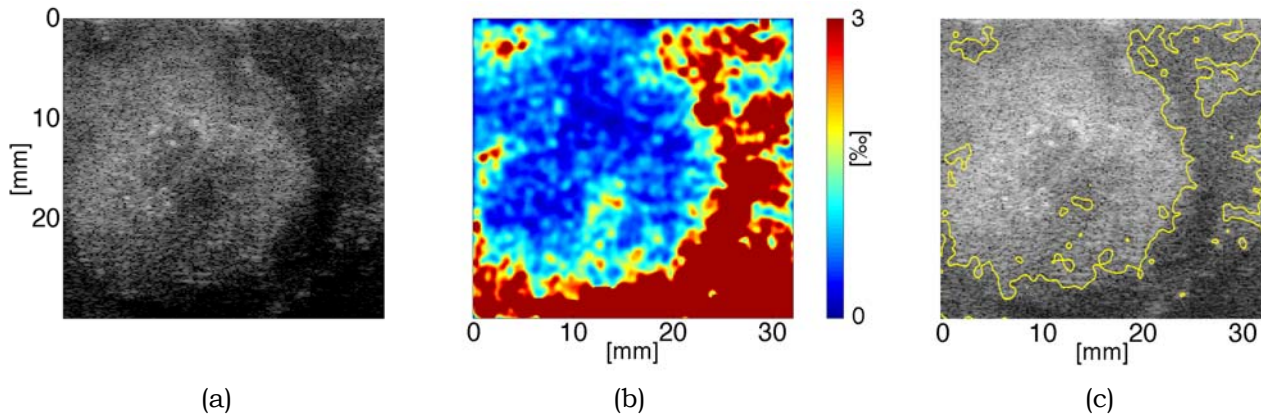(a)   (b)   (c)

Figure 1: Example of strain processing of a brain tumour (metastasis). (a) B-mode image; (b) rectified and smoothed strain results, showing low strain magnitude inside the tumour area and higher strain magnitude outside; (c) the B-mode image overlaid contours at constant strain level derived from (b).

060   INTRA–OPERATIVE ULTRASOUND ELASTOGRAPHY AND REGISTERED MAGNETIC RESONANCE IMAGING OF BRAIN TUMOURS; A FEASIBILITY STUDY.

A Chakraborty[1]*, J Bamber[2], G Berry[2], N Bush[2], N Dorward[1].
[1]Royal Free & University College Hospital Medical School, London, England, UK; [2]Institute of Cancer Research and Royal Marsden NHS Trust, Downs Rd., Sutton, Surrey, SM2 5PT, England, UK.

Brain tumour resection is usually assisted by palpation to gain appreciation of the contrast in mechanical properties of brain to tumour. Ultrasound elastography has potential to improve this process by imaging such properties, possibly quantitatively. At the time of writing, two cases have been evaluated where the aim was to assess the feasibility of using freehand ultrasound elastography intra-operatively to assist brain tumour resection. A "neuro-navigation" system that permits registration between the ultrasound elastogram and a 3D pre-operative magnetic resonance image (MRI) was also evaluated. These two cases contributed valuable preliminary findings that we wish to report, but case acquisition is ongoing and substantially more experience should have been gained by the time this paper is presented.

Ultrasound elastograms of the brain were created using equipment and software similar to that described previously (Doyley et al [1]); radio frequency echo data, from an Acuson™ 128XP scanner, were digitized during freehand palpation of the brain surface with a 7.5 MHz probe in a sterilized rubber sheath, following removal of the appropriate part of skull and dura. The StealthStation™ neuro-navigation system (Medtronic, USA) co-registered the ultrasound plane during palpation onto a pre-operative 3D MRI dataset, and re-sampled the MR image in the plane corresponding to that imaged elastographically. Surface landmarks on the patient provided co-registration between pre-operative MRI and patient cranial anatomy.

Accuracy of co-registration of ultrasound and elastographic images with the MR image data was judged subjectively by comparing structures that appeared on both ultrasound and MRI. An important question concerning feasibility was whether a useful strain distribution could be generated by displacing the brain surface, given that the nearest rigid boundary (the contralateral inner skull) is relatively distant and that fluid-filled ventricles are nearby. This was evaluated from the visual appearance of the strain images but, also, the process of generating strain by ultrasound probe motion was simulated using finite element methods (FEM) and a model consisting of the co-registered MRI data segmented into skull, brain, dura, tumour and ventricle (Young's modulus data were taken from Guillaumme et al [2]). Finally, the brain-to-tumour strain contrast and the visibility of the boundary at the brain-tumour interface were compared, for various applied displacements, to subjective impressions of relative stiffness and adhesion during surgery.

We observed good correspondence between the MR re-sampled images and both the ultrasound and elastographic images, with no requirement to warp image data. Boundaries at tumour margins were best visualized by applying relatively large displacements whereas strain contrast between brain and tumour was most visible at small displacements. Results from the comparison with surgical findings will be apparent when more cases have been studied. The FEM simulation showed that the dura may act as a partially fixed boundary when in the scan field and thus can increase the amount of strain seen for a given displacement.

Intra-operative freehand elastography during brain tumour resection is feasible and may help tumour resection by identifying the biomechanical properties of the tumour and brain-tumour interface. Problems with image interpretation may be overcome by using co-registered MRI neuro-navigation.

References:
[1] Doyley MM, Bamber JC, Fuechsel F, Bush NL (2001). Ultrasound Med Biol; 27: 1347-1357.
[2] Guillaumme A, Osmont D, Gaffe D, Sarron JC, Wuandieu P. (1997) J Biomech; 30: 383-389.

023   **PRELIMINARY EVALUATION OF BREAST DISEASE DIAGNOSIS BASED ON REAL–TIME ELASTICITY IMAGING.**

Takeshi Matsumura[1]*, Satoshi Tamano[1], Ryuichi Shinomura[1], Tsuyoshi Mitake[1], Makoto Yamakawa[2], Tsuyoshi Shiina[2], Ako Itoh[3], Ei Ueno[4].

[1]Research & Development Center, Hitachi Medical Corporation, Chiba, JAPAN; [2]Institute of Information Sciences & Electronics, University of Tsukuba, Tsukuba, JAPAN; [3]Hitachi General Hospital, Ibaraki, JAPAN; [4]Institute of Clinical Medicine, University of Tsukuba, Tsukuba, JAPAN.

It is known that lesions, such as cancer, tend to become harder as the disease progresses. Our group has previously reported that our real-time elasticity imaging system was developed and applied clinically to breast tissue diagnosis where cancers may be displayed as hard tissue.

In this paper, we report the state of our intensive assessments of breast tissue diagnosis and discuss the effects of post-processing algorithms on the clinical usefulness of the elasticity imaging system.

Our system consists of a modified commercial ultrasound scanner with a 7.5 MHz linear array transducer and a PC with dual 2.8 GHz processors, where our strain imaging algorithm (which we call the "Extended Combined Autocorrelation Method") is implemented at 12 frames/s by a highly optimized special task division between the processors.

Through free-hand compression of the body, the echo signals are captured sequentially and using nearest-neighbor RF frames, differences of envelope peak and carrier phase shift are calculated to get the tissue displacement in response to the deformation. Then, tissue strain is color-coded according to its magnitude and translucently super-imposed on the conventional black and white sonogram for easy and fast comparison of the local anatomical position between the strain image and the B-mode image.

For the purpose of higher stability of disease diagnosis based on elasticity images, we tried to implement several post-processing techniques such as
  (1) frame-to-frame smoothing,
  (2) adaptive contrast optimization,
  (3) noise-frame rejection, and
  (4) noise-region reduction (i.e., tissue-region extraction).
In this study those imaging procedures have been studied in relation to each other.

Our system was clinically assessed using 137 patients with breast diseases (76 benign lesions, and 61 malignant lesions). Based on the imaging pattern of the low-strain region inside the lesion that is observed as hypoechoic region in the B-mode image, we introduced 5 grades of elasticity score ranging from 1 (no strain-zero brightness region; benign) to 5 (broader strain-zero brightness region; malignant). The scoring method was applied to all of the lesions, and its diagnostic capability was statistically evaluated as follows:
  (1) The statistically classified group of malignant lesions had the mean score of 4.26 (S.D. = ±0.89) and was significantly separated (p<0.001) from the group of benign lesions, whose mean score was 1.88 (S.D. = ±0.99).
  (2) The elasticity scoring method provided a sensitivity of 86.9%, a specificity of 92.1%, and an accuracy of 89.8%. The details of the elasticity scoring method will be discussed.

In conclusion, due to the post-processing techniques aiming at stable imaging observation, reproducible diagnosis based on elasticity imaging has been realized. Furthermore, we confirmed that our preliminary clinical results derived from the elasticity scoring method represent a promising feature for diagnostic capability.

040   **NEW ELASTOGRAPHIC ALGORITHM FOR *IN–VIVO* STUDY OF THE MECHANICAL BEHAVIOR OF SKIN.**

Yassine Mofid[1]*, Frédéric Ossant[1,3], Claud Imberdis[2], Frédéric Patat[1].
[1]LUSSI, Tours, FRANCE; [2]LMARC, Besançon, FRANCE; [3]University Hospital, Tours, FRANCE.

The aim of this study was to show the value of high-frequency elastography for the *in-vivo* study of the mechanical behavior of skin, which is affected in many human diseases. Our 20MHz real time scanner (DERMCUP 2020™, 256 RF lines per image, 6 mm in width and 8 mm in depth) was combined with a device called an *Extensiometre,* developed by the LMARC laboratory, for *in-vivo* skin creep and relaxation tests [Patent N° FR03/09220]. The latter device permits the application of a stretching stress in the plane of the skin.

We propose a new algorithm called FSSE (Filtered and Staggered Strain Estimation) which is able to improve SNRe without using the temporal pre-stretching. The global stretching was not applicable for complex deformations as we found in the skin because of the presence of both stretched and compressed areas in this tissue.

Using a simulation study (imaging system simulation was similar to the DERMCUP 2020™), we compared elastograms, produced with FSSE, SSE (Staggered Strain Estimation) and CSE (Conventional Strain Estimation – classical method with global stretching) [1] methods without including global stretching, of single and multi-inclusion models. From the point of view of SNRe, CNRe, axial and lateral resolution analysis, FSSE demonstrated the best performance.

In addition, we propose a fast process used for overcoming the restriction due to the step between two adjacent RF A-lines and thus improving the lateral resolution of the estimated lateral displacement images.

In-vivo experiments were conducted with the *Extensiometre* device on several sites of healthy human skin. We used RF sequences of the real time scanner (10 RF images/s) to evaluate axial deformation and lateral displacement with cumulating small deformation steps (up to 10 steps), which allowed measurement up to 20% of local strain in the dermis with a correlation coefficient > 0.9. Good correlation coefficients (ρ>0.8) were obtained in the same way, for axial and lateral displacement of subcutaneous fat (hypodermis): e.g. for the forearm external face, about +6% of axial strain occurred in the dermis with 2mm of stretching and $\pm$60μm maximum symmetrical lateral retraction in the dermis and -60μm in hypodermis. For the forearm lateral face, about +10% axial strain occurred in the dermis and -10% in the hypodermis for 4 mm of stretching. Lateral displacement was $\pm$0.4 mm in the dermis, -0.4 mm in the hypodermis and +0.4 mm in subcutaneous structures (muscle). The dermis has an original mechanical behavior since its thickness increased in the image plane during the creep test. The behavior of the hypodermis depends strongly on the displacement of the dermis and less significantly of surrounding tissues. These *in-vivo* results show the potential of elastography for the study of the mechanical behavior of healthy and diseased skin.

RF Image of Human Forearm

Lateral Displacement   Axial strain image

In-vivo FSSE results
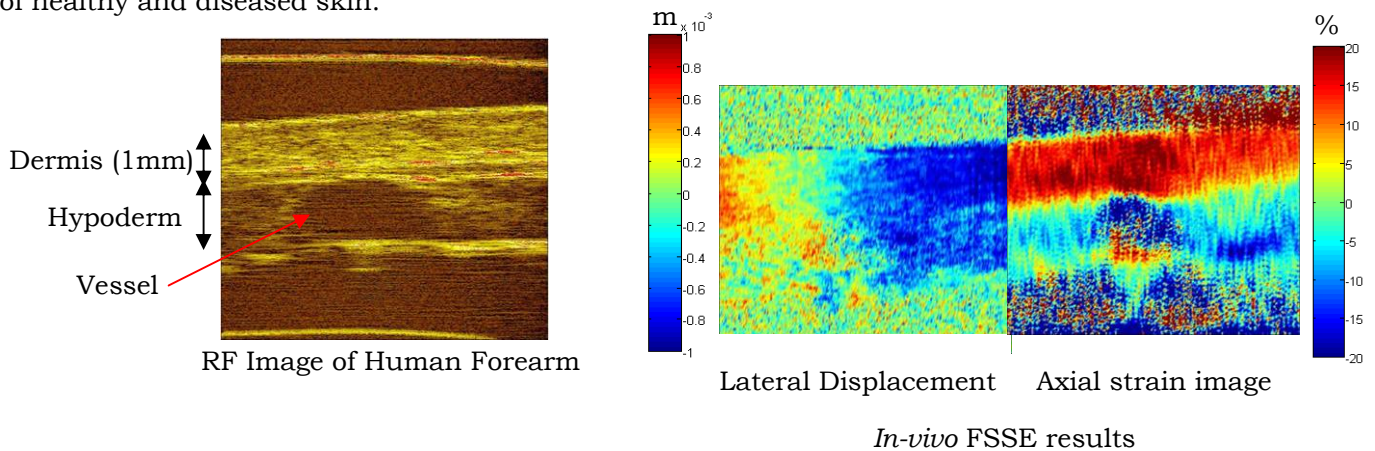
Reference:
[1] S. Srinivasan, J. Ophir, and S. K. Alam, Elastographic Imaging Using Staggered Strain Estimates. Ultrasound Imaging, 2002. 24: p. 229-245.

054   **ON THE TRANSVERSE ANISOTROPY OF HUMAN AND BOVINE CALCIFIED TISSUES.**

JL Katz[1]*, J Kinney[2], P Spencer[1], Y Wang[1], B Fricke[1], M Walker[1], L Friis[3], M Tabib-Azar[4].
[1]UMKC–Center for Research on Interfacial Structure and Properties (UMKC–CRISP), Department of Oral Biology, School of Dentistry and Division of Civil & Mechanical Engineering, School of Computing & Engineering, University of Missouri–Kansas City, Kansas City, MO, USA; [2]Division of Biomaterials and Bioengineering, Department of Preventative and Restorative Dental Sciences, University of California–San Francisco, San Francisco, CA, USA; [3]Department of Mechanical Engineering, University of Kansas, Lawrence, KS, USA; [4]Department of Electrical & Systems Engineering, Case School of Engineering, Case Western Reserve University, Cleveland, OH, USA.

In 1987, Katz and Meunier (1987) published their adaptation of the calculation of the scalar compressive and shear anisotropy factors for single crystal refractory compounds put forth by Chung and Buessem (1968) to calcified tissues. The two scalar anisotropy factors were determined using literature data for a number of ultrasonic measurements of both human and bovine calcified tissues based on transverse isotropic symmetry. Recently, Kinney, et al. (2004) published a study in which they determined the five transverse isotropic elastic constants for both wet and dry human dentin using resonant ultrasound spectroscopy. In 1972, Lees and Rollins modeled wet bovine enamel and dentin as having transverse isotropy elastic based on their limited ultrasonic wave propagation measurements and modeling of related data in the literature. The scalar compressive and shear anisotropy factors have been calculated from both the Kinney et al. and Lees and Rollins sets of data and are compared with a representative set of scalar anisotropy factors from those published previously in 1987 and 1990 by Katz and Meunier for both human and bovine cortical bone. Of note, is that these calculations indicate that dry human dentin is isotropic. This conclusion is supported by Kinney et al. (2001) in a small angle x-ray scattering study of human dentin that indicated that the mineralized collagen fibers were isotropic near the pulp. Also, the scalar anisotropy calculations based on ultrasonic measurements of the transverse isotropic elastic constants for all four aspects of a human femur along its length, Van Buskirk and Ashman (1981), shows that there are significant differences in the shear anisotropy for the anterior aspect, and in the compressive anisotropy for the posterior aspect, relative to the other aspects. In addition, the calculations indicate when the measurements and/or modeling of the transverse isotropic elastic constants for calcified tissues contain artifacts.

Relevant Papers:
Katz JL, Meunier A. The Elastic Anisotropy of Bone. J. Biomech. 20: 1063-1070, 1987.
Katz JL, Meunier A. A Generalized Method for Characterizing Elastic Anisotropy in Solid Living Tissues. J. Mat. Sci.: Mat. in Med. 1: 1-8, 1990.

ANALYSIS OF BLOOD CLOT FORMATION USING TRANSIENT ELASTOGRAPHY.

Jean-Luc Gennisson[1]*, Sophie Lerouge[2] and Guy Cloutier[1].
[1]Laboratory of Biorheology and Medical Ultrasonics, [2]Laboratory of Vascular Biomaterials, University of Montréal Hospital, Pavilion J.A de Sève (room Y-1619), 2099 Alexandre de Sève, Montréal, Québec, H2L 2W5, CANADA.

Blood coagulation process can be beneficial when it serves to prevent hemorrhage from causing tissue damage. However, inappropriate blood coagulation might induce some cardiovascular diseases, like stroke or deep vein thrombosis. Determining the mechanical properties of blood clot may be useful to understand these pathologies and to determine the appropriate treatment. In the last few years, transient elastography has shown its efficiency to map the viscoelastic, anisotropic and non-linear properties of soft biological tissues *in vitro* and *in vivo*. In this study, transient elastography is used to observe and to recover the viscoelastic shear properties of blood clot formation during coagulation.

The 1D shear elasticity probe, composed of a single element 10 MHz ultrasonic transducer mounted on a vibrator, was applied at the surface of blood samples. The shear waves were generated at 100 Hz by the front face of the transducer and 300 RF lines were recorded at 2 kHz frequency rate. From a cross-correlation algorithm between successive ultrasonic signals stored in memory, the longitudinal component of the displacements along the ultrasonic beam was computed. The experiments were performed on 60 ml of pig blood samples anticoagulated with EDTA. The coagulation was initiated *in vitro* at a later time by adding an excess of calcium ions (0.05 g/ml).

From the displacement field, the blood biomechanical properties were recovered during coagulation (150 min) in terms of shear wave speed (V_s) and attenuation (α_s). These measurements also allowed characterization of the process in terms of elasticity (μ_B) and viscosity (η_B) as a function of time (Figure 1). As the shear waves do not propagate in fluids, the parameter assessments became relevant at a precise time t_g = 19 min (when the liquid blood became solid). At the sol-gel transition time t_g, it was found that μ_B = 315.11 Pa and η_B = 0.01 Pa.s. The elasticity and the viscosity evolved as a time power-law and reached a steady state. At the plateau (the last 60 min), the blood clot was mechanically stable (μ_B = 934.79 ± 39.89 Pa and η_B = 1.72 ± 0.07 Pa.s).

The kinetic of blood clot formation was also studied on blood samples modified with the addition of anti-coagulant (heparin), pro-coagulant (thrombin) or fibrinolytic (plasminogen tissue activator) drugs. In these cases, the blood clot behavior in terms of elasticity and viscosity as a function of time was modified. The time t_g also changed due to the coagulation acceleration or deceleration induced by the drugs.

In summary, we showed that transient elastography is able to characterize the mechanical properties of a forming blood clot. This might help for vascular disease diagnosis and reveal new information about the coagulation process. Moreover, by operating non-invasively, this method could provide an *in vivo* evaluation of thrombus formation.
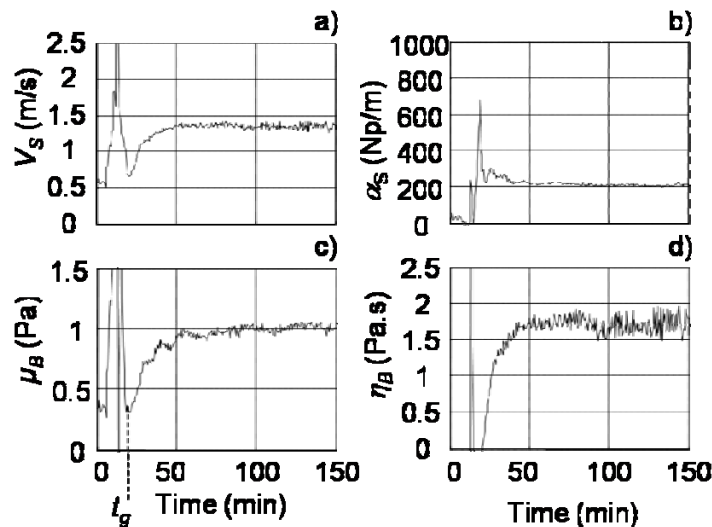

Figure 1: Shear wave speed (a), shear wave attenuation (b), elasticity (c) and viscosity (d) of a blood clot during coagulation as a function of time. The sol-gel transition was found to be at t_g = 19 min, when the blood clot becomes solid.

INTRINSIC LIMITATIONS IN DIFFERENTIAL DIAGNOSTICS BASED ON QUANTITATIVE ELASTOGRAPHY.

Armen Sarvazyan[1]*.
[1]Artann Laboratories, Lambertville, NJ, USA.

Mechanical parameters of soft tissues (such as shear modulus and shear viscosity) influenced by tissue architecture vary by several orders of magnitude between tissues. Even within the same tissue, e.g. in breast with a malignant lesion, the range of variation of elasticity modulus may reach three orders of magnitude, from a fraction of kPa to hundreds of kPa. Such a great variation may seem like a solid physical basis for development of novel methods of differential diagnosis of lesions based on the quantitative elasticity imaging. A whole class of imaging techniques being developed to exploit this. Though a closer look at the problem shows that in reality, the width of the range of the tissue elasticity variations cannot be fully employed for differentiating tissues or lesions.

Current approaches and techniques for elasticity imaging provide the data on tissue mechanical properties in relative units. In other words, the contrast in the elasticity image is defined by the ratio of the elasticity moduli of neighboring tissue structures. To obtain the quantitative data on the elasticity modulus of an imaged tissue structure it is necessary to make certain assumptions on the stress/strain relationship and boundary conditions for the analyzed tissue site.

All methods of elasticity imaging are based on evaluation of strain and/or stress patterns in the tissue subjected to mechanical loading. We conducted theoretical and experimental studies on the dependence of the strain or stress pattern on the hardness of a lesion relative to the surrounding tissue, E/E_0. It was shown that quantitative assessment of the elasticity of inclusions is feasible only in a very limited range of relative hardness E/E_0 from 1 to less than 10 (Figure 1). This estimate is obtained assuming that typical sensitivity of detection techniques to the changes in the strain or stress profiles is about 10%.

Palpable nodules are typically one, two or even three orders of magnitude harder than surrounding tissue. The results of this study show that Elasticity Imaging will not be able to differentiate two nodules one of which is 10 times harder and the second is 1000 times harder than the bulk tissue.
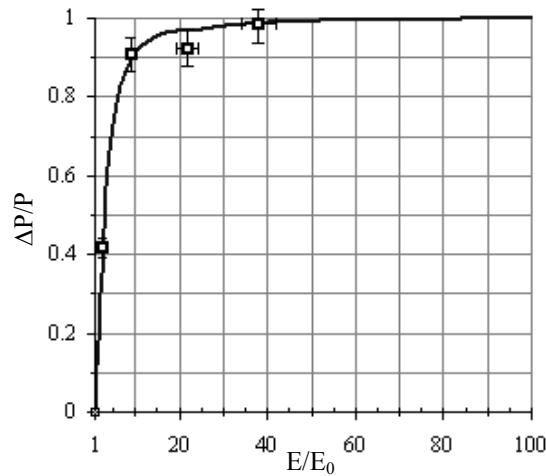
Figure 1: Dependence of the relative increase of the stress profile maximum on the relative hardness of a hard inclusion in the soft tissue. Experimental data were obtained from tissue mimicking phantoms. The solid line is a theoretical curve.

098   **TIME DOMAIN CROSS CORRELATION WITH PRIOR ESTIMATES.**

Reza Zahiri-Azar[1]*, S.E. Salcudean[1].
[1]Department of Electrical and Computer Engineering, University of British Columbia, Vancouver, BC, CANADA.

Following [1], a number of methods have been developed to measure tissue strain and elastic properties. Recent work proposed in our group [2] extends the static ultrasound (US) elastography approach [1] by exciting the tissue with an actuator at multiple frequencies (typically 0 to 25 Hz) and acquiring a sequence of US strain images in real time (typically 50 Hz and above) to generate estimates of relative stiffness, damping and density parameters by solving a local or global inverse parameter identification problem. In order to implement such dynamic elastography methods and in order to realize the numerous potential clinical applications of elastography, such as tumor detection, tissue segmentation, ablation monitoring, etc. there is a compelling need for real-time estimation of tissue strain.

Standard elastography uses a time domain cross correlation technique (TD) to estimate tissue displacement. The TD method has the advantage of being accurate for small strains (0-2%). The problem associated with TD is its high computational requirement that make it inefficient, because it searches exhaustively to find the displacement. This computational inefficiency makes TD an inappropriate choice for real-time strain estimation. Alternative and faster methods of strain estimation have been developed. In particular, real-time strain estimation (30 Hz for 100x90 images) has been reported in [3] based on phase root seeking. In [3], baseband signals instead of real signals are used for strain estimation. There are at least two iteration steps required and signal re-sampling is carried out in each step, which is computationally demanding. In addition, phase root seeking does not work for large values of strain.

We present a new and very efficient strain estimation method, which we call TDPE (time domain cross-correlation with prior estimates) that works as follows. Each RF signal is split into blocks. Each block has four adjacent neighbors – a leading block and a lagging block on the same RF line, and blocks at the same position on the preceding and following RF line. Because of their physical proximity, adjacent blocks have similar displacements and strains. For small strains, we use the displacement estimates of neighbor blocks to bracket the displacement of the current block. Cross-correlation is then used to determine displacements within the bracket. For high strains, we estimate the strain of neighbors and use this information to bracket the strain of the current block, again limiting the displacement search. Typically, only 3 to 5 lags inside the predicted brackets are checked to detect the displacement quickly and with high accuracy.

The TDPE method works best for small values of strain, as typically encountered in dynamic elastography studies (less than 1%). In simulations, our method was shown to work for strains up to 8%. TDPE is 10 times faster and much more accurate than the TD method for both high and low strains. A window length of 1µs and 50% window overlap was used to calculate strains in images. Strain images corresponding to 128x128 pixels B-mode images acquired with a 5MHz US transducer can be computed with Visual C on a Pentium IV 2.53 GHz Desktop PC with 512 MB RAM in less than 30 milliseconds. Therefore, a frame rate well in excess of 30 frames per second is not unlikely in a system that provides real-time access to RF data such as the one used in our group (Ultrasonix RP500, Ultrasonix Medical Corporation, Burnaby, BC). Furthermore, since the TDPE method limits the search area to a very small region around its neighbor, the probability of finding false displacements decreases significantly. As a result, elastograms generated by the TDPE method are much less noisy than those estimated via the TD method.

References:
[1]   J. Ophir et al, "Elastography, a quantitative method for imaging the elasticity of biological tissue", Ultrasonic Imaging Vol. 13, pp. 111-134, 1991.
[2]   E. Turgay, S. MacIntosh, R. Rohling and S. Salcudean. Parameter identification of tissue lumped models based on sequences of ultrasonic strain images. *Second Intl. Conf. on Ultrasonic Measurement and Imaging of Tissue Elasticity.* Corpus Christi, Texas, October 2003.
[3]   A. Pesavento, A. Lorenz, "Real-Time Strain Imaging – a new Ultrasonic Method for Cancer Detection: First Study Results" Proc. Of IEEE 2001 Ultrasonic Symposium, 2001.

019 **DIRECT STRAIN MEASUREMENT BASED ON AN AUTOCORRELATION METHOD.**
Chikayoshi Sumi[1]*.
[1]Department of Electrical and Electronics Engineering, Faculty of Science and Technology, Sophia University, Tokyo 102-8554, JAPAN.

Various tissue displacement measurement methods have been proposed. Usually strain data is obtained by differentiating measured displacement data. In this paper, we present a new real-time method for directly measuring strain without measuring displacement. This method was described in our Japanese patent and USA patent (1993) [1]. However, the method and measurement results have not been reported in the scientific literature.

In the conventional autocorrelation method, displacement is calculated from the phase of the complex autocorrelation signal. In our method, strain is directly obtained by calculating the derivative of the arctangent of the ratio of the imaginary component and real component of the complex autocorrelation signal. That is, the strain can be directly calculated by using the rules of arithmetic of the real and imaginary components and their derivatives, without calculating the phase.

This allows us to directly obtain strain data without unwrapping the phase when the displacement is larger than $\lambda/4$.

We show simulation measurement results below. Ultrasound speed is 1,500 m/s. Ultrasound frequency is 3.5 MHz. Strain is 0.5 percent (tensile). When using the conventional autocorrelation method, as shown in Figure 1(a), the aliasing occurs at the displacement of about 0.107 mm. However, using our direct measurement method, as shown in Figure 1(b), strain can be obtained without phase unwrapping. The high measurement accuracy could be confirmed on this simulation.

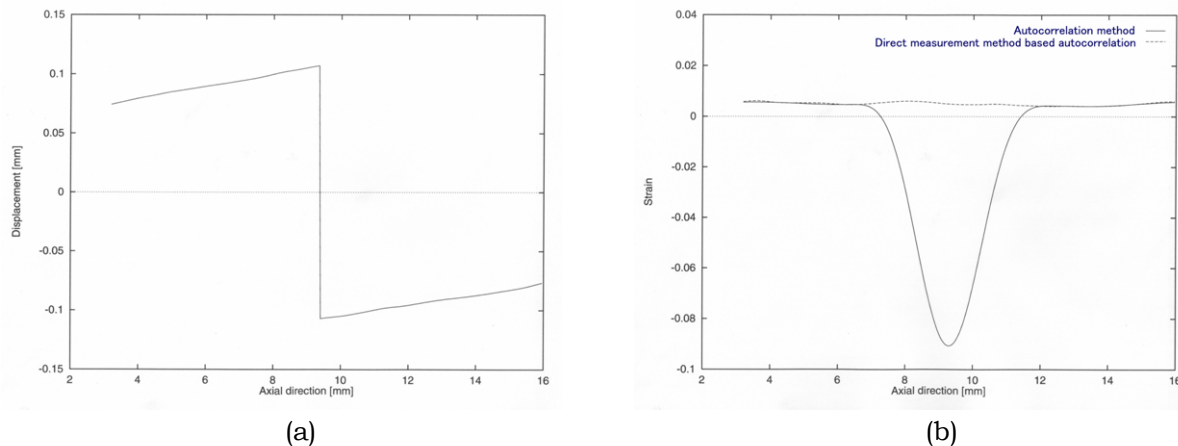(a)   (b)

Figure 1: Simulation (ultrasound speed, 1,500 m/s; frequency, 3.5 MHz, strain, 0.5 percent). (a) Measurement of displacement using the conventional autocorrelation method. (b) Strains respectively obtained by our direct strain measurement method and by differentiating the displacement data of (a) without phase unwrapping.

This direct measurement method can be combined with our previously reported phase-matching method [2] to cope with lateral displacement.

References:
[1] C. Sumi et al., USA Patent 5,495,771, "Elasticity measuring method and elasticity measuring apparatus," 1993.
[2] C. Sumi, "Fine elasticity imaging utilizing the iterative rf-echo phase matching method," IEEE Trans. UFFC vol. 46, no. 1, pp. 158–166, 1999.

083   IMPROVED ELASTOGRAPHIC SIGNAL–TO–NOISE RATIO USING CODED EXCITATION.

Rémi Souchon[1]*, Agnès Pousse[1], Jean-Christophe Béra[1], Jean-Yves Chapelon[1].
INSERM Unité 556, Lyon, FRANCE.

In elastography, image quality can be quantified by elastographic signal-to-noise ratio (SNRe) and axial resolution (Ra). These two parameters trade against each other when using pulsed excitation [1]. Coded excitation [2] was shown to increase sonographic signal-to-noise ratio (SNRs) and penetration depth while preserving axial resolution in sonography. In this study, the use of coded excitation [2] was investigated to augment SNRe without sacrificing axial resolution in ultrasonic elastography.

Theoretical framework: For a constant peak amplitude of the excitation signal, a coded excitation signal of length N provides a $N^{1/2}$ improvement in SNRs compared to an impulse excitation, while the signal bandwidth B is preserved. The strain filter theory [3] predicts that SNRe increases with SNRs in the CRLB region until a maximum is reached for SNRe $\approx 3.5 \; B^{3/2}.T.\Delta T^{1/2}$. For constant bandwidth, window length (T) and window shift (ΔT), constant axial resolution is expected.

Materials and Methods: Both numerical simulations and phantom experiments were carried out to estimate the SNRe in a homogeneous material. These results were compared with those obtained using conventional pulse excitation for constant B, T and ΔT (i.e. constant resolution). Various codes (Golay, Barker and chirp) and code lengths were tested. The numerical simulations used a simple 1D backscattering model to show the theoretical effects of coded excitation on SNRe. Experiments were carried out using a more realistic setup based on multi-compression elastograms acquired with a sector-scan imaging probe in a cylindrical phantom with stiff inclusions.

Results: In noise-free simulations coded excitation induced a slight decrease in SNRe compared to short pulse excitation, probably due to clutter (secondary lobes). When sonographic noise was added into the model, a large improvement in SNRe was observed. The experimental results (Figure 1) showed a significant improvement in penetration depth, while the sharpness of the outline of the inclusions was preserved. As expected from the theory, increased SNRe was observed for low SNRs and low strain, while SNRe remained unchanged (plateau) for high strain and high SNRs (Figure 2).

Conclusion: Coded excitation increased SNRe in areas of low strain and/or low SNRs, without impairing axial resolution. The use of coded excitation resulted in improved sensitivity and dynamic range.
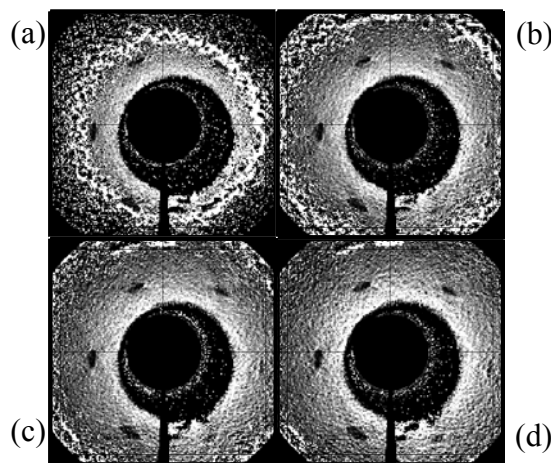

Figure 1: Experimental elastograms for (a) single pulse, (b) Barker 4, (c) Barker 7, and (d) Barker 13 excitation, at constant peak amplitude.
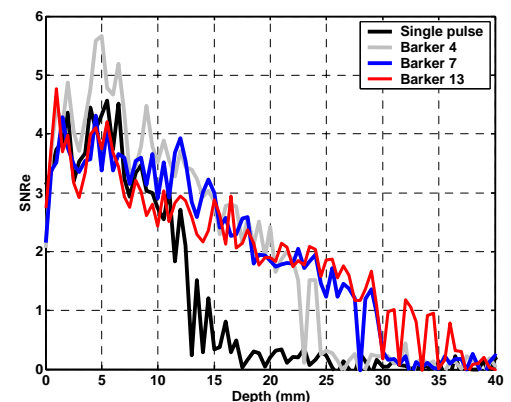
Figure 2: Experimental SNRe vs depth in phantom.

References:
[1] Srinivasan S et al. Trade-offs between the axial resolution and the signal-to-noise ratio in elastography. Ultrasound Med Biol 29(6), 847-866 (2003)
[2] Chiao RY, Hao X. Coded excitation for diagnostic ultrasound: A system developer's perspective. Proc IEEE Ultrasonics Symp 2003 (Vol. 1), 437-448
[3] Varghese T, Ophir J. A theoretical framework for performance characterization of elastography: The strain filter. IEEE Trans Ultrason Ferroelectr Freq Control 44(1), 164-172 (1997)

096   **SYSTEMATIC ERROR CAN DOMINATE IMAGE NOISE IN STRAIN MEASUREMENTS.**

CX Jia[1], NH Gokhale[1], MS Richards[1], LA Nelson[1], MM Doyley[2], AA Oberai[1], PE Barbone[1]*.
[1]Boston University, Boston, MA, USA; [2]Dartmouth College, Hanover, NH, USA.

We report the results of an experiment designed to quantify noise in 2D ultrasound strain measurements. A gelatin agar phantom was fixed and imaged in a mechanical deformation device. Many nominally identical image frames were taken of the phantom in its undeformed configuration. The phantom was then compressed by about 2% strain, and several images were taken in the deformed configuration. The frame repetition provides separate realizations of random electronic noise in each image. In all, about two hundred image pairs are available from which strain can be measured. Two dimensional displacement is estimated using a novel finite-element based image registration method, which gives final image correlations of about 95% on average with a resolution of about 1 mm^2. The technique overcomes the bulk of the so-called "strain-decorrelation" limitations of block matching methods. The displacement results show the following:

(1) The normalized standard deviation of the axial displacement is about 10^{-3}.

(2) The displacement "noise," defined by the difference between the individual displacement estimates and the average displacement, is dominated by a viscoelastic relaxation of overall magnitude about 1.5 microns.

(3) The viscoelastic relaxation strain, though only about one part in a thousand of the overall deformation, can be separated from the elastic deformation and clearly shows features in the phantom.

(4) The individual elastic strain images show comparatively large and obvious fluctuations about a smooth strain distribution; the fluctuations are repeated in each realization, and are therefore not random.

The same fluctuations show themselves in the average strain field. We conclude that the noise in our elastic strain field is dominated not by random electronic image noise, but rather by systematic errors. Two possibilities are contamination by sidelobes and decorrelation of speckle return due to scatterer motion. Finally, we present results of two methods to correct for strain noise: regularization and undetermined elastic constraints. Regularization tends to bias the strains results while the elastic constraint effectively eliminates the elastic strain fluctuations without introducing an obvious bias.

041 **A NOVEL HAPTIC SENSOR ACTUATOR SYSTEM FOR PALPATION IMAGING BASED ON ULTRASOUND ELASTOGRAPHY.**

Walaa Khaled[1]*, Stefan Reichling[2], Otto T. Bruhns[2], Gareth J. Monkman[3], Stefan Egersdorfer[3], Mario Baumann[4], Holger Boese[4], Herbert Freimuth[5], Abdi Tunayar[5], Andreas Lorenz[6], Andreas Pesavento[6] and Helmut Ermert[1].
[1]Institute of High Frequency Engineering, Ruhr-University, Bochum, GERMANY; [2]Institute of Mechanics, Ruhr-University, Bochum, GERMANY; [3]Fachhochschule Regensburg, Electrical Engineering and Mechatronics Department, Regensburg, GERMANY; [4]Fraunhofer-Institut fuer Silicatforschung ISC, Wuerzburg, GERMANY; [5]Institut fuer Mikrotechnik, Mainz GmbH, Mainz, GERMANY; [6]LP-IT Innovative Technologies GmbH, Bochum, GERMANY.

In the field of medical diagnosis, there is a strong need to determine mechanical properties of biological tissue, which are of histological and pathological relevance. One of the established diagnosis procedures is the palpation of body organs and tissue. Palpation is used to locate changes in the pathological state of tissue and organs. Current medical practice routinely uses sophisticated diagnostic tests through magnetic resonance imaging, computed tomography and ultrasound imaging. However, they cannot provide direct measure of tissue elasticity.

Last year, we presented the concept and first results of the haptic sensor actuator system to visualize mechanical properties of tissue using ultrasonic elastography and electrorheological fluids. Using this system, we reconstruct tissue properties on a controllable haptic display capable of emulating and differentiating normal and abnormal biological tissue.

In order to obtain quantitative mechanical properties of tissue noninvasively, we proposed an inverse approach by which the spatial distribution of the relative elastic modulus of tissue can be estimated only from the measured deformation. During the solution of the mechanical forward problem the biological tissue was modeled as a linear isotropic incompressible elastic medium and a 2-D plane strain state model was used. Furthermore, to develop inverse elastography reconstruction approaches, finite element simulations were performed with the software package MSC. Marc 2000 (MSC. Software Corporation, USA) for a number of soft biological tissue models. The results obtained from finite element analysis were confirmed in the ultrasonic experiments on a set of tissue-like phantoms with known acoustical and mechanical properties. The RF-data were acquired using a standard ultrasound system (SONOLINE Omnia, Siemens AG, Germany) equipped with a 9 MHz linear array probe and a conventional AD-board at a sampling frequency of 50 MHz. The axial displacements were calculated using the fast root-seeking technique (A. Pesavento, A. Lorenz and H. Ermert, Electronics Letters, 35, 1999, p. 941-942). Finally, using numerical solution models and solving the inverse problem using two different methods, we deduce relative mechanical properties of tissue. The first method is a modified direct method based on solving the equations of equilibrium proposed by Sumi et. al., IEEE Trans. BME, Vol. 42, 1995, p.193-202, modified by the authors. The second method for solving the inverse elasticity problem is based on recasting the problem as a non-linear optimization problem proposed by Kallel et. al. IEEE Trans. Medical Imaging, 15(3):299–313, 1996. The feasibility of these methods was demonstrated using the measured real time ultrasound data of a tissue-like phantom with a single and a double inclusion problem. The proposed methods seem promising for the quantitative differential diagnosis of lesions in the tissue.

The mechanical properties are then transferred to the actuator system which consists of a 2D piston-array of elements filled with an electrorheological fluid. The array, which is electronically controlled, reconstructs, according to a simplified model of the human sense of touch, the corresponding resistance forces due to the viscosity change of the electrorheological fluid. The spatial resolution of receptors on the finger tip is improved to 1 mm x 3mm. The results show, that our real time ultrasound elastography system is able to differentiate hard lumps from soft tissue, like malignant and benign tissue areas in the prostate or breast, with a high degree of accuracy. This system has the potential of improving diagnosis as a haptic supplement of elasticity visualization and for virtual reality applications like remote palpation, simultaneous multiple actuator palpation, teaching and telemedicine.

MECHANISM FOR HUMAN DETECTION OF ELASTIC LESIONS IN SIMULATED B–MODE MOVIES DURING PALPATION.

Naomi Miller[1]*, Jeffrey Bamber[1].
[1]Joint Department of Physics, Institute of Cancer Research and Royal Marsden NHS Trust, Downs Road, Sutton, Surrey, SM2 5PT, England, UK.

Elastography is showing promise as a technique for imaging the mechanical properties of soft tissue, but these properties can also be assessed by subjective interpretation of tissue motion seen in real-time B-mode images during palpation. This method, which we refer to as relative motion assessment (RMA), can be implemented on unmodified ultrasound scanners and permits simultaneous appreciation of elasticity and backscatter information. We have previously reported that elastic modulus contrast thresholds for lesion detection by RMA are within the range of contrast values that have been measured in normal and diseased breast tissues [1]. The aim of the present study was to learn more about the visual mechanism for lesion detection by RMA. This information could be useful for optimising the method of palpation.

The first part of this study aimed to determine the nature of the signal employed by observers in lesion detection by RMA. Observers were presented with a series of simulated B-mode movies of tissue being palpated that contained lesions of different modulus contrast. They were asked to rate the perceived elastic contrast from 1 to 5. The linearity of the relationship between the perceived contrast and various candidate contrast quantities (e.g., modulus contrast, theoretical strain contrast, different types of measured strain contrast) was used to measure how closely the contrast quantity was related to the signal employed by the observer. The second part of the study aimed to determine whether the axial or lateral component of the signal was more useful to the observer. The simulation of B-mode movies during palpation was modified so that the tissue was only distorted using one component of displacement (Note: Poisson's ratio = 0.495). A perception study was then conducted to determine modulus contrast thresholds for each of these two artificial states (i.e., pure axial compression and pure lateral expansion).

The perceived signal was found to be strain contrast, rather than modulus contrast. We also found that when the observers compared the strain in the lesion with the strain in the background tissue, they ignored (i.e., in effect, compensated for) the low strain region in the background tissue caused by a non-slip boundary (which represented the chest wall). Finally, the observers' ability to detect the lateral RMA signal was considerably greater than their ability to detect either the axial signal or the combined (i.e., original) signal. The most likely explanation is that the lateral signal consists only of an expansive strain, while the axial signal consists of a translational motion (caused by the global motion of the transducer) in addition to the compressive strain, making it more difficult to assess axial strain.

The fact that the perceived contrast is linearly related to strain contrast implies that observers will have a limited ability to assess differences in contrast between lesions of high modulus contrast, due to the non-linear relationship between Young's modulus and strain. However, the same limitation applies to elastographic methods that display strain and this phenomenon might partly explain why Garra et al. [2] reported considerable overlap in the subjective strain of fibroadenomas and cancers. Our observation that humans compensate for low strain near a non-slip boundary suggests that it is acceptable to palpate the breast by pressing against the chest wall. However, it was also found that the global axial motion of the transducer inhibits ability to detect strain. Therefore, as practised by some breast ultrasonographers, it might be better to implement RMA of the breast by holding the transducer still, immobilising the lesion between the fingers, and then applying a lateral strain from both the left and right hand sides. Alternatively, a processing method could be devised to remove the global motion from the RMA movie [3].

We have demonstrated that observer studies are a useful means of optimising RMA. There is considerable scope for further enhancement, for example, by determining the optimum applied strain and strain rate. In the meantime, the routine use of RMA in ultrasound breast examination should be widely encouraged.

References:
[1] Miller NR and Bamber JC. Thresholds for visual detection of Young's modulus contrast in simulated ultrasound image movies. Phys Med Biol 2000; 45:2057-2079.
[2] Garra BS, Céspedes I, Ophir J, Spratt S, Zuurbier RA, Magnant CM and Pennanen MF. Elastography of breast lesions: initial clinical results. Radiology 1997; 202:79-86.
[3] Bamber JC. Method and apparatus for tissue-centered scan conversion in an ultrasound imaging system. 1996 US Patent Number: 5,538,004.

* indicates Presenter

100 **SHEAR WAVE ELASTICITY IMAGING WITH THE USE OF TIME REVERSAL ACOUSTICS.**

Armen Sarvazyan[1]*, Alexander Sutin[1].
[1]Artann Laboratories, Lambertville, NJ, USA.

Shear Wave Elasticity Imaging (SWEI) has promising applications both in ultrasonic imaging and MRI. In the SWEI, dynamic shear stress is remotely induced in soft tissue by the radiation force of the pushing ultrasound beam. There are several ways to generate this pushing focused ultrasound beam. In addition to conventional means of generating, focusing and steering of ultrasonic beams, there is a novel technique based on Time Reversal Acoustics (TRA) developed by Mathias Fink at the University of Paris.

In this talk, we present initial result of the studies on the use of the TRA transmitters for generation of radiation force in soft tissue and discuss the potential of the TRA technique in the applications related to elasticity imaging.

There are numerous advantages of TRA systems for focusing ultrasonic beams over conventional phased arrays. TRA provides concentrating ultrasound energy both in space and in time. TRA focusing transmitters can be made very broad band and can generate arbitrary form signals using very simple means. A TRA transmitter with just a few piezotransducers can generate and steer focused ultrasonic beam with the efficacy comparable to that achieved with a phased array comprising hundreds of elements.

We have developed several TRA focusing systems. Electronic unit for the TRA systems provides receiving, digitizing, storing, time reversing and transmitting of acoustic signals in a wide frequency range from 0.01 to 10 MHz. The TRA focusing was investigated in the water tank, in tissue phantoms and *ex vivo* animal tissues. The tests demonstrated that TRA system can produce highly focused ultrasound pulses with large variation of frequencies and waveforms, which is important for optimizing generation of radiation force in specific applications. The pulse duration can be varied from 1 to 500 µs and frequency range from 0.1 to several MHz. The amplitude of the focused signal reached tens of MPa.

A theoretical model for calculation of radiation force produced by TRA system is developed. The model is based on an assumption that the radiating part of the resonator works as a phase conjugation screen for a spherical wave radiated from the focal point. Theoretical dependencies of the field structure on the position of the focus point and ultrasound frequency are in a good agreement with experimental results

We are currently exploring application of TRA in both MR SWEI, where the propagation of shear waves is visualized by MRI, and ultrasonic SWEI, where the detection of generated shear waves is achieved using acoustic means.

NONCONTACT ULTRASOUND INDENTATION SYSTEM FOR MEASURING TISSUE MATERIAL PROPERTIES USING WATER BEAM.

Minhua Lu[1], Yongping Zheng[1]*, Qinghua Huang[1].
[1]Rehabilitation Engineering Center, The Hong Kong Polytechnic University, Hong Kong, China.

To measure or image the mechanical properties of tissue has been attracting increasing research efforts during the recent decades as changes in tissue stiffness are often related to pathological process. Ultrasound indentation techniques have been proved to be a useful tool for measuring the stiffness of tissue specimens as well as body tissues *in vivo* [1]. However, the direct contact manner makes it difficult for the present ultrasound indentation systems to be use with focused ultrasound beams for high resolution or with fast scanning for elasticity imaging. We have therefore developed a noncontact ultrasound indentation system by using water beam compression.

The system was comprised of a focused high-frequency ultrasound transducer, a water beam ejector and a pressure sensor. The water beam served as a compressor as well as a medium for ultrasound propagation. The tissue deformation was estimated from the ultrasound echoes reflected from the tissue using a cross-correlation algorithm. We have earlier reported the system. In this study, we tested different phantoms using this water beam indentation technique.

Various phantoms with different stiffness made from silicones were prepared for experiments. The sizes of the phantoms were about 1cm×1cm×0.5cm (width×length×height), 1cm×1cm×1cm, 1cm×1cm×1.5cm. Each phantom was indented by loading and unloading for three cycles in each indentation test, and each one was indented three times. The pressure applied on the phantoms was calculated by assuming a uniform stress distribution in the contacting area between the water beam and the phantom surface. The pressure/relative deformation (P/RD) slopes were used as an index of the phantoms' stiffness (Figure 1). The mechanical properties of the phantoms were also measured using uni-axial compression [2], and their compressive Young's modulus and Poisson's ratio were obtained. Good correlation between the slopes of P/RD and Young's modulus was find (R^2= 0.75) (Figure 2).

In summary, we were able to demonstrate the effectiveness of the new system to measure the phantoms with different stiffness. The system repeatability was good. We will further investigate the derivation of elasticity parameters from ultrasonic water indentation.

References: [1] Zheng YP and Mak AFT. IEEE Trans Biomed Eng 43: 912-918, 1996.
[2] Zheng YP, et al. Phys Med Biol 47: 3165-3180, 2002.
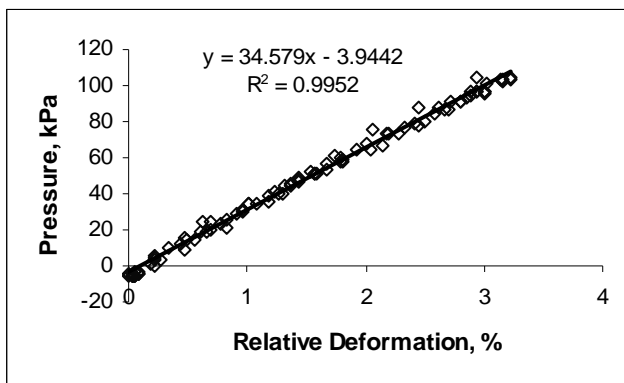

Figure 1: Relationship between pressure and relative deformation under water indentation.
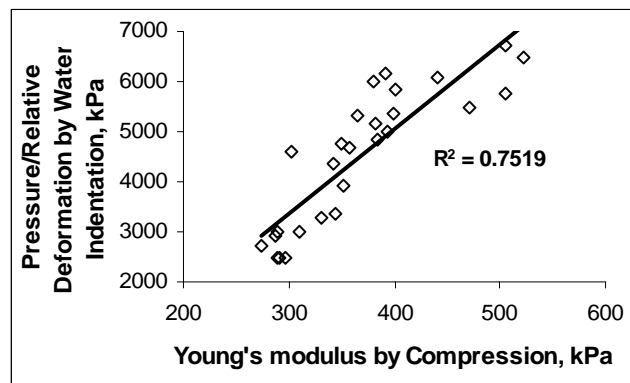

Figure 2: The correlation between the slopes of P/RD and Young's modulus of the phantoms.

***IN–VITRO* IMAGING OF HIFU–INDUCED LESIONS IN BOVINE LIVERS USING THREE DIMENSIONAL SONOELASTOGRAPHY.**

Man Zhang[1], Lawrence S. Taylor[1], Deborah J. Rubens[2], Kevin J. Parker[3]*.
[1]Department of Biomedical Engineering, [2]Department of Radiology, [3]Department of Electrical and Computer Engineering, University of Rochester, Rochester, NY, USA.

High intensity focused ultrasound (HIFU) is a non-invasive therapeutic method which creates coagulation necrosis for killing malignant tumors within a well-defined volume in the tissue. In this study, sonoelastography was investigated for the visualization of HIFU-induced lesions in the bovine livers *in vitro.*

Tissue samples (~4×4×4 cm^3) were cut from fresh bovine liver and then degassed overnight. Lesions were created in tissue samples by a single-element HIFU transducer. The compound lesion volume was determined by the number of individual lesions treated with identical HIFU exposure dose. A volumetric series of 2D sonoelastography images were acquired from the liver-embedded agar phantom. Each lesion displayed as a dark area surrounded by a bright green background in the image. IRIS Explorer was used to reconstruct 3D lesion images. After imaging lesions were examined by gross pathology to verify their size, shape and volume.

The gross pathology results showed that HIFU-induced compound lesions were relatively uniform, palpably harder and brighter than the normal tissue. The mean volumes of three 1×2 compound lesions, three 2×2 lesions and three 3×3 lesions measured by fluid displacement were 1.8cm^3, 2.4cm^3 and 6.0cm^3, respectively. As the smallest lesion in the test, a single HIFU lesion with 1.3cm^3 in volume was also successfully detected by 3D sonoelastography. The edge of each lesion in the image was ambiguous in a range of ~3mm. When only the darkest region in the image was delineated as the lesion, the mean sonoelastography volume of the 10 lesions was 84% of the volume measured by fluid displacement. Good correlation between the lesion dimensions determined from sonoelastography images and gross pathology was also found. This study demonstrates that sonoelastography is a potential real-time method to accurately monitor the HIFU therapy of cancerous lesions.
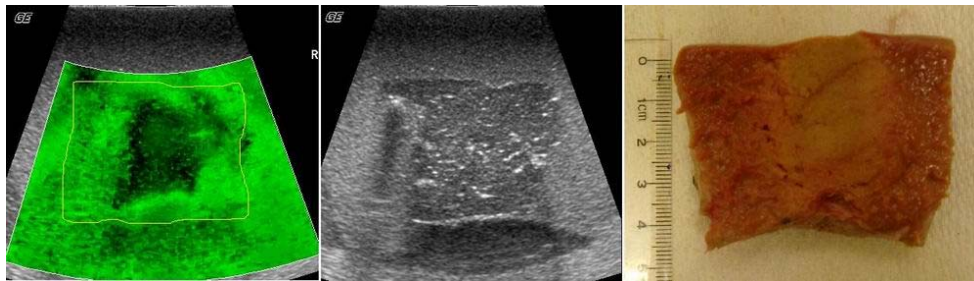

Figure 1: Sonoelastography and B-scan images of a HIFU lesion verified by dissection.
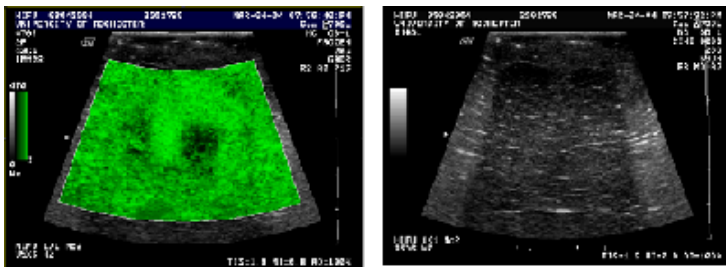

Figure 2: The smallest HIFU lesion with 1.3cm^3 in volume detected by sonoelastography.
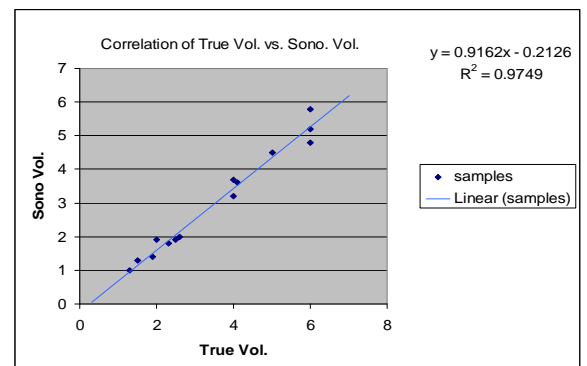

Figure 3: Correlation between true volume and sonoelastography volume.

077   SONOMYOGRAPHY ANALYSIS OF THE MORPHOLOGICAL CHANGES OF FOREARM MUSCLES IN ACTION.

Yongping Zheng[1]*, Xin Chen[1].
[1]Rehabilitation Engineering Center, The Hong Kong Polytechnic University, Hong Kong, CHINA.

Electromyography (EMG) signal has been widely used for the control of upper limb prosthetic devices for many years. Various signal processing methods have been developed to improve the quality of the EMG control algorithm. Nevertheless, some inherent factors in the use of EMG limit its use as an ideal control method. In addition, multiple degrees of freedom (DoF) are difficult to achieve using EMG. Since sonography is widely used in assessment of human muscles and nerves, it has the potential of being applied as one control signal. In this study, 2D ultrasound images were used to detect morphological changes of the forearm. We called the signal derived from ultrasound images or signals about the muscle activities as sonomyography (SMG). The relationship between SMG, EMG and the wrist flexion-extension angle of normal subjects was investigated.

The subject was asked to perform wrist extension and relaxation repeatedly with the guidance of audio beats. Sonography of wrist extensor muscles was recorded using a B-mode ultrasound scanner (180 Plus, Sonosite) with a 10 MHz 38mm transducer (L38, Sonosite). EMG signals were acquired by biploar Ag-Agcl electrodes (Axon Systems) at the same site. The wrist motions were monitored simultaneously by an electronic goniometer. The B-mode video signal was sent to computer and captured by an image acquisition board (NI PCI-1411, National Instruments). Both EMG and goniometer signals were recorded simultaneously by a signal acquisition board (NI PCI-6024E, National Instruments). Motion analysis and data processing were implemented by customer-developed software.

Ten normal subjects were recruited in the experiment. They were asked to perform several cycles of flexion-extension in three trials. The muscle deformation profile was derived from the sonography data, and the wrist angle profile was derived from the motion data. The root mean square (RMS) value of EMG signal was also extracted. Figure 1 illustrates a typical result of the wrist flexion-extension angle versus the muscle deformation. The results of all subjects showed a similar pattern. It is shown in this figure that the wrist angle was closely followed by the muscle deformation. The relationship between the wrist angle and the muscle deformation was further studied, and the slope of the linear regression of the first cycle was computed. A typical illustration is shown in Figure 2. The EMG signal also had a similar relationship with angle, but compared with SMG signal, there are more fluctuations in the EMG result.

In this study, sonography was employed to investigate the morphological changes of muscles. The good linear relationship between muscle deformation and wrist angle shows the potential feasibility of using SMG as a control signal. Compared with the EMG signal, the SMG signal has several advantages. It is not affected by the skin conditions and is immune to electromagnetic interference that affects EMG. Besides muscle deformation, there exists more valuable information about the muscle activities in the sonogram. In addition, motions of multiple degrees of freedom can be detected using SMG, as ultrasound can be used to easily differentiate the motion of different muscles. Future work on this aspect will improve this SMG control algorithm. Furthermore, more effort is needed to establish the model to study the basic relationship between SMG and underlying muscle activities.
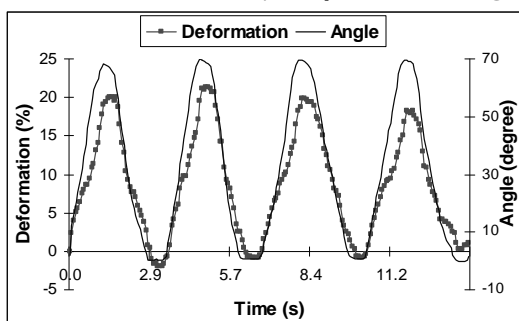
Figure 1: Wrist angle and muscle deformation

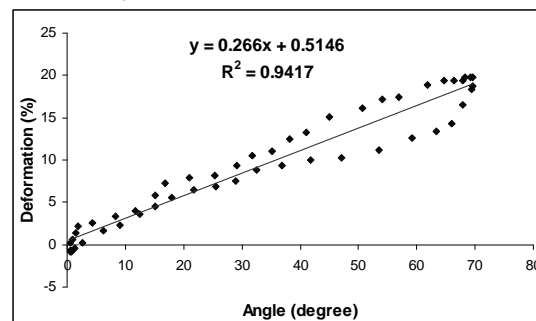Figure 2: Linear regression of angle and deformation in the first cycle of wrist flexion and extension

* indicates Presenter

021 **THERMAL PROPERTIES RECONSTRUCTION TECHNIQUE BASED ON TEMPERATURE MEASUREMENT.**

Chikayoshi Sumi[1]*.

[1]Department of Electrical and Electronics Engineering, Faculty of Science and Technology, Sophia University, Tokyo 102-8554, JAPAN.

For various soft tissues, we are developing the ultrasonic strain measurement-based mechanical properties (shear modulus, density, Poisson's ratio) reconstruction/imaging technique. On human *in vivo* liver, and breast etc., we reported the effectiveness as a differential diagnosis technique and a monitoring technique of low invasive therapies such as chemotherapy (e.g., anticancer drug and ethanol), cryotherapy, and thermal therapy (e.g., HIFU, micro and rf electromagnetic waves). On these tissues, we also confirmed the inhomogeneity of thermal-elasticity, for instance, between parenchyma and blood vessels [1].

In this report, we propose to reconstruct thermal properties such as thermal conductivity and thermal diffusivity in addition to the mechanical properties for diagnosis and treatment (planning). Temperature can be measured by measuring strain generated by temperature change. Provided that the reference values of thermal properties are given in the ROI as initial conditions, by solving the simultaneous first order partial differential equations (PDEs) having the temperature distributions as inhomogeneous coefficients, we can determine the thermal properties distributions.
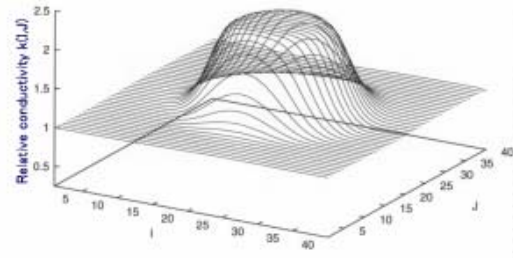
$$\rho c \frac{dT_i}{dt} = \nabla T_i \cdot \nabla k + k \nabla^2 T_i + Q,$$

where, k, D, c, T_i, Q are respectively thermal conductivity, density, specific heat, temperature, and heat source or heat sink. Realization of a proper reference region allows reduction of the required number of independent temperature distributions. This can be delineated by considering characteristic curves of the PDEs. To stabilize the reconstruction, so-called regularization method is applied. Infrared temperature measurement can also be utilized.

The figure below shows simple simulation results of reconstruction of the thermal conductivity distribution obtained using a proper reference region and a steady temperature distribution. The proper reference region extends in a direction which crosses the direction of heat flux.
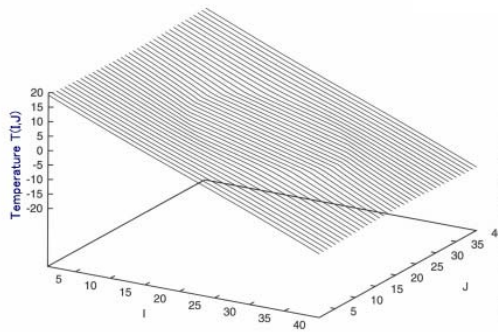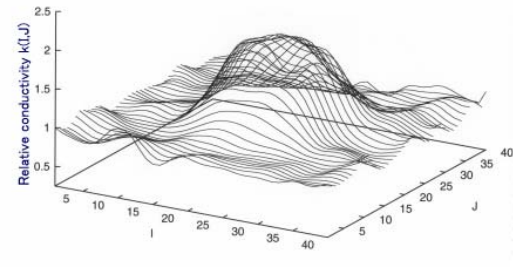

(a) No noise-filled temperature data.　　(b) Thermal conductivity reconstruction from (a).
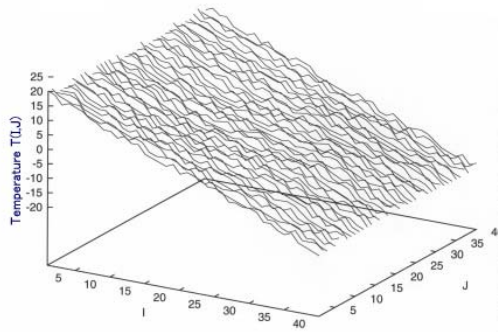
(c) Noise-filled temperature data.　　(d) Regularized conductivity reconstruction from (c).

Reference:
[1] C. Sumi, Proc. of 23rd Ann. Int. Conf. of the IEEE Eng. in Med. and Biol. Soc., Istanbul, October '01.

* indicates Presenter

099   **THERMAL LESION MONITORING USING MINIATURIZED IMAGE–TREAT ARRAYS.**
Inder Raj S. Makin[1], T. Douglas Mast[2]*, Waseem Faidi[2], Megan M. Runk[2], Peter G. Barthe[1], Michael H. Slayton[1].
[1]Guided Therapy Systems, Mesa, AZ, USA; [2]Ethicon Endo–Surgery, Cincinnati, OH, USA.

A key potential advantage for ultrasound therapy is the ability to treat and image tissue using the same device. Recent development of miniaturized dual-functionality (image and treat) probes, capable of both high power (*e.g.*, > 80 W/cm^2 at 3.1 MHz) and broad bandwidth (*e.g.*, 50% centered at 3.5 MHz), has allowed real-time imaging and monitoring of thermal lesioning with complete co-registration of image and treatment regions of interest. Using 3–10 mm diameter probes with 32–64 elements operating at center frequencies 3–8 MHz, high-quality B-scan images and useful monitoring information can be obtained during therapy planning and treatment.

Monitoring of thermal lesioning by these arrays can be performed simultaneously using the same array elements. In addition to real-time B-scan visualization, techniques employed include echo strain imaging to map small temperature rises and analysis of echo waveform changes to detect boiling and tissue modification. Echo strain maps are computed using a simple estimator based on the depth-dependent phase change between echo signals before and after tissue heating. Echo waveform changes are mapped using a cumulative measure of signal differences related to signal decorrelation. Both of these monitoring methods have been implemented using simple operations on analytic echo signals, allowing real-time display of parameter maps superimposed on B-scan images.

086 **TISSUE DISPLACEMENT AND STRAIN PATTERNS DURING ACUPUNCTURE FOLLOW CONNECTIVE TISSUE PLANES.**

Elisa E. Konofagou[1]*, James R. Fox[2], Helene M. Langevin[2].
[1]Department of Biomedical Engineering, Columbia University, New York, NY, USA; [2]Departments of Orthopaedics & Rehabilitation and Neurology, University of Vermont, Burlington, VT, USA.

Introduction:
Acupuncture has been shown to cause mechanical stimulation of connective tissue. Since a correspondence has been shown between acupuncture meridians and inter-muscular connective tissue planes, we hypothesized that tissue displacement and strain patterns during acupuncture needle manipulation along an acupuncture meridian (longitudinal connective tissue plane) would be spatially related to that connective tissue plane seen on B-scan ultrasound.

Methods:
To test this hypothesis, we performed *in vivo* ultrasonic imaging using a System Five (Vingmed) ultrasound scanner at 6.7 MHz on the thigh of four human subjects. The ultrasound probe was placed both longitudinally and transversely (relative to the meridian) at acupuncture point GB32, located between the biceps femoris and vastus lateralis. After insertion, the acupuncture needle was rotated (8 revolutions) followed by upward and downward 2 mm needle movements using a computer-controlled acupuncture needling instrument. Disposable stainless steel needles (0.25 mm diameter) were used. Axial displacement and strain images were generated using the RF data and cross-correlation techniques between successively acquired RF scans during all needle movements. Seventy RF scans were acquired continuously during each experiment at the rate of 12.9 frames/s.

Results:
In longitudinal images, clear bands of tissue displacement were observed, corresponding to the perimuscular fascia running parallel to the skin surface (along the meridian). In the longitudinal strain images, a difference between the behavior of the tissue layers (subcutaneous tissue and muscle) was noted, one being stretched while the other being compressed during rotation, downward and upward motion of the needle. In the transverse images, the predominant organized displacement and strain patterns during needle movement followed the intermuscular fascial plane running diagonally across the image.

Discussion:
Our preliminary results support the hypothesis that acupuncture needle manipulation causes mechanical stimulation of tissue (manifested as rigid motion, compression and/or stretching) along connective tissue planes. The sonogram provides the anatomical information while the displacement and strain images highlight the regions of high concentration of mechanical effects resulting from the needle movement. Further testing and analysis will aim at studying whether this mechanical stimulation occurs preferentially longitudinally or transversely to the planes of meridians.

102 **COMBINED ULTRASOUND, PHOTOACOUSTIC AND ELASTICITY IMAGING.**

Stanislav Emelianov[1]*, Salavat R. Aglyamov[1], Srivalleesha Mallidi[1], Jignesh Shah[1], Suhyun Park[1], Shriram Sethuraman[1], Andrei Karpiouk[2], Massoud Motamedi[2], Alexander Oraevsky[3], Richard D. Irving[4], Rainer M. Schmitt[4], W. Guy Scott[4].
[1]Department of Biomedical Engineering, The University of Texas at Austin, Austin, TX, 78712, USA; [2]Center for Biomedical Engineering, The University of Texas Medical Branch, Galveston, TX, 77555, USA; [3]Fairway Medical Technologies, Houston, TX, 77099, USA; [4]WinProbe Corporation, North Palm Beach, FL, 33408, USA.

There presently is a definite and urgent clinical need for an imaging technique that can visualize both morphological and functional properties of tissue. In this paper, we present a combined diagnostic imaging system capable of simultaneous imaging of tissue structure (ultrasound imaging) and functional changes (photoacoustic and elasticity imaging) of tissue.

Ultrasound imaging is commonly used in clinical practice while elasticity and photoacoustic imaging are relatively new. Despite the great enthusiasm that the latter two techniques have generated among investigators in the medical imaging field, neither elasticity nor photoacoustic imaging have yet been adopted in clinical medicine due to several shortcomings. Elasticity imaging must retain the dynamic and interactive (i.e., real-time) nature of medical ultrasound, but existing ultrasound systems are not designed for integration with computation-intensive elasticity imaging. Therefore, clinical implementation of elasticity imaging has thus far been limited by hardware design and, consequently, unacceptably long off-line processing time. Photoacoustic imaging (i.e., imaging based on the absorption of short pulses of electromagnetic energy, such as light, and the subsequent emission of acoustic waves) failed to visualize tumors in context of the anatomical structure of surrounding tissue. This is partially attributed to the fact that photoacoustic imaging cannot be directly integrated with existing ultrasound imaging systems due to significant differences in ultrasound transducer design and underlying hardware specifications. However, these complementary techniques – ultrasound, photoacoustic and elasticity imaging – can be combined to take full advantage of the many synergistic features that none of the individual imaging systems alone can offer.

To evaluate our approach, numerical and experimental studies were performed using heterogeneous phantoms where ultrasonic, optical and viscoelastic properties of the materials were chosen to closely mimic soft tissue. The phantoms were imaged using pulsed, dual-frequency Nd:YAG laser interfaced with a custom designed ultrasound imaging system. The images clearly demonstrate that various properties of the phantom materials can be assessed using the combined imaging system.

The results of this study suggest that combined ultrasound-based imaging is possible and can provide additional diagnostic information based on functional changes associated with tissue pathology. Application of the combined imaging include cancer detection, diagnosis and treatment monitoring, biopsy guidance and microscopic imaging of engineered tissue are discussed. Practical and experimental aspects of combined imaging will be presented with emphasis on data capture and signal/image processing algorithms. The paper will conclude with a discussion of the advantages and limitations of the combined imaging technique.

062 **DEVELOPMENT OF HIGH BANDWIDTH TRANSDUCERS USING INJECTION–MOLDED 1-3 LOW PITCH COMPOSITES: A NUMERICAL STUDY.**

RM Schmitt[1]*, WG Scott[1], S Emelianov[2], RD Irving[1].
[1]WinProbe Corporation, North Palm Beach, FL, USA; [2]Dept of Biomedical Engineering, University of Texas at Austin, Austin, TX, USA.

Ultra wide bandwidth transducers are highly desirable for ultrasound-based elasticity imaging since they increase both accuracy and spatial resolution of tissue displacement and strain estimates. Compared to solid piezo-ceramic, the 1-3 piezo composite materials exhibit lower impedance, higher internal damping (low Q, and increased electromechanical coupling). In concert with the development of a new ultrasound imaging research platform and a 3x3 matrix of partially overlapping phased array beams to identify out of plane tissue motion, we evaluate the use of injection molded 1-3 composites to construct the 1.5-D matrix array consisting of 12 x 64 array elements.

The basic approaches to achieve high bandwidth are a) the classical approach of multilayer matching and b) using stacks of 1-3 composites of different layer thicknesses, where each layer defines a different "pass-band". Since 1-3 composite material samples the aperture by its pillar to pillar pitch design, constraints impacting the bandwidth are imposed. In addition, cross-talk between neighbor elements limits the beam steering for phased array.

Using the Finite Element Analysis (FEA) [1] we have investigated both approaches and compared the results to a modeled gold standard consisting of piezo-ceramic plate perfectly matched by a fully absorbing backing. The analysis of the transient performance of 1-3 composite, where all elements were driven in parallel, revealed that an upper bandwidth limit is defined by the pillar pitch rather then the pillar aspect ratio. Low acoustic impedance and absorption of the material forming the composite matrix support the approach of electroplating arrays. In this case, additional mechanical cutting suppressing mechanical cross-talk is not needed. Stacking composites for ultra-wide bandwidth are currently investigated and results will also be presented at the meeting.

[1] PzFlex, Weidlinger Associates,

079   **DEVELOPMENT OF AN ULTRASOUND RESEARCH PLATFORM.**

W.G. Scott[1]*, R.M. Schmitt[1], R.D. Irving[1].
[1]WinProbe Corporation, North Palm Beach, FL, USA.

A programmable ultrasound system has been developed where the researcher designs the operation by entering parameters into a PC which calculates transmission, beamforming, signal processing and scanconversion coefficients that are downloaded into a printed circuit board set containing the analog electronics and Field Programmable Gate Arrays (FPGA). The coefficients determine the operation of the instrument through increments of 10 nanoseconds during the acquisition of Radio Frequency (RF) acoustic lines and frames. The algorithms of the operations are designed in the MatLab environment and coupled through Simulink and System Generator into code that is downloaded from the PC to the FPGAs in seconds. Multiple memories are available for storage of the RF data facilitating correlation methods for tissue shift estimations in elastography.

The past year of development has been devoted to providing the researcher with a toolbox of programs that allow easy implementation of the functions of an ultrasonic scanner. An executive program provides communication via a USB2 link to all memories for downloading coefficients and uploading RF acoustic lines, processed lines or images. A C[++] based Graphical User Interface (GUI) provides the tools for visualizing and controlling the ultrasound functions. Program operations are scripted. Scripting provides the researcher with an automated, programmable repeatable method of set-up and operation.

The FPGAs provide a computational power in the multiples of trillions of operations per second exceeding the capacity of Digital Signal processors by several orders of magnitude.

Thirty-two acoustic channels are implemented on each set of printed circuit boards allowing multiples of boards to comprise a system.

The first of the installations are beginning to provide feedback on system performance. An example of B-mode imaging, demonstrating the re-configurable hardware using the Matlab-Simulink-System Generator linkage is given.

008 **AN ACTIVELY SHIELDED ELECTROMAGNETIC TRANSDUCER FOR MR–ELASTOGRAPHY DEDICATED TO MAMMOGRAPHY.**

Heike Hörning[1]*, Michael Dargatz[2], Ralph Sinkus[2].
[1]Philips Medical Systems, Hamburg, GERMANY; [2]Philips Research, Hamburg, GERMANY.

Dynamic MR-Elastography measuring the displacement field in steady-state requires a source of sinusoidal mechanical vibrations. These vibrations penetrate as longitudinal/transversal waves into the object of interest and represent the source of information for Elastography. A prerequisite for the technique to work properly is a mechanical transducer with several properties: a) oscillating monochromatically, b) providing phase stability and c) vibrating with an amplitude as large as possible to ensure optimal penetration of the wave [1]. Moreover, MR-Elastography additionally requires the absence of an electromagnetic stray-field, as this would lead to artifacts in the final MR-image. We present a novel design of such a transducer fulfilling all these requirements and being dedicated to the application of Mammography.

The typical patient position in MR-Mammography is prone with the breasts inside a dedicated MR-receiver coil. Mechanical compression plates are attached to each breast in feet-head direction (i.e. pushing each breast apart in the left-right direction) in order to obtain a similar pattern of compression as in X-ray Mammography. Both plates are attached to a frame which is mechanically connected to a "driving" coil (Figure 1a). The driving coil (driven by a sinusoidal current) is oriented such, that the coupling between its magnetic moment and the main magnetic field of the MR-scanner leads to oscillations in the feet-head direction. The driving coil is surrounded by a "shielding" coil, which exhibits the same magnetic moment but opposite in sign. This actively shields the stray-field of the driving coil. Each breast is mechanically excited by an independent transducer unit with all four coils (two driving coils and two shielding coils) electrically connected in series (Figure 1b). The phase of the two transducer units is opposite to minimize residual stray-field effects.

Figure 1c shows the spectra of the transducer unit as measured with an accelerometer at 85 Hz under different loading conditions. The resonance curve exhibits a prominent narrow peak at the driving frequency indicating little attenuation. An upper frequency at 255 Hz is visible. The resonance peaks neither shift nor change in amplitude under addition of a mechanical load (breast phantom of 1.5kg weight) [2]. Operating in addition, the MRE sequence is only adding white noise but not influencing the resonance properties of the transducer unit at all. The residual influence of the electromagnetic stray-field is assessed via MRE measurements carried out with a water phantom located inside the MR-receiver coil without mechanical contact to the compression plates. The local displacement field is measured in dynamic MRE typically at 8 time points equally distributed over one oscillator cycle. Figure 1d shows the corresponding values of the phase inside the water phantom with/without the transducer unit turned on. The phase errors as obtained with an actively vibrating unit are of similar order of magnitude (80 phase units of 2B*1000) as the normal noise within the phase. The presence of the active transducer leads to a DC of about 40 phase units. In general, measurements inside a phantom or the breast yield a span of typically 1000-2000 units and sometimes even include phase-wraps! *In-vivo* MRE measurements demonstrate a sinusoidal temporal behavior of the wave to very high precision.

References: [1] Braun et. al, MRM 50 : 220-222 (2003)   [2] Rossman et. al, 11th ISMRM 2003, p.1075
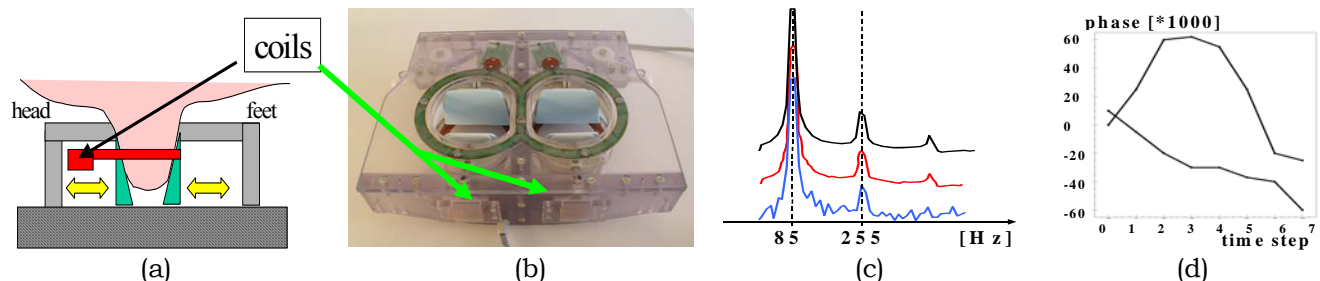

Figure1: (a) Sketch of the experiment. Mechanical excitation of the breast is done in feet-head direction via two plates (green triangles). These plates are connected to a frame which is driven by a coil (red rectangles). (b) Front view. (c) Spectra of one transducer unit with an excitation at 85 Hz: black line=no load, red line=with load, blue line=with load and MRE sequence running. (d) Phase values as measured inside a water phantom without mechanical contact to the transducer unit, but located between the compression plates (i.e. sensitive to stray-field effects of the coil units). Lower curve: phase values as measured via MRE without vibration (i.e. representing phase noise), upper curve: phase values with transducer unit working at a power level equal to the one used for *in-vivo* measurements.

002   **TRANSCUTANEOUS MEASUREMENT OF MYOCARDIAL VISCOELASTICITY.**

H. Kanai[1]*.
[1]Dept. of Electronic Eng., Tohoku University, Sendai 980-8579, JAPAN.

Introduction: The viscoelasticity of the myocardium is essential in the evaluation of diastolic function. However, the viscoelasticity of the myocardium has not yet been noninvasively measured *in vivo*. Based on our new finding that some impulse vibrations propagate along the interventricular septum (IVS) just after the aortic-valve (AV) closure timing (T0) (Kanai, H., et. al. Ultrasound Med Biol 2001;**27**:481), we developed a new method to measure the viscoelasticity of the myocardium. The results of this work are reported in this paper.

Methods: Based on our novel method (Kanai, H., et. al. IEEE Trans UFFC 1997;**44**:752, Kanai, H., et. al. Circulation 2003;**107**:3018), the vibrations are measured almost simultaneously at about 160 points set from the base to the apex along the IVS. Although the delay time of the impulse wave from the root of the aorta (Ao) to the apex is very small (several milliseconds), which cannot be measured by conventional equipment, the phase value of the measured impulse wave reveals the propagation of the impulse along the IVS. Its propagation speed is determined for each frequency component. By comparing the dispersion characteristics of the resultant speed with the theoretical speed of the guided shear wave (Lamb wave), the viscoelasticity of the IVS is noninvasively determined.

***In Vivo* Experimental Results:** For a healthy subject, the propagation situation of the impulse wave was clearly obtained. It propagates from the root of the Ao to the apex along the IVS as shown in Figure 1. As shown in the consecutively obtained motion pictures of Figure 1, just around the time of AV closure, a few impulses are radiated from the root of AV and propagated along the IVS. The delay due to the propagation of the steep impulse from the root to the apex-side is several milliseconds, which has not been recognised at all by any other clinical technique. By fitting the theoretical characteristics of the propagation speed for the Lamb wave to the measured instantaneous phase velocities $\{v_p\}$ from 10 to 100 Hz, the instantaneous Lame coefficients—elasticity parameter μ_1 and viscosity parameter μ_2—were determined. Since the phase velocity v_p approached zero for low frequency f_0, the shear elasticity μ_1 was negligibly small and the shear viscosity μ_2 corresponds to the gradient of the dispersion. For end-systole to the beginning of the isovolumic relaxation (IR) period, the instantaneous viscosity of the myocardium rapidly decreased from about 2.1 kPa·s to 0.1 kPa·s. This would be due to the rapid decrease in the LV inner pressure from about 120 to several mmHg, which is caused by relaxation of the myocardium. These viscosity values have same order of magnitude as those measured for canine hearts by Templeton, G. H., et al. (*J. Applied Physiology* 1974; **36**:123).

Conclusions: We found that the impulse is spontaneously actuated due to the closure of the Ao valve at the beginning of diastole, and it propagates along the IVS. By definitely detecting its propagation speed, we noninvasively determined the viscoelasticity characteristics of the IVS. This method offers potential for *in vivo* imaging of the tissue characteristics and diastolic function, which cannot be obtained by conventional echocardiography, CT, or MRI.
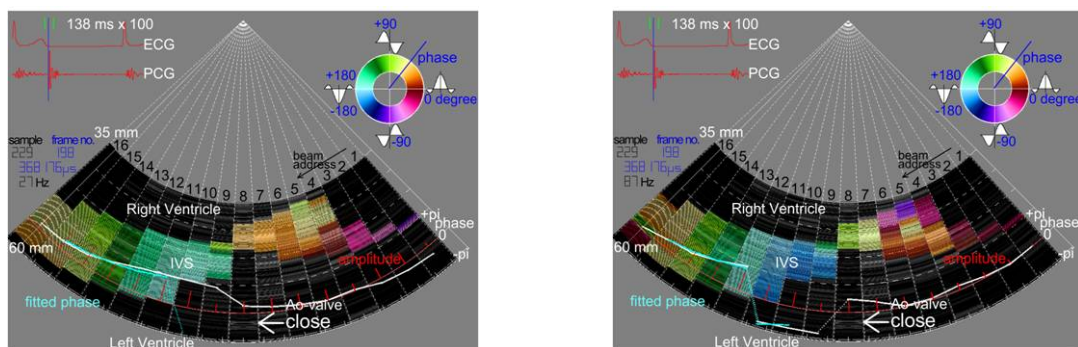

Figure 1: The spatial distribution of the colour-coded phase values of the measured wavelets just at the aortic-valve closure timing (left: 27 Hz, right: 87 Hz).

004   **ADAPTING THE LAGRANGIAN SPECKLE MODEL ESTIMATOR FOR ENDOVASCULAR ELASTOGRAPHY: THEORY AND VALIDATION WITH SIMULATED RADIO–FREQUENCY DATA.**

R. Maurice[1]*, J. Ohayon[2], G. Finet[3], G. Cloutier[1].
[1]University of Montréal Hospital Research Center, Montréal, Québec, CANADA; [2]Institut A. Bonniot, Lyon, FRANCE; [3]Claude Bernard University, Lyon, FRANCE.

Intravascular ultrasound (IVUS) is known to be the reference tool for pre-operative vessel lesion assessments and for endovascular therapy planning. Nevertheless, IVUS echograms only provide subjective information about vessel wall lesions. Since changes in the vascular tissue stiffness are characteristic of vessel pathologies, catheter-based endovascular ultrasound elastography (EVE) has been proposed in the literature as a method for outlining the elastic properties of vessel walls. In this paper, the Lagrangian Speckle Model Estimator (LSME) is formulated for investigations in EVE, i.e. using a polar coordinate system. The method was implemented through an adapted version of the Levenberg-Marquardt minimization algorithm, using the optical flow equations to compute the Jacobbian matrix. The theoretical framework was validated with simulated ultrasound RF data of mechanically complex vessel wall pathologies. The results, corroborated with Ansys finite element software, demonstrated the potential of EVE to provide useful information about the heterogeneous nature of atherosclerotic plaques.

017 **INVESTIGATION OF "RING RESONANT FREQUENCY" FOR ESTIMATION OF ARTERIAL ELASTICITY.**
Xiaoming Zhang[1], James F. Greenleaf[1]*.
[1]Department of Physiology and Biomedical Engineering, Mayo Clinic College of Medicine, 200 First Street SW, Rochester, MN, 55905, USA.

Background: According to recent statistics by the American Heart Association, cardiovascular disease (CVD) has been the number one killer in the United States. It has long been recognized that a high percentage of all cardiovascular disease is associated with a stiffening of the arteries. Increased stiffness of the arteries has recently gained acceptance as an independent risk factor for cardiovascular and many other diseases. Pulse wave velocity (PWV) is widely used for estimating the stiffness of an artery. The pulse wave velocity is directly related to the elastic modulus in the circumferential direction of the artery by the well known Moens-Korteweg equation (1878). Usually, PWV is measured using the "foot-to-foot" method. However, the "foot" of the pressure wave is not clear due to reflected waves and blood noise. PWV is an average indicator of artery stiffness between the two measuring points, and therefore does not identify local stiffness variations. From measured PWV, the diameter and thickness of the artery are needed to calculate the elastic modulus of the artery. We recently proposed producing a bending wave in the arterial wall using low frequency localized ultrasound radiation force and measuring the resulting wave velocity along the arterial wall [X. Zhang et al., Proc. 2003 Ultrason. Symp., 1883-1886], [X. Zhang et al., Proc. 2004 SPIE, Medical Imaging]. The wave velocity can be measured accurately over a few millimeters using this method.

Objective: We have now identified a "ring resonant frequency" that can be used for estimation of arterial elastic modulus. The objective of this paper is to address the theory and measurement techniques of this new method.

Methods: To generate the "ring resonance", a harmonic localized radiation force of ultrasound is remotely and non-invasively applied at the artery. The vibration response of the artery to this force is measured by optical or Doppler techniques. Three ring resonant modes are identified for estimation of the elastic modulus of the artery. These three modes contain basically "local" or "cross sectional" information of the artery. Therefore, "local" elastic modulus can be estimated.

Results: Experiments on ring resonant frequencies were carried out on a porcine artery. The length of the artery is 10 cm and its outer diameter is 6 mm. The artery was sealed in a gelatin phantom box. The artery was pressurized by internal saline at 70 mm Hg. The measurement results of the three resonant frequencies are, respectively, 356 Hz, 718 Hz, and 968 Hz. Estimation of the circumferential Young's modulus by the three measured frequencies are, respectively, 135 kPa, 137 kPa, and 125 kPa. The estimated modulus is very consistent with the three resonant frequency measurements. The values of these three estimations are well within the range of arterial elastic modulus from published papers.

Conclusions:
1) Three ring resonant modes are identified for estimation of the elastic modulus of arterial wall. Only one of the three resonant frequencies is required for estimating the Young's modulus of the artery.
2) The estimation of the Young's modulus of the artery only requires the diameter of the artery, but doesn't need the thickness of the artery which is difficult to measure with accuracy and precision.

029 **CHARACTERIZATION OF VULNERABLE CORONARY PLAQUE BY STRAIN POWER IMAGE.**
T Shiina[1]*, N Nitta[2], M Yamagishi[3].
[1]University of Tsukuba, Tsukuba, JAPAN; [2]National Institute of Advanced Industrial Science and Technology, Tsukuba, JAPAN; [3]National Cardiovascular Center, Osaka, JAPAN.

Pathological diagnosis of atherosclerotic coronary plaque is important for preventing plaque rupture, which can induce acute ischemic syndromes. Recent research on atherosclerotic plaque revealed that lipid rich plaque with a thin fibrous cap is vulnerable, i.e., susceptible to rupture. In order to prevent plaque rupture, it is necessary to discriminate among different types of plaque and detect vulnerable plaques. Elasticity imaging by intravascular ultrasound (IVUS) is a useful technique because the plaque components such as lipid, fibrosis and calcification can be directly assessed by the difference in tissue stiffness. We previously reported on the usefulness of intravascular elasticity (strain) imaging based on our method, which had a significant ability to precisely detect strain over a large dynamic range from RF data acquired during interventional procedures.

However, the spatial resolution and accuracy of intravascular strain imaging became blurred when catheter rotation induced by the heartbeat was severe. Therefore, for the purpose of obtaining more accurate assessments of any plaques under interventional conditions, we propose for the first time a method of strain power imaging by analyzing the time-varying strain profiles. For each point or ROI on the instantaneous strain images obtained between consecutive pairs of echograms, strain profiles as a function of time are obtained by two-dimensionally tracking the ROI. Next, the strain power near the heart beat frequency is calculated from the power spectrum of the time varying strain profiles over a single cardiac cycle. As a result, the high-resolution and stable strain power image is obtained.

The performance of this method was evaluated using coronary interventional data acquired at a frame rate of 30Hz during 20s using 240MHz sampling, with 1024 scan lines for an investigation depth of 5 mm. *In vivo* tests were conducted in several patients suffering from vulnerable coronary plaque with lipid-rich plaque. Results showed that strain power imaging can provide stable information on characteristics of plaque under interventional conditions, and has the ability to detect vulnerable plaque with high contrast.

(a) B-mode Image of coronary artery.

(b) Strain Power Image High strain power region at the surface adjacent to low-strain region is prone to vulnerable plaque.
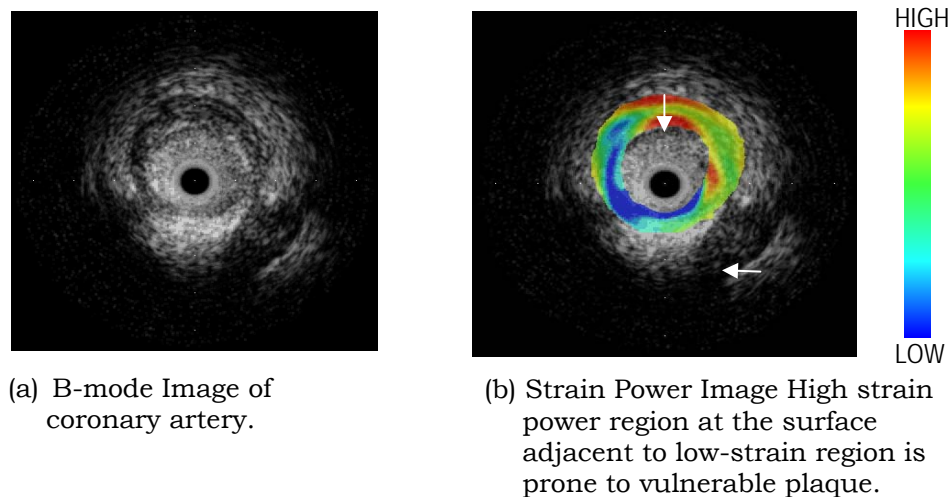
Figure 1: An example of strain power imaging of coronary plaques.

037 **CLINICAL EVALUATION OF 3D INTRAVASCULAR ULTRASOUND PALPOGRAPHY FOR VULNERABLE PLAQUE DETECTION.**
Antonius F.W. van der Steen[1,2]*, Johannes A. Schaar[1,2], Frits Mastik[1], Chris L. de Korte[3], Patrick W. Serruys[1].
[1]Biomedical Engineering, Thorax Centre, Erasmus MC, Rotterdam, The NETHERLANDS; [2]Interuniversity Cardiology Institute of the Netherlands, Utrecht, The NETHERLANDS; [3]University Medical Centre, Nijmegen, The NETHERLANDS.

Background:
3D palpography is a technique that is capable of measuring radial strain in an atherosclerotic plaque. The development of this technique has been reported at this conference. It had been hypothesizes and has been shown *in vitro* that high strain spot in plaques are indicators for vulnerable atherosclerotic plaques. In this paper, the first clinical experience is described. Reproducibility in patients and the relation between number of high strain spots and clinical presentation of the patient are discussed.

Methods:
3D palpograms are acquired in patients during percutaneous transluminal coronary angioplasty (PTCA) procedures. For this goal, a Volcano InVision echo apparatus was equipped with an rf-output. Intravascular rf-ultrasound data are acquired with a PC based acquisition system. Frames acquired at end-diastole are taken to determine the palpograms. A pull back of 1 mm/s was used to acquire data of a full segment of a vessel in 3D. The systemic pressure is used to strain the tissue. This strain is determined using cross-correlation analysis of sequential frames.

In 12 patients a total of 14 3D palpograms were acquired twice at the same location. Palpograms were displayed as map representing the continuous strain distribution of the vessel wall. The maps were subdivided in regions covering 3 mm by 22.5 degrees. The median strain of the corresponding regions of first and the second recording were compared.

Furthermore, we performed 3 D palpography in 55 patients that were divided into three groups based on clinical presentation (stable or unstable angina, acute myocardial infarction). In patients with myocardial infarction, the non-culprit vessel was studied. The number of high strain spots, which are related to vulnerable plaques, are counted and related to clinical appearance.

Results:
For reproducibility 512 regions were compared using orthogonal regression. The R^2 of the model is 0.89 with a $p < 0.0001$, revealing a good reproducibility.

Stable patient group (n=19) had 0.7 ± 0.5 high strain spots, the unstable group 1.7 ± 0.4 and the post myocardial infarction 2.0 ± 0.8. There was a significant difference between the stable vs. unstable group (p<0.001) and stable vs. post MI group (p<0.0001). No difference was seen between the unstable group and post MI group (p<0.056).

Conclusion:
Palpography can be used to assess vulnerable plaques in human. This pilot study revealed a clear association between clinical presentation and the amount of vulnerable plaques. However, additional validation has to be performed to assess the predictive value of the technique to identify vulnerable patients.

051 **ROBUST ASSESSMENT OF ARTERIAL PLAQUE COMPOSITION *IN VIVO* USING A PARAMETRIC PLAQUE MODEL–BASED YOUNG'S MODULUS RECONSTRUCTION METHOD.**
Radj A. Baldewsing[1]*, Frits Mastik[1], Johannes A. Schaar[1,2] and Antonius F. W. van der Steen[1,2].
[1]Biomedical Engineering, Thorax Centre, Erasmus MC, Rotterdam, The NETHERLANDS; [2]Interuniversity Cardiology Institute of the Netherlands, Utrecht, The NETHERLANDS.

Background and Goal: Assessment of vulnerable plaque material composition by calculating a modulus elastogram, i.e., image of the Young's modulus, allows for monitoring of atherosclerosis. Intra-Vascular UltraSound (IVUS) elastography generates radial strain elastograms of arterial cross-sections. We developed a method to reconstruct a modulus elastogram from a strain elastogram. This paper (a) describes the reconstruction of a modulus elastogram from an *in vivo* measured strain elastogram of a patient using that method, and (b) evaluates the method's robustness by quantifying the effect of geometry and material properties of plaque components and catheter position upon a reconstruction.

Materials: Data were acquired from a non-culprit artery in a patient referred for Percutaneous Transluminal Coronary Angioplasty (PTCA); this artery contained a non-obstructing plaque.

Methods: From this patient, a compounded *in vivo* strain elastogram was processed (pressure-differential 1 mmHg and strain < 2%) using radio-frequency data obtained with a 20 MHz phased array IVUS catheter (Volcano Therapeutics, Inc.). Compounding was done to increase the signal-to-noise ratio and only in conjunction with strain elastograms obtained during the diastolic phase of a cardiac cycle where catheter motion was minimal. Reconstruction was done by a minimization algorithm. It minimizes the Root-Mean-Squared (RMS) error between the strain elastogram calculated with a Parametric Finite Element Model (PFEM) representation of a vulnerable plaque, and a measured strain elastogram by iteratively updating the PFEM geometry and material parameters. These PFEM parameters define a media region containing a lipid-pool covered by a cap; these three regions have a constant Young's Modulus (YM) and their borders are defined by circles. A reference plaque was defined as the modulus elastogram that was reconstructed from the strain elastogram measured *in vivo*. This reference plaque was then used to simulate different strain elastograms, by varying the geometry and material properties of its plaque components (i.e., plaques were defined with small/large, thin/thick, eccentric, or soft/stiff lipid-pool and/or cap) and used catheter position (i.e., towards and opposite the plaque, and near a plaque shoulder, all with 50% catheter eccentricity). Strain noise (N_i) was added to each strain value (S_i) in a strain elastogram; each N_i is drawn from a normal distribution with mean 0 and standard deviation = $0.2*S_i+0.04$. These coefficients are obtained from strain data measured in patients. Robustness was evaluated by comparing each reconstructed modulus elastogram with the corresponding reference plaque: the agreement in size and shape between a reconstructed plaque component region and corresponding reference plaque component region was quantified by their percentage of Area Overlap (AO); the disagreement in their YM value was quantified by their Relative Error (RE).

Results: The modulus elastogram of the patient's plaque revealed a media area (YM 111 kPa) containing a large lipid-pool (YM 1 kPa) covered by a stiff cap (YM 118 kPa). Vulnerable plaques (e.g., those with intrinsic high strain and strain-gradients) could be correctly reconstructed from their simulated strain elastogram(s), and resulted in the following averages ± standard deviation (n=21): lipid-AO = 93% ±6%, cap-AO = 89% ±6%, YMlipid-RE = 26% ±19%, YMcap-RE = 23% ±5% and YMmedia-RE = 6% ±4%; some reconstructions resulted in a slightly 'thinner and stiffer' or 'thicker and softer' cap. However, for non-vulnerable plaques it was not possible to compute a correct modulus elastogram. This occurred when the cap was thick and stiff or when the modulus ratio (i.e., YMcap/YMlipid) was low. Using 2 or 4 times higher noise-model coefficients only modestly compromised the computation of a correct modulus elastogram.

Conclusions: We described how to obtain a plaque composition image from an *in vivo* measured strain elastogram using the reconstruction method. This seems a robust method for assessing vulnerable plaque material composition, since the results show that the primary factors that change the information in a strain elastogram still allow the reconstruction of a correct modulus elastogram. These results support the use of this method in the monitoring of atherosclerosis *in vivo*.

067 **A NEW METHOD FOR TWO–DIMENSIONAL MYOCARDIAL STRAIN ESTIMATION BY ULTRASOUND: A COMPARISON WITH SONOMICROMETRY *IN VIVO*.**
Stian Langeland[1], Jan D'hooge[2]*, H. Alex Leather[3], Piet Claus[1], George R. Sutherland[1], Patrick F. Wouters[3] and Bart Bijnens[1].
[1]Dept. of Cardiology, [2]Dept. of Electrical Engineering, [3]Dept. of Anesthesiology, Catholic University Leuven, Leuven, BELGIUM.

Introduction: One-dimensional strain (S) and strain rate (SR) imaging have been shown to be angle dependent. Fully resolved two-dimensional (2D) strain would solve this problem. Therefore, a new methodology for estimation of 2D strain based on 2D radio frequency (RF) processing has been developed in our lab. It has been shown earlier to give accurate angle independent strain values in an *in vitro* setup.

Aim: To validate this new methodology in the *in vivo* setting.

Methods: In 5 open chest sheep, ultrasound (US) RF data were acquired in a parasternal long axis view using a Toshiba PowerVision 6000 equipped with an RF interface for research purposes. Myocardial radial (R) and longitudinal (L) strains were simultaneously estimated in the inferolateral wall using the new methodology from single RF data sets. Four segment-length sonomicrometry crystals (SM) were placed in a tetrahedral configuration just lateral to the imaging plane giving a continuous reference for the L and R strains. After baseline (BL) acquisitions, the deformation was modulated by 1) esmolol infusion (ES), 2) dobutamine infusion (DOB) and 3) inducing ischemia by occlusion of a distal branch of the circumflex coronary artery. Peak systolic strains (Smax) were compared by means of linear regression and the correlation coefficient.

Results: For both the R and L Smax strong correlations were found between the US and the SM measurements (r = 0.95 and r = 0.98 respectively, p<0.001). Example strain curves are given in Figure 1 (a) and (b) for BL and ISC respectively.

Conclusion: Simultaneous estimation of 2D myocardial L and R strain using US RF tracking showed to be a robust method in an *in vivo* setting. Myocardial strain could thus be assessed independent of insonation angle.
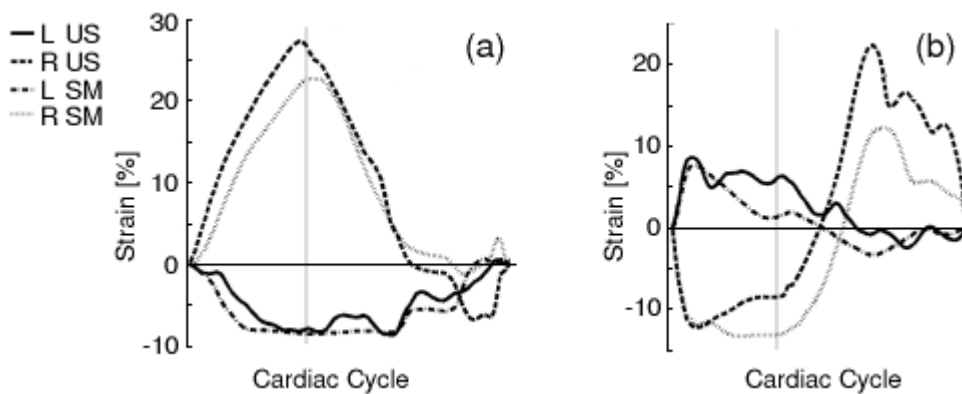

Figure 1: Examples of strain curves for BL (a) and ISC (b).

087   **TWO–DIMENSIONAL FUNCTIONAL INFORMATION CAN BE USED FOR AUTOMATED LEFT-VENTRICULAR SEGMENTATION.**

Elisa E. Konofagou[1]* and Todd C. Pulerwitz[2].
[1]Department of Biomedical Engineering, Columbia University, New York, NY, USA; [2]Department of Cardiology, Columbia Presbyterian Hospital, New York, NY, USA.

Introduction:
In echocardiography, left-ventricular (LV) myocardial abnormalities are usually characterized by dyskinetic or akinetic wall motion and/or poor contractile properties. In order to determine the first characteristic, the ventricular cavity is often manually traced by a cardiologist at different steps of the cardiac cycle and an average estimate of the wall motion around the ventricular cavity highlights the potential abnormal regions. This is because automated segmentation analysis of sonograms has often been shown futile due to the high speckle noise. The second characteristic can be inferred by using a variety of different techniques, such as Tissue Doppler, Strain Rate Imaging and Myocardial Elastography [1]. In this paper, we determine whether Myocardial Elastography can be used to assist in the automated segmentation of the left ventricle. The hypothesis is that blood and muscle scatterers have distinct motion and deformation characteristics that allow for their successful separation when motion and deformation are imaged using Myocardial Elastography.

Methods:
Normal, human volunteers were scanned using a 2-MHz phased array and a Terason ultrasound scanner (Teratech, Inc., Burlington, MA) both in short- and long-axis views of the left ventricle. RF data were acquired over three cardiac cycles during natural contraction of the myocardium. The maximum scanning depth was 15 cm with a sampling rate of 20 MHz and an associated frame rate of approximately 20 frames/s. Corrected (or, recorrelated) two-dimensional (i.e., axial and lateral) displacement and strain estimates were imaged after using a modified, reference-independent version of a previously described technique [2] that utilizes interpolation, cross-correlation and correction techniques to decouple and estimate the two main motion components. Axial and lateral, motion, deformation and correlation coefficient images were utilized and compared in order to segment the left-ventricular wall, i.e., separate the cavity region from the myocardial wall.

Results:
In both short-axis and long-axis views, during diastole, the elastograms were shown to highlight the displacement difference between the LV wall and cavity through the well-known "underline effect" that results from high gradients in the displacement. During systole, the elastograms were very noisy, mainly limited by the low frame rate used. On the other hand, during both diastole and systole, axial and lateral correlation images indicated an approximately twice higher average correlation coefficient in the LV wall compared to that inside the cavity. Contour plots of thresholded correlation coefficients, therefore, successfully delineated the borders of the LV cavity throughout all three cardiac cycles.

Discussion:
Even at low frame rates, two-dimensional elastographic information was shown to be useful in the automated differentiation between the LV wall and the LV cavity based on the fact that the cavity will deform (or, decorrelate) in a different fashion to the myocardial wall. Compared to motion and deformation, the use of correlation coefficients was shown to be the most successful in underlying the highly decorrelating cavity and assisting a simple segmentation technique to generate automated contours throughout several full cardiac cycles in two distinct views. It is expected that higher frame rates will increase the elastographic precision in systole and, thus, allow for higher resolution necessary for refined, automated tracing and better comparison to manual tracings.

References:
[1] Konofagou E.E., D'hooge J. and Ophir J., *IEEE-UFFC Proc Symp,* 1273-1276, 2000.
[2] Konofagou E.E. and Ophir, J., *Ultras Med Biol 24(8),* 1183-1199, 1998.

020   **SIMULATION STUDY OF RECONSTRUCTION OF SHEAR MODULUS, DENSITY, AND POISSON'S RATIO DISTRIBUTIONS.**

Chikayoshi Sumi[1]*.

[1]Department of Electrical and Electronics Engineering, Faculty of Science and Technology, Sophia University, Tokyo 102-8554, JAPAN.

Shear modulus may be an important parameter for differentiating malignancies of normal soft tissues, e.g., in the breast, liver, kidney etc. With such consideration in mind, we previously proposed a reconstruction method of shear modulus distribution of tissues *in vivo* from only measured static strain tensor data, where the Poisson's ratio is assumed to have a known constant value. Arbitrary mechanical sources are assumed to exist outside the ROI. Furthermore, at the last conference [1], we reported an extended reconstruction method to reconstruct the distributions of the Poisson's ratio and density as well. In actual *in vivo* tissues, since the Poisson's ratio is also inhomogeneous, the extended method allows improvement of the accuracy of shear modulus reconstruction. Moreover, by handling dynamic tissue deformation, the extended reconstruction method also yields reconstructions of density distribution simultaneously.

The feasibility of the method is verified by simulations, where the deformation data is obtained by using the successive over-relaxation (SOR) method. A simulated cubic phantom (50.0 mm on a side) was uniformly vibrated in the axial direction (x-axis) with a frequency of 1.0 Hz (displacement of 0.25 mm). The phantom includes a spherical inhomogeneous region at a depth x = 25.0 mm with 5-mm radius. The shear modulus value of the inhomogeneous region is set 10 times higher than that of the surrounding medium, i.e., $1.0 \vee 10^6$ N/m^2 versus $1.0 \vee 10^5$ N/m^2, and the Poisson's ratio is uniformly set at 0.47. A cubic ROI is used (30.0 mm on a side) having an inhomogeneous region in the central part. Using the resultant strain tensor data from the ROI, 3D reconstruction is performed under the assumption of a 3D stress distribution. The reference region is set at the upper surface of the ROI.

Figure 1a shows 3D the shear modulus reconstruction (elevational position z = 25.0 mm), while Figures 1b and 1c respectively show 3D reconstructions of the Poisson's ratio and the density (z = 25.0 mm). The bulk modulus can also be reconstructed (Figure 1d). These reconstructions were quantitatively obtained.
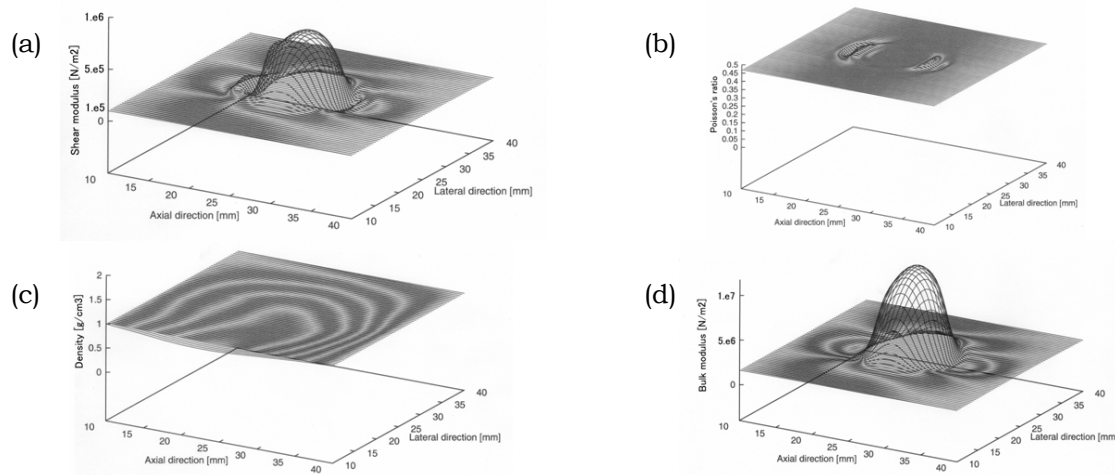

Figure 1: Simulation of reconstruction of shear modulus, Poisson's ratio, and density. Reconstructions were obtained under the assumptions of 3D (x,y,z) stress distributions on a simulated cubic phantom of 50.0 mm sides including a 10 times higher shear modulus spherical region at a depth x = 25.0 mm with 5-mm radius ($1.0 \vee 10^6$ N/m^2 versus $1.0 \vee 10^5$ N/m^2). This phantom was vibrated in the axial direction (x-axis) with a frequency of 1.0 Hz (displacement of 0.25 mm). Cubic ROIs (30.0 mm on a side) are set at the central part of the inhomogeneous spherical region. The reference region is set at the upper surface of the ROI. (a), (b), (c), and (d) are respectively 3D reconstructions in the plane z = 25.0 mm of shear modulus, Poisson's ratio, density, and bulk modulus.

Reference: [1] C. Sumi, Proc. of the 2nd Int'l. Conf. on the Ultrason. Meas. and Imag. of Tissue Elasticity, p. 43, '03.

* indicates Presenter

031 **INFLUENCE OF VISCOSITY ON SHEAR WAVES INDUCED BY THE ACOUSTIC RADIATION FORCE.**

Jeremy Bercoff[1], Mickael Tanter[1], Mathias Fink[1]*.
[1]Laboratoire Ondes et Acoustique, E.S.P.C.I, C.N.R.S. (UMR 7587), Paris, FRANCE.

In this work, a 3D analytical formulation of the mechanical Green's function in a viscoelastic medium is derived and presented. Based on a Voigt model to take into account viscoelasticity, this mathematical formulation is validated experimentally using the supersonic shear imaging technique (SSI). Taking benefit of the ultrasonic remote generation of a moving shear source radiating low-frequency shear waves in the medium, this technique has been studied and validated for soft tissue elasticity mapping in previous works. It is shown here that the spatial and temporal shape of shear waves induced in soft tissues using SSI can be accurately modeled with the viscoelastic Green's function. The influences of important parameters such as viscosity, elasticity, or diffraction on the shear wave shape are carefully studied and discriminated. In a second part, taking advantage of the previous modeling, the inverse problem consisting of recovering shear elasticity and viscosity is presented and validated using the Green's function-based simulation tool. Experiments on tissue-mimicking phantoms presenting different viscoelastic properties are presented. The influence of out-of-plane shear propagation on the inversion algorithm is discussed.

033   **THE INVERSE PROBLEM OF SHEAR WAVE PROPAGATION: RECOVERING BOTH SHEAR MODULUS AND VISCOSITY IMAGES FROM SUPERSONIC SHEAR IMAGING DATA.**

Jeremy Bercoff[1], Mickael Tanter[1]*, Mathias Fink[1].
[1]Laboratoire Ondes et Acoustique, E.S.P.C.I, C.N.R.S. (UMR 7587), Paris, FRANCE.

During the last six years, the ability of ultrafast imaging scanners to image the transient shear wave propagation in human tissues has been investigated extensively by our group. These shear waves can be generated either by mechanical vibrators located at the surface of the body (transient elastography) or remotely deeply into tissues using the acoustic radiation force concept (supersonic shear imaging). From the movie of these propagating shear waves, it is possible to recover the local elastic properties of soft tissues. To date, we had only derived a local inverse problem that allowed us to recover shear modulus images of the region of interest. Here, we propose to take into account shear viscosity in the formulation of the inverse problem. Simulations based on a 3D Green's formalism as well as simulations based on 3D finite differences time domain (FDTD) are used to validate the ability of our local inversion to recover both shear modulus and viscosity in non-noisy or noisy conditions. Finally, experiments conducted in tissue mimicking phantoms containing hard inclusions and viscous inclusions allowed us to demonstrate the potential of the inversion technique. A complete map of the shear viscosity can be recovered with good resolution and contrast. The influence of various parameters such as ultrasonic frequency, shear diffraction effects, noise filtering are discussed.

097   **ENHANCING THE PERFORMANCE OF MODULUS ELASTOGRAMS.**

Marvin M. Doyley[1]*, Seshadri Srinivasan[2,3], Ziji Wu[1], Brian S. Garra[4], Jonathan Ophir[2,3].
[1]Department of Radiology, Dartmouth Medical School, Hanover NH, USA, [2]The University of Texas Medical School, Department of Radiology, Ultrasonics Laboratory, Houston, TX, USA; [3]University of Houston, Electrical and Computer Engineering Department, Houston, TX, USA; [4]University of Vermont College of Medicine–Fletcher Allen Health Care, Burlington, VT, USA.

Elastography is an emerging imaging modality that images the intrinsic mechanical properties of tissue by ultrasonically imaging externally or internally-induced local tissue strains. Strain by itself represents an incomplete measure of tissue elasticity. Furthermore, artifacts are often incurred when strain elastograms are interpreted as modulus elastograms based on the assumption of stress uniformity. Despite these limitations, various groups, including ours, have demonstrated that elastographic images that possess good spatial and contrast resolution can be produced within the clinic using strain-based elastographic imaging.

It is generally envisaged that a better approach to elastographic imaging is to compute modulus elastograms from ultrasonically measured internal tissue displacements by solving the inverse elasticity problem. Although this approach to elastographic imaging generally takes proper account of the internal stress distribution when computing modulus elastograms, the technique is often fraught with problems due to the *ill-posed* nature of the inverse elastographic problem. Consequently, the performance (spatial and contrast resolution) of modulus elastograms is often inferior to strain elastograms, especially when reconstruction is performed under physiological conditions.

Consequently, a constraining reconstruction technique was developed to improve the performance of an iterative inversion technique. Reconstructed values were constrained using *a-priori* information regarding the size and location of suspicious breast tissues that were obtained from strain elastograms. Performance was evaluated using a) gelatin based phantoms, b) excised kidney and prostate tissues, and c) three breast cancer patients. Figure 1 shows an example of modulus and strain elastograms obtained from a phantom containing four circular inclusions. Note that all four inclusions are discernible in the strain elastogram (Figure 1A). Despite the complexity of the phantom, the inclusions are discernible in the modulus elastogram (Figure 1B) computed using the unconstrained inversion technique; however, it apparent that spatial resolution of modulus elastogram is inferior to that of the strain elastogram. Note that the spatial resolution of the modulus elastograms was substantially improved by constraining the reconstruction procedure (see Figure 1C). This was also observed in the *in vivo* and *in vitro* studies. It was concluded that the constrained inversion technique performed sufficiently well to warrant more in-depth clinical evaluation.

A   B   C
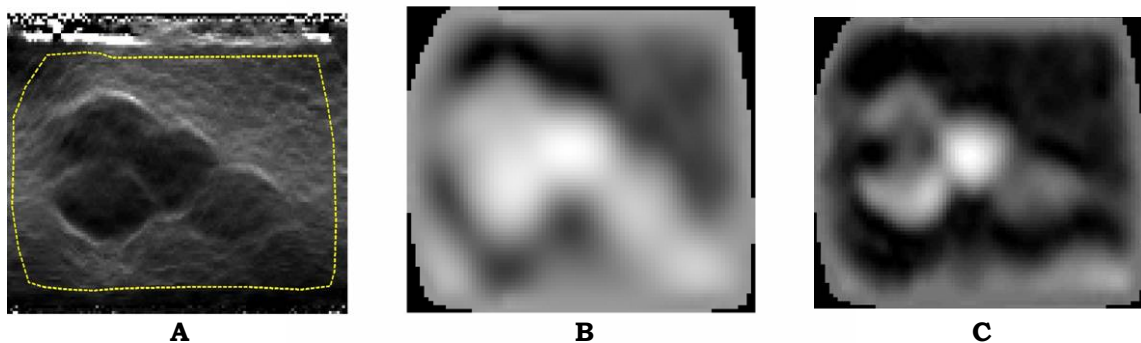
Figure 1: Strain (Figure 1A) and modulus (Figure 1B & Figure 1C) elastograms obtained from a phantom containing four cylindrical inclusions. Elastogram computed using the unconstrained and constrained reconstruction techniques are shown in (Figure 1B) and (Figure 1C), respectively. The broken yellow lines shown in Figure 1A denote the reconstruction field of view.

084 TRANSIENT ELASTOGRAPHY: ALGORITHMS AND MODELS.

Joyce McLaughlin[1]*, Daniel Renzi[1], Jeong-Rock Yoon[1], Alexander Glasman[1].
[1]Rensselaer Polytechnic Institute, 110 8th Street, Troy, NY, USA.

In transient elastography a low central frequency pulse is initiated either on the surface of the body or, using supersonic shear imaging, along a line interior to the body. A propagating wave, with a front, is produced and measured by an ultrafast ultrasound based measurement system developed in the laboratory of M. Fink. We consider models of the tissue and the experiment. We develop and report on the implementation of algorithms that find shear wave speed changes, including directionally dependent changes present in anisotropic media, from propagating fronts. Data is from experiments performed in the laboratory of Mathias Fink.

094   **IMAGING LOCALIZED VISCOELASTIC PROPERTIES USING HARMONIC MOTION IMAGING.**

Elisa E. Konofagou[1]* and Timothy P. Harrigan[2].
[1]Department of Biomedical Engineering, Columbia University, New York, NY, USA; [2]Exponent, Inc., Framingham, MA, USA.

Introduction:
All tissues are viscoelastic [1]. However, most elasticity imaging techniques make the assumption that the tissues are purely elastic so that the measured mechanical response can be more directly associated to the elastic modulus of the tissue. Harmonic Motion Imaging (HMI) [2] is a technique that applies an oscillatory radiation force in a small tissue region (on the order of a beamwidth) and images the resulting localized harmonic displacement. In this paper, we investigate the potential of the technique to determine both the elastic modulus and the viscous damping coefficient by comparing the amplitude and phase of the resulting displacement to those of the applied radiation force.

Methods:
Finite-element simulations (FEA) of a 2D, plane strain three-layered model were generated on Algor software (Algor, Inc, Pittsuburgh, PA). The Young's modulus of the middle layer was allowed to change relative to the adjacent layers of fixed modulus equal to 10kPa. In order to simulate the experimental application of HMI, a sinusoidal force of frequency equal to 200Hz sequentially on each node of the FEA model. Simulated ultrasonic RF data were generated for each step of vibration and for each node using a convolutional model and the calculated displacements. Crosscorrelation techniques using a 2mm window and 80% overlap were applied on the RF data in order to image the incremental displacement in the direction of the applied force across the model. Eight different cases were studied; four of different moduli (5-40kPa) and same relative viscous damping coefficient equal to 10 while the other four had different damping coefficients (0-10) and same modulus (40kPa). The mean-squared amplitude and the phase shift of the estimated displacements relative to the applied force were studied in each FEA case in order to identify their distinct viscoelastic properties.

Results:
In M-mode HMI images, the amplitude of the displacements decreased exponentially with higher modulus and higher damping coefficient. However, only the increase of the viscous coefficient was shown to lead to a positive phase shift on the order of 50µs between the input radiation force and the resulting displacement. The estimated effect of the local viscous coefficient on the displacement amplitude was then removed so that the latter only indicated the effect of the change in modulus. Spatial HMI images were then generated indicating the regions of different elastic modulus and different viscous coefficients in all eight cases.

Discussion:
HMI was shown capable of mapping local viscoelastic properties through *a priori* knowledge of the applied radiation force and the estimated localized harmonic displacement. The localized oscillatory response of the tissue allowed for successful decoupling of the elastic modulus and the viscous damping coefficient and, thus, for the correct estimation and mapping of both properties. Current investigations consider the imaging quality of mapping viscoelastic responses and the experimental verification of these results using viscoelastic phantoms.

References:
[1] Fung Y.C., Biomechanics, Second Edition, Springer-Verlag, New York, 1993.
[2] Konofagou E.E. and Hynynen, K., Ultras Med Biol, 1405-1413, 2003.

089 POISSON'S RATIO IMAGING AND POROELASTOGRAPHY IN BIOLOGICAL TISSUES: A FEASIBILITY STUDY.

Raffaella Righetti[1,2]*, Jonathan Ophir[1,2] and Thomas A. Krouskop[1,3].
[1]The University of Texas Medical School, Department of Radiology, Ultrasonics Laboratory, Houston, TX, USA; [2]University of Houston, Electrical and Computer Engineering Department, Houston, TX, USA; [3]Baylor College of Medicine, Department of Physical Medicine and Rehabilitation, Houston, TX, USA.

Objective: To investigate the feasibility of imaging the Poisson's ratio and the time-dependent behavior of homogeneous and non-homogeneous phantoms and biological tissues.

We have recently demonstrated the feasibility of generating both Poisson's ratio elastograms, which convey information about the local compressibility within the imaged material, and poroelastograms, which convey information about the time-dependent behavior of the imaged material, in uniform porous phantoms. This was demonstrated through experiments, simulations and independent mechanical tests. In this paper, we extend the previous study to investigate the feasibility of Poisson's ratio imaging and poroelastography to non-uniform phantoms and biological tissues.

Methods: Poisson's ratio elastograms and poroelastograms were generated in non-homogenous porous phantoms, obtained by combining materials with different elastic and permeability properties, and in porcine muscle samples *in vitro*. The instantaneously-acquired Poisson's ratio elastograms were aimed at depicting the short-term behavior of the samples. Therefore, the spatial variations in the instantaneous Poisson's ratio elastograms might be attributable either to very fast fluid translocation phenomena or to an inherently non-homogenous distribution of the local compressibility of the samples. The poroelastograms obtained from samples under sustained compression were aimed at characterizing the long-term behavior of the materials. In this case, interstitial fluid flow and subsequent viscoelastic effects were determined primarily by the intrinsic permeability of the porous materials.

The sample materials used for the experiments were previously characterized through independent mechanical measurements. Simulations were also performed, which, together with the mechanical measurements, were used in order to predict and better interpret the experimental results.

Results: Figure 1 shows the generation of a Poisson's ratio elastogram from a pair of lateral strain and axial strain elastograms obtained from a porcine muscle specimen with high water holding capacity (DFD). An optical image of the cut specimen at approximately the same plane as the imaged plane is shown as well. A corresponding poroelastogram taken from the same specimen is shown in Figure 2. Note the subtle changes that occur in the poroelastogram with time, possibly due to the high water holding capacity of this tissue.

Conclusions: On a local basis, it appears from our preliminary results that at least some tissues respond nearly instantaneously as a spatially complex structure, where some areas are incompressible, while others exhibit various degrees of compressibility, which may be related to perfusion effects. When subjected to a more sustained compression, the time-dependent mechanical behavior of a tissue is related to the tissue water content and to the freedom with which this water can move within the tissue, which may in turn be related to diffusion effects. These preliminary results also show that Poisson ratio elastography and poroelastography may have the potential to image the diffusion and perfusion characteristics of tissues.
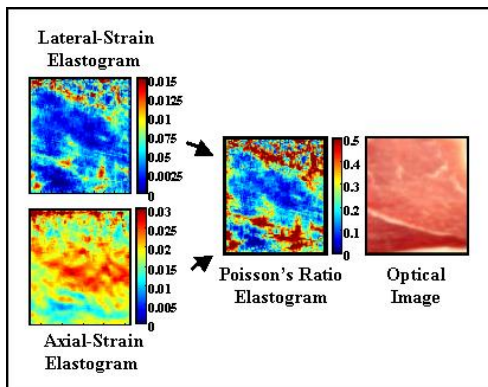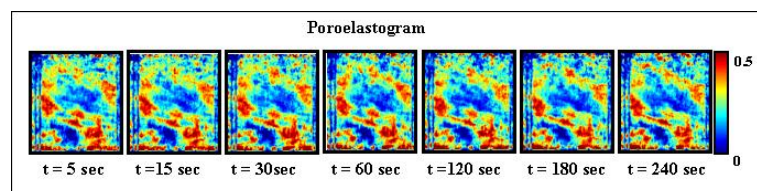

Figure 1

Figure 2

088   **A METHOD FOR GENERATING PERMEABILITY ELASTOGRAMS USING POROELASTOGRAPHY.**

Raffaella Righetti[1,2]*, Jonathan Ophir[1,2] and Thomas A. Krouskop[1,3].
[1]The University of Texas Medical School, Department of Radiology, Ultrasonics Laboratory, Houston, TX, USA; [2]University of Houston, Electrical and Computer Engineering Department, Houston, TX, USA; [3]Baylor College of Medicine, Department of Physical Medicine and Rehabilitation, Houston, TX, USA.

Objective: To investigate the feasibility of using poroelastography for imaging the permeability of porous media. Since permeability is one of the fundamental parameters that control the time-dependant mechanical behavior of porous media, a method that would allow its local estimation may be of value for better characterizing the mechanical behavior of porous materials and tissues and might even be useful for diagnosis of some pathological conditions, such as edema.

Methods: Permeability elastograms were generated for homogenous porous phantoms with different elastic and permeability properties, and for non-homogenous porous phantoms obtained by combining different poroelastic materials. The sample materials used for the poroelastographic experiments were previously characterized through independent mechanical measurements. The drained elastic modulus and Poisson's ratio of the samples were estimated using an Instron testing device and basic geometrical considerations. In order to mechanically characterize the time-dependent behavior of the samples, stress relaxation experiments were also performed on selected samples. Finally, the coefficient of permeability of the sample materials was estimated using standard soil mechanics tests.

The method used to create permeability elastograms involved first the generation of poroelastograms from the porous samples under sustained compression (for more details on the procedure for acquiring and generating poroelastograms, we refer to Righetti et al. 2004). Then, the permeability of the sample was estimated from the application of a biphasic theoretical model to the time history of each pixel in the poroelastogram. For comparison, the same methodology was also applied to the stress-relaxation curves obtained from the same sample materials using indentation. In this case, the procedure was applied to the normalized axial stress history obtained from each sample during the relaxation phase.

Results: Figure 1a-c shows (a) poroelastogram (depicting the evolution of the local Poisson's ratio vs. time after compression), (b) global stress-relaxation curve, and (c) corresponding permeability elastogram of a homogeneously porous phantom. The averaged permeability as obtained from the permeability elastogram was $3.06*10^{-9} \pm 2.1*10^{-9}$ [m^4/Ns]**.** This value was found to be in good agreement with the permeability value as estimated from the corresponding stress relaxation test.

Conclusions: The results suggest that poroelastography may have significant potential for imaging the permeability of media characterized by different poroelastic properties, provided that a theoretical model whose assumptions are in agreement with the poroelastographic experimental conditions is available.

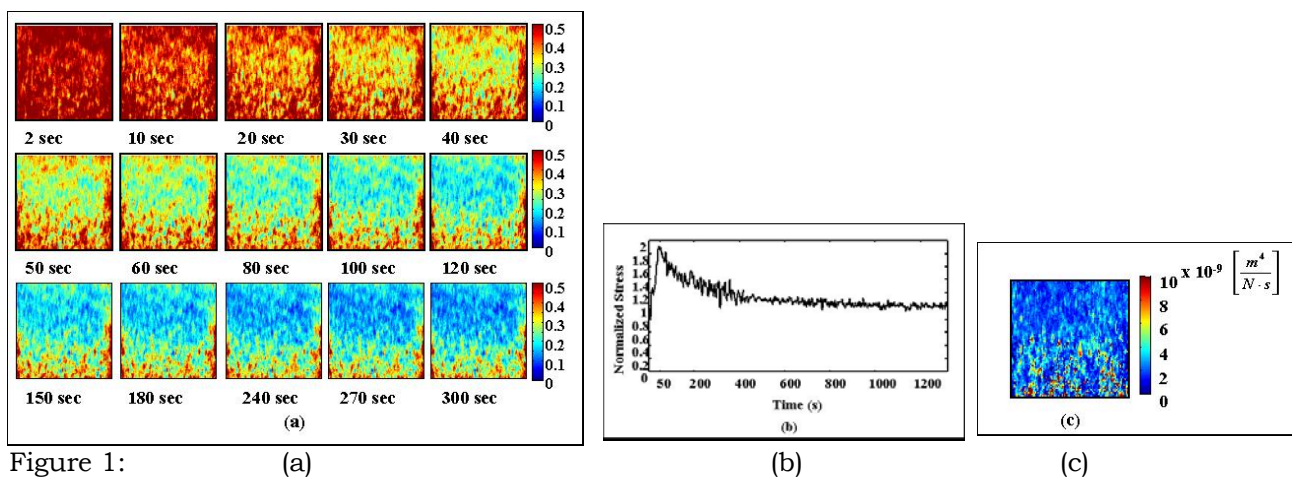Figure 1:   (a)   (b)   (c)

Reference:
Righetti R, Ophir J, Srinivasan S, Krouskop TA. The feasibility of using elastography for imaging the Poisson's ratio in porous media. Ultras. Med. Biol., vol. 30 215-228, 2004.

066 TOWARDS A MODEL–BASED POROELASTIC IMAGING METHOD.

Gearóid Berry[1]*, Jeffrey Bamber[1], Naomi Miller[1].
[1]Joint Department of Physics, Institute of Cancer Research and Royal Marsden NHS Trust, Downs Road, Sutton, Surrey, SM2 5PT, England, UK.

Poroelastic materials belong to a class of viscoelastic materials that are composed of two phases: a sponge-like, elastic, porous, permeable, solid phase and a liquid phase that inhabits the pores of the solid matrix. The fluid is mobile and is free to move through the solid phase. When the surface of such a material is subjected to a step compressive strain, a time-dependent strain field is induced inside the material. The nature of this strain field can reveal information about the poroelastic properties of the material such as the Young's Modulus of the solid matrix, the Poisson's Ratio of the solid matrix and the permeability of the solid matrix to the pore fluid [1].

Many soft tissues are believed to be poroelastic in character. It is further believed that the onset and progression of disease can alter the poroelastic properties of the affected tissue. Consequently, a poroelastic imaging technique has the potential to be diagnostically useful and may provide a means of monitoring the progress of a disease as well as assessing response to treatment.

Preliminary investigations into the use of elastographic methods as the basis for a poroelastic imaging method have been carried out previously [2][3][4]. This investigation builds on this foundation in the following ways:
a) A new analytical expression is derived describing the time-dependent strain field inside (as opposed to on the surface of) a homogeneous cylinder of poroelastic material undergoing stress relaxation. The equation assumes perfect-slip boundary conditions between the compressor and the poroelastic material.
b) The time-dependent strain field inside a relaxing cylindrical sample of tofu is experimentally imaged using elastographic techniques with a strain signal-to-noise ratio sufficient to permit a detailed comparison between theory and experiment.
c) By curve-fitting to the analytical expression, a method is developed to produce poroelastic images by relating the imaged time-dependent strain field back to the underlying poroelastic properties.

Detailed structure in the time-dependent strain field, which was not anticipated from previous work, was predicted by the new analytical expression. While this was seen in some of the experimental results, which were broadly similar to the predictions of the analytical theory, perfect agreement between theory and experiment was not found. Departures of the experimental results from the predicted response were consistent with the existence of imperfect-slip boundary conditions between the compressor and the sample, as confirmed by finite element simulation. Efforts to curve-fit to the analytical theory were frustrated by the lack of perfect agreement between theory and experiment.

This work confirms the usefulness of elastographic techniques for imaging the time-varying strain field in a relaxing poroelastic material. The analytical expression provides a first step towards model-based imaging of the poroelastic properties by relating the strain field to these properties. In order to produce images of the poroelastic properties using this analytical approach, further work is required: either the theory must be generalized to allow for imperfect-slip boundary conditions or the experimental methods must be refined to produce boundary conditions that are as near to perfect-slip as possible.

References:
[1] Armstrong CG, Lai WM, Mow VC. An analysis of the unconfined compression of articular cartilage. Journal of Biomech. Eng. 1984;106:165-173.
[2] Konofagou E, Harrigan T, Ophir J, Krouskop T. Poroelastography: imaging the poroelastic properties of tissues. UMB 2001;27(10):1387-1397.
[3] Righetti R, Ophir J, Srinivasan S, Krouskop T. The feasibility of using elastography for imaging the local lateral-to-axial strain ratios in homogeneously porous media. Proceedings of the Second International Conference on the Ultrasonic Measurement and Imaging of Tissue Elasticity, 2003.
[4] Righetti R, Ophir J, Srinivasan S, Krouskop T. The feasibility of using elastography for imaging the Poisson's Ratio in porous media. UMB 2004;30(2):215-228.

032 **MONITORING OF HIFU LESIONS USING SUPERSONIC SHEAR IMAGING: A UNIQUE THERAPY AND IMAGING SYSTEM.**
Jeremy Bercoff[1], Mathieu Pernot[1], Mickael Tanter[1]*, Mathias Fink[1].
[1]Laboratoire Ondes et Acoustique, E.S.P.C.I, C.N.R.S. (UMR 7587), Paris, FRANCE.

Thermally induced lesions are generally stiffer than surrounding tissues. We propose here to use the Supersonic Shear Imaging technique (SSI) for monitoring high intensity focused ultrasound (HIFU) therapy. This new elasticity imaging technique is based on remotely creating shear sources using the acoustic radiation force at different locations in the medium. In these experiments a HIFU probe is used to generate lesions in fresh tissue samples. A diagnostic transducer, controlled by our ultrafast scanner, is located in the therapeutic probe focal plane. It is used for both generating the shear waves and imaging the resulting propagation at frame rates reaching 5000 images/s. Movies of the shear wave propagation can be computed off-line. The therapeutic and imaging sequences are interleaved, and a set of propagation movies is performed during the heating process. From each movie, elasticity estimations have been performed using an inversion algorithm. It demonstrates the feasibility of detecting and quantifying the hardness of HIFU-induced lesions using SSI. Images of the Young's modulus acquired during the treatment clearly prove the ability of SSI to monitor the lesion formation.

007   **3D *IN–VIVO* LIVER MR–ELASTOGRAPHY.**

Ralph Sinkus[1]*, Heike Hörning[2], Leon ter Beek[3], Michael Dargatz[1] and Bernhard Van Beers[4].
[1]Philips Research, Hamburg, GERMANY; [2]Philips Medical Systems, Hamburg, GERMANY; [3]Philips Medical Systems, Brussels, BELGIUM; [4]UCL St. Luc, Brussels, BELGIUM.

Chronic diffuse liver diseases as well as focal liver lesions are typically accompanied by changes in the stiffness of the organ [1]. Often, metastases of colorectal cancer (which is the third most common cancer both in men and in women) spread initially to the liver. Early detection of those metastases as well as correct differential diagnosis can help to reduce mortality. Here, Elastography has the potential to provide valuable diagnostic information, because malignant focal lesions within the liver typically appear much harder than the surrounding tissue. We present an approach to measure the shear modulus of the liver utilizing a full 3D approach for reconstruction [2] and respiratory motion compensation via MR-navigators to allow for free breathing. Current scan times are about 25min.

The patient is in prone position with the mechanical transducer placed underneath pushing upwards against the last rib and parts of the liver lobe (Figure1a). MR-signal reception is performed via a four-element surface coil. Thereby, good SNR is ensured within the liver. MR reconstruction utilizes the SENSE technology to provide amplitude and phase information of the MR-image, which is crucial for Elastography since the information about the mechanical wave (amplitude/phase) is "stored" in the phase of the MR-image. Respiratory motion is measured by an interleaved MR-navigator (NAV), which measures the position of the diaphragm and enables acceptance/rejection of "wrong" respiratory motion states in real-time (Figure 1b). The so-called seed-position is the end-expiratory position, because it represents the most stable state during the respiratory cycle. Typically, respiratory gating leads to a reduction of the scan efficiency of 30-50%. Slice orientation is transversal or sagittal with the latter leading to reduced interferences with the navigator. Saturation slabs (REST) in A-P direction prevent back-folding artifacts. The field of view is 160mm, 64^2 pixels resolution with a slice-thickness of 3mm. Seven adjacent slices are measured utilizing a motion-sensitized spin-echo sequence (SE) with TE/TR=50/500ms. The MR-sequence is consisting of (NAV–REST–SE)-(NAV–REST–SE)-.... and measures the 3D steady-state motion field during end-expiration.

Mechanical excitation is applied longitudinally at ν=85 Hz. Very good penetration of the mechanical wave into the entire liver is observed by pushing against the rib (Figure 1d). Although mechanical excitation is applied only at one location, waves are observed being generated everywhere on the surface of the liver. Here, the thoracic cage is functioning as a resonator. This leads to an efficient mechanical excitation within the entire liver, which is crucial for achieving high quality Elastography results. Initial measurements from healthy volunteers show the outer region of the liver appearing softer than the inner core (Figure 1e).

This work demonstrates the technical feasibility of free-breathing *in-vivo* liver Elastography. Scan times of about 25 min are currently prohibitive for clinical applications. However, speed-ups by a factor 3-5 are feasible by utilizing fast imaging techniques such as Echo-Planar-Imaging. Clinical studies of various pathologies are now required to evaluate the diagnostic potential of the method.

References: [1] Sandrin et. al, Ultrasound in Med. & Bio **29** (12), 1705-1713 (2003)
          [2] Sinkus et. al, Physics Medicine Biology **45** (2), 1649-1664 (2000)

| (a) | (b) | (c) | (d) | (e) |
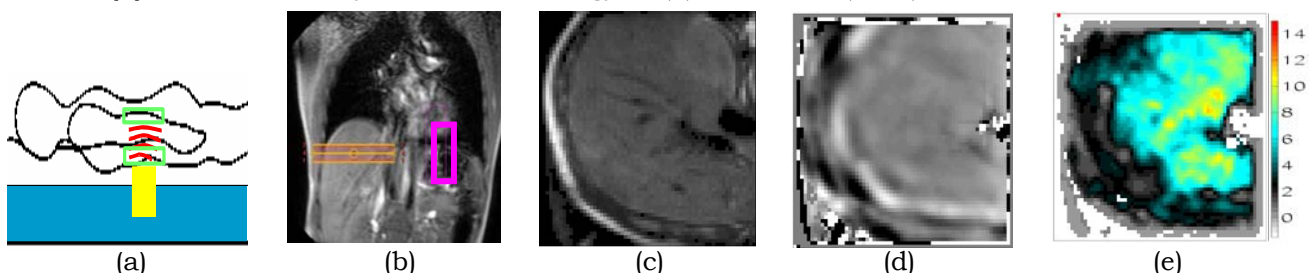
Figure1: (a) Sketch of the set up: the patient is in prone position, yellow block=mechanical transducer pushing upwards against the ribs, red lines=mechanical wave propagating into the liver, green squares=surface coils; (b) scout scan depicting the thoracic cage, orange lines indicating the location of the transversally orientated MRE scan, pink rectangle=MR navigator measuring the position of the diaphragm; (c) MR-magnitude image of the MRE scan showing the liver; (d) corresponding image of the mechanical wave in through-slice direction and (e) image of the reconstructed shear modulus in units of [kPa]. The outer parts appear softer than the inner core of the liver.

DETERMINATION OF ANISOTROPIC ELASTICITIES OF *IN VIVO* SKELETAL MUSCLE USING A GEOMETRIC ANALYSIS OF MR–ELASTOGRAPHY WAVE PATTERNS.

S. Papazoglou[1]*, J. Braun[2], M. Taupitz[1], I. Sack[1].
[1]Institute of Radiology–Charité, Berlin, GERMANY; [2]Institute of Biometry and Medical Informatics–Charité, Berlin, GERMANY.

In MR-Elastography, shear vibrations of tissue are depicted in terms of phase-contrast wave patterns that enable the reconstruction of elasticity maps [1]. While the wavelength is directly related to the shear modulus, the wave pattern can reveal information about the anisotropic elastic properties of the tissue. The correlation of wave patterns to the anisotropy of the tissue has most directly been observed in skeletal muscle tissue [2]. It could be shown that shear waves can propagate either parallel or as *V*-shaped waves through the tissue depending on the position of the actuator with respect to the muscle [3].

Here, a strategy is introduced to gain information about the complete three-dimensional anisotropy of the elasticity using two-dimensional MRE shear wave patterns. Therefore, the solution of the wave equation in *k*-space was approximated by ellipses to analytically describe the form of shear waves depending on the constitutive parameters.

The new method is applied to *in vivo* MRE experiments of the biceps brachii. Two shear moduli parallel ($\mu_=$) and perpendicular ($\mu_\perp$) to the main direction of the muscle fibers could be determined from a single 2D wave image. $\mu_=$ was found to be four times larger than $\mu_\perp$ resulting in *V*-shaped shear wave patterns with approximately 37° inclusion angle between the propagating wavefronts. These results are in good agreement with sonoelastography data presented in the literature [4].

References:
[1] Muthupillai, R; Lomas, D. J.; Rossman, P. J.; Greenleaf, J. F.; Manduca, A.; Ehman, R. L. Science 1995, 269, 1854-1857
[2] Dresner, M. A.; Rose, G. H.; Rossman, P. J.; Muthupillai, R; Manduca, A.; Ehman, R. L. J. Magn. Reson. Imaging 2001, 13, 269-276
[3] Sack, I.; Bernarding, J.; Braun, J. Magn. Reson. Imaging 2002, 20, 95-104
[4] Gennisson, J. L.; Catheline, S.; Chaffai, S.; Fink, M. J. Accoust. Soc. Am. 2003, 114 (1), 536-541

065 MEASURING THE MECHANICAL PROPERTIES OF SMALL BIOLOGICAL TISSUES USING MICROMAGNETIC RESONANCE ELASTOGRAPHY (µMRE).

Shadi F. Othman[1]*, Huihui Xu[1], Thomas J. Royston[1], Richard L. Magin[1].
[1]University of Illinois at Chicago, Chicago, IL, 60607, USA.

Introduction: Measurement of shear wave motion in soft biological tissues provides unique spatially-localized information about the tissue's material properties. Such information can reflect the development of pathology and in some cases biomechanical integrity. Many disease states significantly change tissue material parameters, such as the elastic moduli, which in turn significantly affect shear wave propagation through the tissue. Recently, this concept has been combined with the medical imaging modalities of ultrasound (US) and magnetic resonance imaging (MRI) to establish a noninvasive means of visualizing shear wave motion for diagnosis in a clinical setting. When combined with US, for example, the Doppler effect is used to provide localized information about tissue motion that can be used to map shear wave propagation following excitation of mechanical waves. On the other hand, when mechanical vibration of tissue is combined with MRI, a phase contrast imaging technique is used to visualize the spatial and temporal pattern of strains associated with the propagation of the acoustic waves in the tissue, and these data are used to construct a map of the "shear stiffness" throughout the tissue. Variations of this approach have been most commonly referred to as "MR elastography (MRE)" or dynamic MRE [e.g. Muthupillai 95].

In this study, we are presenting micromagnetic resonance elastography (µMRE) as new technique for measuring the viscoelastic mechanical properties of small biological tissues [Othman 04]. The proposed study is unique in its goal to develop an integrated mechanical actuator/RF coil detector system suitable for µMRE experiments in 10 mm diameter clear imaging bore available in an 11.74 T NMR spectrometer (500 MHz for proton). This approach is significantly different from the majority of magnetic resonance elastography (MRE) studies that are performed in relatively low field whole body MRI systems.

Methods: Shear waves were introduced into agar gel phantoms of different concentrations (0.5%-2%) by a piezoelectric actuator (Piezo system, MA) driven at its structural resonance frequency (570 Hz). The actuator was placed inside a 1 cm test tube and mechanically coupled to the gel via a thin needle (0.5 mm). All experiments were conducted at 500 MHz in a 56-mm vertical bore 11.74 T magnet (Oxford Instruments, Oxford, England, UK) using a Bruker DRX 500 MHz Avance spectrometer (Bruker Instruments, Billerica, MA). The samples and the imaging coils (10 and 5 mm saddle coils) were inserted in the Bruker Micro5 imaging probe with a triple axes gradients (200 Gauss/cm maximum). A modified gradient echo pulse sequence with variable number of bipolar gradients was implemented [1]. Tissue engineered constructs, bovine articular cartilage were also tested using the proposed method.

In order to validate the method, a simple composite phantom (two media of different stiffness) was tested.

Results: To validate our method shear wave propagating through a two component medium is shown in Figure1. We observe the shear wave propagating though both materials (agarose gel 0.25% and 0.4%, respectively) with different wavelengths. Shear waves traveling through an adipogenic (fat-like) tissue engineered construct and an agarose gel phantom are shown in Figure 2. µMRE can be used to evaluate the mechanical properties of a tissue-engineered construct at different growth stages as shown in Figure 2. The wavelength inside the construct is smaller than that observed in the agarose gel.

Conclusion: µMRE has the potential of visualizing the biomechanical properties of small biological samples such as articular cartilage and tissue engineered constructs with high spatial resolution. Future work should include the design of a high frequency mechanical actuator with lower electromagnetic coupling, and the development of an advanced reconstruction algorithm that takes into account the heterogeneity of the material at the microscopic level.

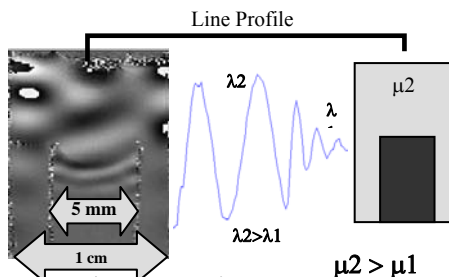References: [1] Muthupillai et al., science 95, [2] Othman et al., ISMRM 04.

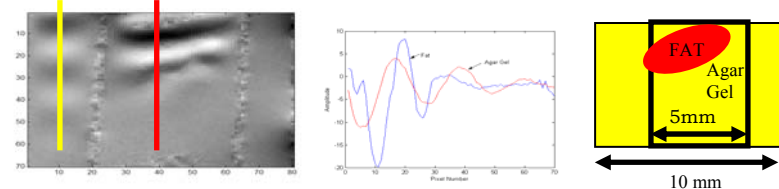Figure 1: Shear wave in two compartment media, inplane resolution 140µm x 140µm

Figure 2: Shear waves traveling through adipogenic construct and agarose gel (0.25% agar), acquisition time = 52s.

064   FAST GENERATION OF 3D SYNTHETIC RF DATA OF NONLINEARLY ELASTIC OBJECTS FOR SPECKLE TRACKING PERFORMANCE EVALUATION.

Ramon Q. Erkamp[1]*, Paul L. Carson[1], Matthew O'Donnell[1].
[1]University of Michigan, Ann Arbor, MI, USA.

A major component of developing ultrasound elasticity imaging algorithms is verification. This can be done by synthetically generating an RF data set where all the properties to be imaged are exactly known. Elastic properties of biological tissue are highly nonlinear; the elastic modulus for example can increase threefold over less than a 10% deformation range. With 3D elasticity imaging an emerging field and even 2D speckle tracking being affected by the 3D scattering distribution, a 3D dataset is desirable. If nonlinear elastic behavior over a large deformation range is to be imaged, many of these RF volumes need to be generated. Moreover, as some speckle tracking algorithms can be strongly affected by the speckle statistics, a high scatterer density is needed to ensure fully developed speckle, especially in regions that are expanding during the deformation process. These factors fuel the need for efficient algorithms that can generate RF data within an acceptable timeframe.

An example of breast imaging simulation is presented, where a 1cm spherical intraductal carcinoma is surrounded by glandular tissue and a small fat layer. Elastic properties are taken from [1] and a Mooney-Rivlin strain energy function is fit to each material. The breast geometry is simulated in Abaqus (Hibbit, Karlsson & Sorensen, Inc., Pawtucket, RI) using a hyperelastic model and exploiting axial symmetry. The resulting displacement fields warp a set of scatterer locations to the desired deformation stage. The 3D pointspread function (psf) of an 8MHz 1.25D imaging array was experimentally measured and is modeled as an amplitude modulated sinusoidal function, with a separable polynomial function for the modulation. The psf does not have positional dependencies. This limits the complexity of the simulated psf, but results in much faster code. The scatterer strengths are set to a random Rayleigh distribution to further approximate tissue speckle statistics. Calculations are in the time domain, and because of the analytical model there are no timing/interpolation type errors. For an imaging volume that is 4cm deep and 3cm in the other dimensions, with a sample frequency of 40MHz , center frequency of 8MHz, and 16 scatterers per ultrasonic wavelength, there are more than 22×10^9 scatterers, and the calculation takes about 2 days on a Pentium 4 2.6Ghz PC (at 4 scatterers per wavelength, it takes 45 minutes).

As we have full control over the scan plane, psf, sampling frequency, beam density, etc., the effects of those parameters on speckle tracking can be analytically examined in terms of signal and contrast to noise values. Below is a preliminary (low 4 scatter/wavelength density) analysis of the effect of out of plane motion on conventional 2D speckle tracking. A 1.4% average strain is applied to a breast model, and it is also translated by 0.05mm increments elevational to the imaging plane. Shown are the resulting strain images, and below it the corresponding contrast to noise ration as a function of elevational shift. Clearly, even relatively small elevational shifts can significantly degrade 2D speckle tracking.

Reference:
[1] T. A. Krouskop, T. M. Wheeler, F. Kallel, B. S. Garra, and T. Hall, "The elastic moduli of breast and prostate tissues under compression," *Ultrason. Imag.*, vol. 20, pp. 151–159, 1998.
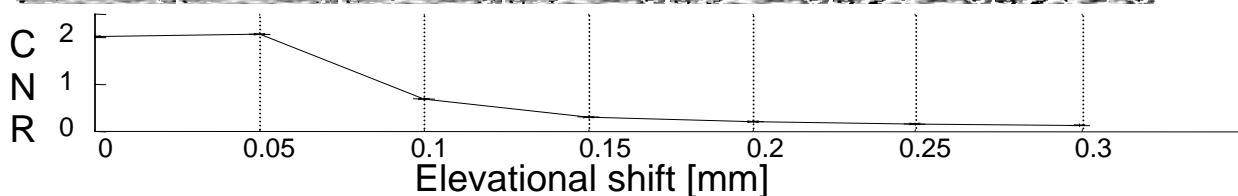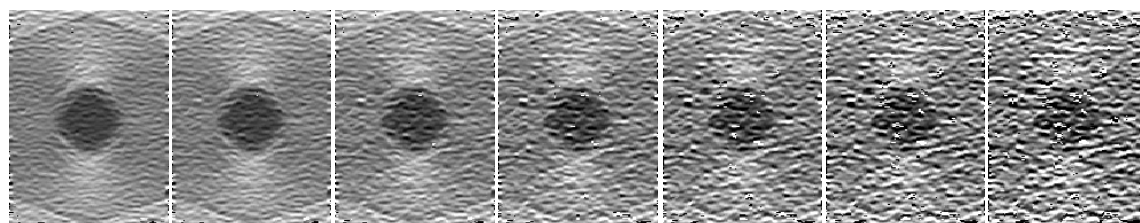
048 **TISSUE–MIMICKING SPHERICAL LESION PHANTOMS FOR ELASTOGRAPHY WITH AND WITHOUT ULTRASOUND REFRACTION EFFECTS.**
EL Madsen[1]*, G Frank[1], M Hobson[1], H Shi[1], T Varghese[1], J Jiang[1], TJ Hall[1], TA Krouskop[2,3], J Ophir[3], J Weaver[4], MM Doyley[4].
[1]University of Wisconsin–Madison, Madison, WI, USA; [2]Baylor College of Medicine, Houston, TX, USA; [3]The University of Texas Medical School, Houston, TX, USA; [4]Dartmouth College, Hanover, NH, USA.

Spherical lesion phantoms have been constructed from two different types of materials. One type is a mixture of agar, gelatin, water, microscopic glass beads, CuCl2, EDTA, HCHO, NaCl and a preservative. The ultrasound (US) attenuation coefficient slope is about 0.4 dB/cm/MHz, depending on the glass bead concentration, and the US propagation speed is about 1530 m/s in both lesions and background. T1's range from 400 to 500 ms and T2's from 40 to 70 ms. Two phantoms have been made from these materials, one with elastic contrast ≡ C ≡ (inclusion Young's modulus) ÷ (background Young's modulus) = 2.5 and the other with C = 5.8.

The other type of material is an oil-in-gelatin dispersion in which the volume fraction consisting of safflower oil determines the value of the Young's modulus [1]. HCHO cross-links the gelatin and helps prevent bacterial invasion. One such phantom has been constructed with the following properties: C = 3.6; T1 = 290 ms and T2 = 110 in the background; T1 = 1300 ms and T2 = 240 in the lesions; US speed = 1498 m/s in the background and 1547 m/s in the lesions providing US refraction effects typical of tissues *in vivo*.

Each phantom is a 10cm x 10cm x 10cm cube with four planar arrays of spheres. One array contains 4-mm diameter spheres, another 3-mm diameter spheres, another 2-mm diameter spheres, and another 1.6-mm diameter spheres. The distance between spheres is more than four times the sphere diameter to avoid significant mechanical cross-talk. Spheres in each array lie at 1-cm intervals through a depth of 9 cm.

In the agar/gelatin type phantoms US refraction effects are minimal, whereas in the oil-in-gelatin type there is significant refraction at the sphere-to-background boundaries. Thus, comparison of detectability on US elastograms as a function of presence or absence of refraction is of interest.

Note that spherical lesion phantoms made from agar/gelatin materials were reported at last year's meeting (Proceedings of the Second International Conference on the Measurement and Imaging of Tissue Elasticity, Corpus Christi, Texas, USA, October, 2003). However, the agar/gelatin phantoms described in this abstract represent significant improvements in that realistic US attenuation and scattering levels are represented and positions of spheres in arrays have been changed to insure negligible mechanical cross-talk.

To date, US elastography employing a 7.5 MHz linear array, focused at 5.5 cm, on an Aloka SD 2000 scanner has detected lesions in depth ranges shown in the table below. Additional results for Siemens and ATL US systems and for MR elastography using a 1.5 tesla GE Signa unit will also be presented.

Phantom identification	Depth range of detection (cm)			
	4-mm spheres	3-mm spheres	2-mm spheres	1.6-mm spheres
agar/gelatin with C = 5.8	1 to 8 cm	1 to 7 cm	2 to 5 cm	none
agar/gelatin with C = 2.5	1 to 7 cm	1 to 7 cm	2 to 5 cm	none
oil-in-gelatin with C = 3.6	1 to 6 cm	1 to 6 cm	none	none

For these preliminary results, refraction seems to play a greater role in detectability than elastic contrast. It should be noted, however, that the technique used for making elastograms of the agar/gelatin phantom with C = 2.5 was likely superior to that used for the other phantoms.

Reference:
[1]   Madsen EL, Frank GR, Krouskop TA, Kallel F and Ophir J, *Ultrasonic Imaging* **25**: 17-38 (2003).

049 **TISSUE–MIMICKING ANTHROPOMORPHIC BREAST PHANTOMS FOR ULTRASOUND AND MR ELASTOGRAPHY.**

EL Madsen[1]*, G Frank[1], M Hobson[1], H Shi[1], T Varghese[1], J Jiang[1], TJ Hall[1], TA Krouskop[2,3], J Ophir[3], J Weaver[4], MM Doyley[4].
[1]University of Wisconsin–Madison, Madison, WI, USA; [2]Baylor College of Medicine, Houston, TX, USA; [3]The University of Texas Medical School, Houston, TX, USA; [4]Dartmouth College, Hanover, NH, USA.

A set of materials has been developed, which form the basis for production of anthropomorphic breast phantoms with realistic elastic, ultrasound (US) and MR properties. Materials representing fat, glandular parenchyma, and abnormal tissues can be formed and bonded in direct contact without long-term change in geometric or physical properties. The materials consist of oil-in-gelatin dispersions where the physical properties depend primarily on the volume percent safflower oil (droplets) suspended in the (solid) gelatin matrix. The volume percent oil ranges from 0% (tumors) to 70% (fat). A 30% concentration is considered representative of glandular parenchyma. Versions of these materials have been reported previously [a]. The major improvement is that the maximum volume percent oil has been increased from 50% to 70%, allowing more realistic mimicking of fat.

Values of Young's moduli at 0.1 Hz, US speeds and US attenuation coefficient slopes at 6 MHz and MR T_1's and T_2's at 60 MHz are given in the table below for a set of test materials. Glass beads for attenuation and scattering enhancement were not included. All measurements were made at 22EC.

Volume percent safflower oil	Young's modulus (kPa)	US attenuation coefficient slope (dB/cm/MHz)	US propagation speed (m/s)	T_1 (ms)	T_2 (ms)
0	70	0.15	1572	1150	253
10	52	0.24	1559	1000	172
30	34	0.34	1536	400	130
50	21	0.44	1510	310	109
70	11	0.44	1490	253	96

Note that US refraction will occur between fat (70% oil), glandular (30% oil) and tumor (0%), which may challenge US elastography. Because of the varying volume percent oil, there will also be chemical shift artifacts which may challenge MR elastography in a similar way as in the *in vivo* case.

Addition of microscopic glass bead scatterers in any section of a phantom can raise the US attenuation coefficient slope by as much as 1 dB/cm/MHz with little affect on the MR relaxation times; modest increase in Young's modulus is anticipated, based on experience with previous materials.

Stable anthropomorphic breast phantoms for use in US have been produced previously using similar materials [b, c]. Production of molds for making phantoms with geometries suitable for current US and MR breast elastography with internal structures representative of the human breast remains to be achieved. Simulated cancers can be produced with spiculations.

Two subtleties in mechanical properties will be simulated in the phantoms. One is suspected "slipping" that can occur at the boundary between a fibroadenoma and the surrounding tissue. Simulated fibroadenomas can be coated to prevent bonding with the surroundings during manufacture. The other subtlety is the increase in Young's modulus with increasing stress exhibited by cancers. A material that is compatible with the oil-in-gelatin dispersions and that can be bonded to its surroundings will be used for such tumors. The Young's modulus of the oil-in-gelatin dispersions is essentially independent of stress.

References:
[a] Madsen EL, Frank GR, Krouskop TA, Kallel F and Ophir J, *Ultrasonic Imaging* **25**: 17-38 (2003).
[b] Madsen EL, Zagzebski JA, Frank GR, et al. *J Clinical Ultrasound* **10**: 67-75 & 91-100 (1982).
[c] Madsen EL, Kelly-Fry E, Frank GR. *Ultrasound in Med and Biol* **14**:183-201 (1988).

DESIGN AND CHARACTERISATION OF A COMPLIANT WALL VASCULAR PHANTOM OF VARYING ELASTICITY FOR ULTRASOUND INVESTIGATION OF ARTERIAL WALL MOTION (AWM).

Judith Dineley[1], Peter R. Hoskins[1]*.
[1]Dept. of Medical Physics, University of Edinburgh, Edinburgh, Midlothian, Scotland, UK.

Introduction: Changes in mechanical properties of the arteries induced by the onset and development of arteriosclerosis and atherosclerosis may be inferred from the arterial wall motion (AWM) together with blood pressure data [1]. Compliant wall vascular phantoms have the potential to provide physiologically realistic AWM, assisting in the evaluation of AWM measurement techniques and in the understanding of haemodynamic phenomena in an environment that is relatively simple compared to *in vivo*. This paper presents a detailed characterisation of such a phantom in which the mechanical properties of the carotid artery are matched, a task previously unreported in the literature.

Phantom design: A longitudinally stressed compliant tube of polyvinyl alcohol cryogel (wall thickness 1.55mm) is embedded in a gelatin based tissue mimick. Movement of the vessel walls is produced by pulsatile blood mimicking fluid flow through the vessel, driven by a pc-controlled gear pump. The wall modulus is varied according to the length and number of the freeze-thaw cycles to which it is subjected.

Material characterisation: Static and dynamic mechanical properties of the mimicks were evaluated by using an INSTRON tensile testing rig. Samples were prepared at weekly-fortnightly intervals for one month and subsequently tested in order to evaluate stability of the materials. Variation of vessel mimick elastic modulus with number of freeze-thaw cycles was also quantified. Preliminary results established an available range of $57\pm5.2-153.2\pm22$kPa for 2-10 freeze-thaw cycles.

Phantom characterisation: AWM phantom data were acquired using Tissue Doppler Imaging and a Philips prototype AWM software. Various volume flow waveforms were applied to the phantom, varying key characteristics such as peak flow in order to achieve a physiologic AWM curve. Preliminary AWM waveforms produced by realistic wall velocities (peak 10-14mm/s), with realistic rapid rise times (≥0.16s) have been generated (Figure 1). Variation in AWM with longitudinal position for a uniform vessel was investigated, revealing a standard deviation of 5.4% in the mean dilation for measurements across the phantom length. Quantification of this variation will allow AWM data for more complex arrangements of elasticity and geometry to be interpreted with greater confidence. Variations in AWM symmetry with geometry were examined, demonstrating non-uniform AWM (0.51 ± 0.24mm) in vessels with non-uniform wall thickness compared to AWM in vessels with relatively uniform wall thickness (0.65 ± 0.09mm).

Conclusion: A compliant wall vascular phantom for use with ultrasound scanners has been designed and characterised, the results of which are presented. Mechanical characterisation confirms the potential for elastic moduli in the physiologic range. The phantom will aid in the investigation of AWM measurement technique efficacy, in particular the evaluation of vessel elastic properties using fluid pressure data, and the investigation of haemodynamic phenomena.
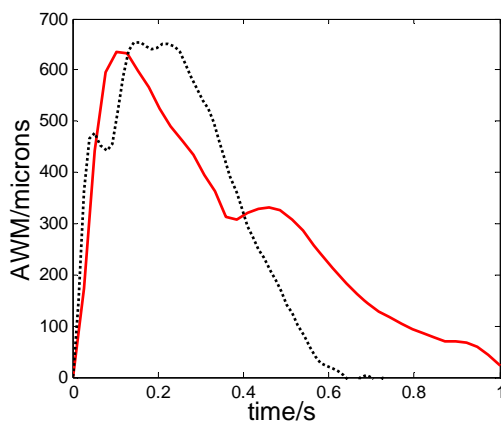

Figure 1: Comparison of preliminary phantom AWM (dashed) with physiologic common carotid artery AWM (solid).

References:

[1] Bank A.J et al. Direct Effects of Smooth Muscle Relaxation and Contraction on *In Vivo* Human Brachial Artery Elastic Properties. Circ Res 1995; 77:1008.

## 043 DEVELOPMENT OF A NEW TISSUE–EQUIVALENT GEL FOR WALL–LESS FLOW AND WALL MOTION PHANTOMS.

TL Poepping[1]*, PR Hoskins[1], WJ Easson[2].
[1]Medical Physics, University of Edinburgh, Edinburgh, Scotland, UK; [2]Institute of Materials and Processes, University of Edinburgh, Edinburgh, Scotland, UK.

A new gel has been developed for use in ultrasound tissue-mimicking materials (TMM) in wall-less flow phantoms. Similar to other TMM, this work aims at a material with tissue-equivalent acoustic properties and elasticity, but with improved strength in order to withstand physiological stresses. Previous ultrasound-compatible, wall-less vessel phantoms have been based primarily on agar gels. However, these wall-less phantoms suffer rupture and leakage problems under physiological flow conditions, especially at stress concentration points, such as bifurcations in anatomically realistic flow phantoms. This new gel has been designed for use with a lost-material casting technique in order to produce anthropomorphic phantoms, which can be used for flow or wall motion studies. The gel must be poured into the mould at a temperature below the melting point of the metal arterial cast, allowed to set to a solid gel, then reheated above the melting point of the metal core without melting the gel; this requires the gel to be thermally irreversible. A unique method for rendering a semi-irreversible form will be discussed.

The new gel may be made with a range of elasticities to simulate that in normal healthy arteries and in diseased arteries with increased stiffness. Elasticity and tensile strengths were determined using an Instron system with a 1 kN load cell and 0.5 mm/s constant extension rate. Preliminary results have revealed formulations that have a tensile strength up to 9 times greater than agar alone, as shown below, and can withstand up to 20 times greater tensile strains. The elastic moduli range from 90 to 250 kPa, depending upon component concentrations. Gel components and method of gel and phantom fabrication will be presented.

In conclusion, the new gel allows the use of a lost-material casting technique to produce anthropomorphic flow phantoms capable of withstanding mechanical stresses present during physiologically realistic, pulsatile flow. This gel may also be of interest for the manufacture of other general ultrasound phantoms in which the elastic properties of the TMM need to be varied.
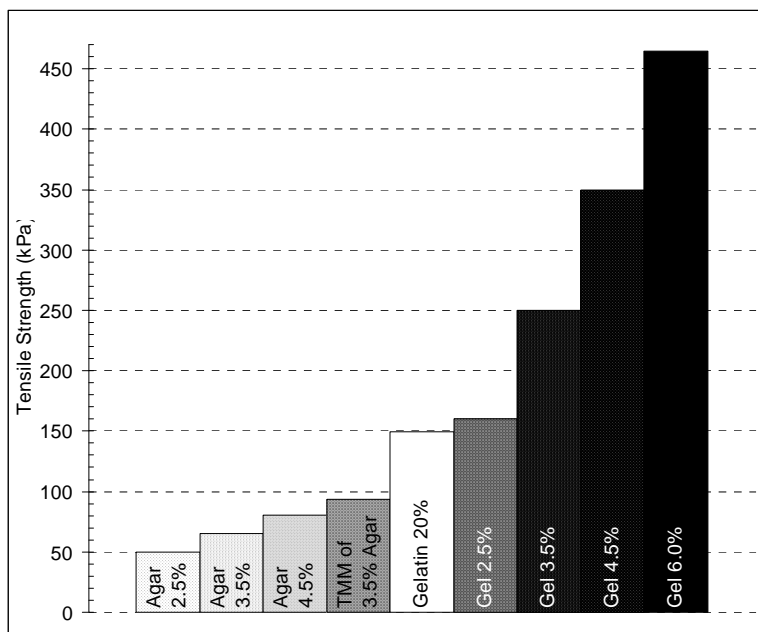
005   **A STUDY OF VIBRATION CHARACTERISTICS FOR ULTRASONIC ELASTICITY IMAGING.**

J Park[1], S Kwon[2], and MK Jeong[2]*.
[1]Department of Physics, [2]Department of Electronics and Telecommunication Engineering, Daejin University, Pocheon, Kyeonggi, 487-711, KOREA.

Elastographic imaging using vibration in ultrasonic imaging is receiving attention as a new diagnostic method of visualizing tissue pathology. Tissues subjected to vibration exhibit different vibration characteristics depending on their stiffness [1, 2]. This study investigates by simulation and experiment the vibration characteristics of tumors whose shapes are modeled as cylinders and spheres and which are harder than their surrounding media in an infinite homogeneous medium upon which a shear wave is incident, by varying their stiffness, lesion diameter, and vibration frequency. In particular, the difference in vibration characteristic between cylinder and sphere is highlighted.

The ratio of vibrational amplitudes between a lesion and its surrounding medium due to external vibration applied to them is found to increase with increasing external vibration frequency, stiffness difference between lesion and background, and lesion diameter. This tendency is more pronounced for cylindrical targets than spherical ones. This finding suggests that one can obtain better contrast elastographic images of cylinders than spheres and that there is a definite limit to which one can increase the vibration frequency to obtain better resolution. As the vibration frequency increases, the elastographic contrast increases, but a resonance phenomenon appears with the resonance frequency determined according to the object diameter and its difference in stiffness from the background. When the vibration frequency exceeds the resonance frequency, the ratio of vibrational amplitudes between object and background ceases to increase further. The resonance frequencies of the spheres were found to be higher than those of the cylinders.

In order to verify these lesion vibration characteristics, we carried out an experiment with a commercial elastographic phantom (CIRS, USA) embedded with cylinders and spheres wherein low frequency vibration was applied to 10 and 20 mm diameter lesions. The vibration was applied using a low frequency vibrator built around audio speakers, and the displacement distribution was computed from the echo signal phase in dedicated software on a PC embedded ultrasonic scanner (ACCUSION, Medison Co, Korea) with the resulting elasticity images obtained and displayed in real time. The vibration frequencies ranged from 50 to 300 Hz, and the experimentally determined elastographic contrast showed the same tendency as the underlying theory and simulation results.

References:
[1] M. K. Jeong and S. J. Kwon, "Tissue stiffness imaging method using temporal variation of ultrasound speckle pattern," IEEE Trans. UFFC, vol. 50, no. 4, pp. 457-460, April 2003.
[2] M. K. Jeong, S. J. Kwon, J. M. Park, and M. H. Bae, "Tissue stiffness measurement using temporal variation of ultrasound speckle pattern," SPIE Medical Imaging, San Diego, 2003.

012 **COMPUTER–BASED VIBRATIONAL VISCOELASTOC MEASUREMENT OF SOFT TISSUES.**

Evgeny M. Timanin[1]*, Evgeny V. Eremin[1].
[1]Institute of Applied Physics, Nizhny Novgorod, RUSSIA.

Together with different approaches to "ultrasonic elastography" [1], traditional measurements of mechanical characteristics of biological soft tissues continue to be vital for characterizing their condition as affected by different physical or physiological factors: heat, chill, humidity, zero gravity, electrical stimulation, massage, athletic drill, drug treatment etc. One of the most suitable ways of measuring the mechanical parameters of tissues for this purpose is based on registration of dynamic mechanical characteristics of tissues (stiffness K and impedance Z) when in contact with a vibrating disk. This methodology has been under development by several researchers, including the authors [2-9].

Results of this work are the following. A computer based technique has been built for measuring tissues' viscoelastic characteristics [7-9]. This operates in Windows 2000/XP/ME/9x and works in part on portable computers. The main parts of the devices are special probes and special managing programs. The method is realized by registering the frequency dependencies of tissue stiffness and impedance, as well as by single-frequency measurements, and provides the possibility of monitoring tissue viscoelastic characteristics with a temporal resolution of less then 0.1 s. The second part of our work is the development of models of vibrating disk interaction with layered tissues [6-8]. Tissues are considered as a half-space, as a layer bound to a rigid base, or as a set of layers (two or three) bound to each other and to the rigid base. The vibration source is considered as a pressure source, providing different pressure distributions, as a source of normal and shear stresses (pressure source with friction), or as a source of displacements. The resulting models were used for interpreting experimental data by solving the direct problems, as well as for the estimation of rheological parameters of tissues via the impedance characteristics by solving the inverse problems. The third part of this work involves experimental studies of impedance characteristics of biological tissues with physiological and biomechanical goals [9].

Models of mechanical impedance were used also as a basis for the development of models of vibration penetration into layered tissues from a surface source [10] for "ultrasonic elastography". Tissues are considered here as a three-layered half-space (skin-fat complex, muscle, liver) with bound or sliding layers. Some experiments [11] have been carried out in this direction on gelatin phantoms by an automated setup based on ultrasonic pulse Doppler technique.

References:
1. Proceedings of the Second International Conference on the Ultrasonic Measurement and Imaging of Tissue Elasticity. Corpus Christi, Texas, U.S.A., October 12-15 2003, P.1-100.
2. Franke E. Mechanical impedance of the surface of the human body J. Appl. Physiol. 1951. 3(1). P.582-590.
3. Oka H., Nakamura T. Estimation of internal structure and viscoelasticity from mechanical impedance Electrical Engineering in Japan. 1998. 125(3). P.31-39.
4. Skovoroda A.R., Aglyamov S.R. Reconstruction of the elastic properties of layered viscoelastic media using impedance measurements Biophysics. 1998. 43(2) P.348-352.
5. Zhang X., Royston T.J., Mansy H.A., Sandler R.H. Radiation impedance of a finite circular piston on a viscoelastic half-space with application to medical diagnosis JASA. 2001. 109(2). P.795-802.
6. Timanin E.M. On contribution of shear waves into a transverse stiffness of soft biological tissues in vibrating indentor investigations 13 Intern. Congr. on Acoustics. Belgrade, 1989. V.4. P.215-218.
7. Eremin E.V., Timanin E.M. Interpretation of a Layer Mechanical Impedance Measured Using a Hard Round Die Acoustical Physics. 2000. 46(4). P.421-426.
8. Timanin E.M., Eremin E.V. Interpretation of Mechanical Impedance of Biological Tissues in the Three-Layered Model with the Pressure Source of Vibrations Biophysics. 2003. 48(2). P.324-331.
9. Timanin E.M., Eremin E.V. Monitoring of Biceps Characteristics in Sustained Isometric Contractions by the Methods of Impedance Mechanomyography and Electromyography Acta of Bioengineering and Biomechanics. 2002. V. 4, Suppl. 1 Proceedings of the 13-th Conference of European Society of Biomechanics. Wroclaw, 2002. P.616-617.
10. Timanin E.M. Displacement Field Produced by a Surface Source of Vibrations in a Layered Biological Tissue Acoustical Physics. 2002. 48(1). P.87-93.
11. Timanin E.M., Eremin E.V. Ultrasonic Doppler Imaging of Nonlinear Elastic Shear Properties of Biological Tissue Phantoms Nonlinear Acoustics at the Beginning of the 21-st Century / Edited by O.V.Rudenko and O.A.Sapozhnikov. Moscow: Faculty of Physics, MSU, 2002. V.1. P.449-452.

018 **TWO–DIMENSIONAL ELASTIC MODULUS DISTRIBUTION RECONSTRUCTION BASED ON A MODIFIED THREE–DIMENSIONAL FINITE–ELEMENT MODEL.**

Makoto Yamakawa[1]*, Tsuyoshi Shiina[1].
[1]University of Tsukuba, Tsukuba, JAPAN.

Strain imaging is useful for visualizing information relating to tissue hardness. However, strain is a parameter that depends on the amount of tissue compression or the distribution of pressure. As the result, tissue hardness cannot be quantitatively evaluated from the strain distribution. Therefore, reconstruction of the elastic modulus (Young's modulus) distribution has been investigated for quantitative evaluation of tissue hardness. Assuming a tissue to be a 3-dimensional elastic object is desirable for evaluating tissue elastic modulus more accurately. However, measurement of the 3-D distribution of strain is usually required to reconstruct the elastic modulus on the assumption of a perfect 3-D state. In addition, numerical analysis based on a 3-D model such as a finite-element model generally takes vast processing time.

Therefore, we propose a method for rapidly reconstructing an elastic modulus distribution using the 2-D strain distribution. The method is based on a modified 3-D finite-element model where each element has a certain thickness in the elevational direction. Using this model, we estimate the tissue elastic modulus distribution by an iterative reconstruction technique [1] based on the 3-D elastic equation from the 2-D axial strain distribution and the pressure distribution on the body surface.

The performance of the proposed method using the modified 3-D model is evaluated and compared with methods using 1-D or 2-D models (plane strain state, plane stress state). Results show that the accuracy of reconstruction based on the modified 3-D model is about 4 times better than that of a 1-D model, and about 3 times better than that of a 2-D model. Moreover, comparing with a method based on a strict 3-D model, the proposed method can reconstruct elastic modulus from the 2-D strain distribution to almost the same accuracy as the 3-D model, which needs the 3-D distribution of strain, around the area near the center of the ROI. Furthermore, the proposed method can attain high-speed processing which is about 170 times faster than the method using a 3-D model.

These results validate that the proposed method based on the modified 3-D finite-element model enables us to reconstruct the tissue elastic modulus distribution at high speed and with high precision from only the 2-D strain distribution.

Reference:

[1] M. Yamakawa and T. Shiina, "Tissue Elasticity Reconstruction Based on 3-Dimensional Finite-Element Model", Jpn. J. Appl. Phys., Vol.38, No.5B, pp.3393-3398, 1999.
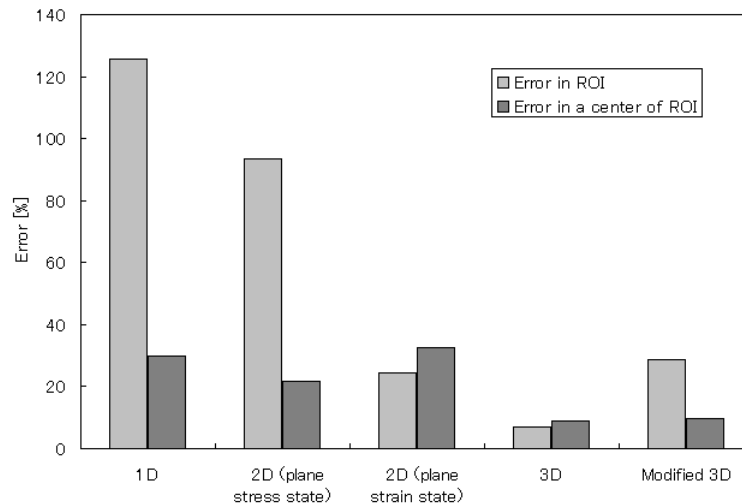
Figure 1: Results of tissue elastic modulus distribution reconstruction based on each model.

027   **AN ARTERIAL WALL MOTION TEST TOOL TO ASSESS PHILIPS AWM SOFTWARE.**
Steven James Hammer[1]*, Judith Dineley[1], William J. Easson[2], Peter R. Hoskins[1].
[1]Medical Physics, School of Clinical Sciences and Community Health, The University of Edinburgh, Edinburgh, Midlothian, Scotland, UK; [2]Institute for Materials and Processes, School of Engineering and Electronics, The University of Edinburgh, Edinburgh, Midlothian, Scotland, UK.

Introduction: With onset and progression of arteriosclerosis and atherosclerosis, the large arteries undergo diffuse and focal changes in mechanical properties respectively. These mechanical properties can be inferred by evaluating the arterial wall motion (AWM) and blood pressure. Test tools are necessary to evaluate AWM measurement technique efficacy. A flat reflective layer which moves relative to a fixed layer simulates AWM. This is more easily controllable and quantifiable than flow phantoms [1,2]. The design of such a test tool is presented. Results of the evaluation of an AWM technique comprising of a Philips prototype software coupled with Tissue Doppler Imaging (TDI) are also presented. These provide a more comprehensive evaluation, complementing previous results [1,2].

Methods: To assess the accuracy and precision of the AWM software, a controlled *in-vitro* test tool has been developed. A moving wall made of polyvinyl alcohol (PVA) cryogel is moved below a fixed PVA cryogel layer to provide a B-mode ultrasound (US) image akin to a cross-section through a straight artery. The moving wall is controlled using a stepper-motor driven linear table and a Parker L25i intelligent stepper drive. Lower wall displacements and velocities are similar to those of the carotid artery, peaking at 5mm and 2.2 cm/s respectively. By collecting TDI cineloops using a Philips HDI5000 scanner, the Philips AWM software derives the relative wall displacement, and the known movement of the wall can be compared to the measured output from the software to assess its accuracy and precision.

Results: Constant velocity waveforms ranging from 0.05cm/s to 0.25cm/s were produced and cineloops acquired with a range of scanner settings including velocity scale, colour box size and TGC settings. Six measurements were acquired at each tool velocity/scanner setting in order to establish inherent variability (Figure 1). Similar tests were performed for physiological velocity waveforms. Early results revealed an overestimate of AWM cycle length and an underestimate of maximum AWM for one particular tool velocity/scanner setting combination (Figure 1). In addition, the AWM/TDI technique performance varies with velocity scale setting (Figure 2). Ongoing work includes calibrating the test tool to ensure the accuracy of the movement that is produced by the moving wall compared to the commanded movement. Further assessments of the accuracy of the AWM software will be presented.

Conclusion: The wall motion test tool provides a convenient and accurate means of assessing the results given by the Philips AWM/TDI technique. The AWM technique evaluation provides a more comprehensive understanding of the uncertainties associated with the technique when used in a clinical setting.

References:
[1] Bonnefous O. et al. New TDI developments for vascular and cardiac applications. Ultrasonics Symposium, 2000 IEEE; 2:1285-1290.
[2] Germond L. et al. Quantitative assessment of the artery dilation measurements with an arterial phantom. Ultrasonics symposium, 2001 IEEE; 2:1413-1416.
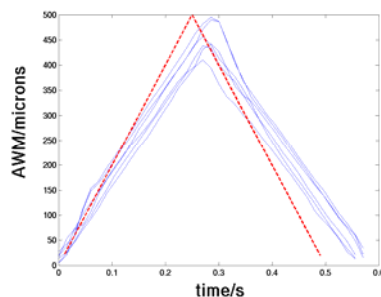
Figure 1: Variability of AWM measurements with actual movement
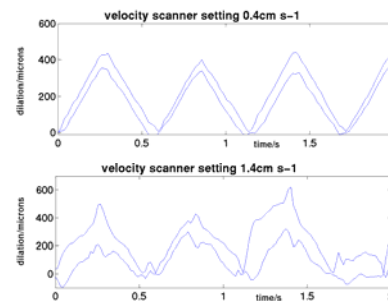

Figure 2: AWM measurement variation with velocity scale settings

038 **INTRAVASCULAR ULTRASOUND PALPOGRAPHY FOR DETERMINING THE AGE OF A THROMBUS: AN ANIMAL STUDY *IN VIVO*.**

Johannes A. Schaar[1,2], Frits Mastik[1], Elsa D. van Deel[1], Cornelis J. Slager[1], Patrick W. Serruys[1], Dirk J.Duncker[1], Antonius F.W. van der Steen[1,2]*.
[1]Biomedical Engineering, Thorax Centre, Erasmus MC, Rotterdam, The NETHERLANDS; [2]Interuniversity Cardiology Institute of the Netherlands, Utrecht, The NETHERLANDS.

Background: Vulnerable plaques can lead to thrombus development, which may cause acute coronary syndrome. The age of a thrombus cannot be assessed *in vivo* with currently available imaging methods. It is well accepted that a thrombus stiffens over time; nevertheless nothing is known about the time course of this process especially in the very early phase of development.

Palpography – an IVUS based technique that has been reported at this conference before – assesses the mechanical properties of biological tissue and can be used to measure the stiffness of thrombi *in vivo*. We hypothesize that the organization process in a thrombus starts early after introduction and that stiffness is increasing over time.

Methods: In 7 anesthetized and surgically prepared pigs thrombus formation was introduced in both femoral arteries by applying electrical DC current (90mA, 9V) to the outer vessel wall. The current caused a vessel injury with the signs of endothelial erosion. Over this erosion a thrombus was formed, which left a lumen through which the blood pressure could act as the driving force to strain the thrombus. Ten thrombi were formed, while in 4 cases the process failed. Before applying the current a 20MHz phased array intravascular ultrasound catheter (Volcano) was introduced at the location where the thrombus was created. Radio-frequency (RF) data were acquired at 30 frames per second. Data were recorded at 6 time points after thrombus introduction (5, 20, 45, 75, 105, 180 minutes). Cross-correlation based analysis of the RF data revealed the radial strain of the luminal layer of the thrombus.

Results: Initially thrombi are soft and stiffened dramatically in the first 20 minutes with a strain reduction of about 50%. The strain between frames in a thrombus decreased from (0.27 ± 0.16) at 5 minutes through (0.17 ± 0.10) at 20 minutes to (0.11 ± 0.10) after 45 minutes. Further stiffening took considerably more time, but could be observed towards the end of the experiment. The inverse relation between the time and strain over the first 3 hours is highly significant ($R2=0.59$; $p < 0.0001$).

Conclusion: This is the first time the *in vivo* development of a thrombus in an artery could be monitored with special emphasis on the organization of the thrombus. A vast part of the organization process takes place within 20 minutes after thrombus introduction.

039　**OPTICAL FLOW TISSUE TRACKING USING REAL–TIME 3D ULTRASOUND.**

P. Jordan[1]*, R.D. Howe[1], D.P. Perrin[1].
[1]Division of Engineering and Applied Sciences, Harvard University, Cambridge, MA 02138, USA.

Our long-term research goal is to develop accurate mathematical models of tissue and organ elasticity, which may be calculated in real-time and thus utilized in medical simulation for trauma and surgical training. We propose to use real-time three-dimensional ultrasound to perform *in-vivo* elastography and validation of elasticity measurements obtained with mechanical compression devices.

Real-time 3D ultrasound (Philips SONOS 7500 Live 3D Echo, Philips Medical Systems, Andover, MA, USA) is capable of providing volumetric data at frame rates up to 30 volumes per second with near 1mm spatial resolutions. Due to its low operating cost, temporal resolution, and non-ionizing nature, real-time 3D ultrasound is an ideal modality for elastographic imaging.

We report on our current approach to *in-vivo* and *ex-vivo* tissue deformation tracking. The aim of the *in-vivo* experiments is to validate elasticity measurements performed on porcine liver with mechanical compression devices, while the *ex-vivo* experiments are intended to validate our proposed tissue tracking algorithm. *Ex-vivo* studies are performed on samples of partially constrained muscular tissue subjected to slowly applied loading conditions.

A three-dimensional multi-resolution optical flow algorithm was implemented based on the original approach of Horn and Schunck [1]. The volumetric sequences are preprocessed with spatiotemporal filters described by Simoncelli [2], improving our ability to obtain accurate spatio-temporal derivatives. A four level Gaussian pyramid is constructed, in order to allow for a fine-to-coarse approximation of the optical flow, improving the robustness of our approach.

We also report on our preliminary results based on *ex-vivo* studies performed on muscular tissue and further discuss our ability to accurately track tissue deformation with real-time three-dimension ultrasound.

References:
[1]　Horn B.K.P. and Schunck B.G.: Determination of Optical Flow. Artificial Intelligence, 17, 1981, pp185-204.
[2]　Simoncelli E.P.: Design of multidimensional derivative filters. IEEE Int. Conf. Image Processing, Vol 1, 1994, pp 790-793.

045 **FEASIBILITY OF SKIN SURFACE ELASTOGRAPHY BY TRACKING SURFACE TOPOGRAPHY.**
Louise Coutts[1]*, Jeffrey Bamber[1], Naomi Miller[1].
[1]Joint Department of Physics, Institute of Cancer Research and Royal Marsden NHS Trust, Downs Road, Sutton, Surrey, SM2 5PT, England, UK.

The measurement of skin elasticity has potential to become an important factor in the clinical diagnosis and assessment of a wide range of skin conditions, examples being psoriasis, acne scars, wounds (during healing), skin cancer, radiation fibrosis and lymphoedema. Existing methods of measuring skin elasticity, such as measuring overall strain while applying suction, torsion or a uniaxial load to the skin, provide only an overall value of skin stiffness, and hence do not enable regional variations in stiffness to be assessed on a scale smaller than many centimeters. Although ultrasound elasticity imaging of the skin is under investigation, an optical method would have the attractions of low cost, simplicity and utility when skin contact is undesirable. Compatibility with existing methods of examining the skin would also be an advantage, but the optical appearance of the skin surface is highly dependent on, amongst other variables, the angle of incidence of the illumination. It is, therefore, likely to decorrelate rapidly with strain. We have hypothesized that the microscopic skin surface topography (i.e. surface height) should represent a reliable and relatively stable signal for displacement tracking. Such a signal can easily be measured by a variety of optical methods to a lateral spatial resolution of a few tens of microns and a height resolution of a few microns. Furthermore, strain-induced decorrelation of the two dimensional (2D) surface profile may (in the longer term) be amenable to model-based prediction.

A study has been carried out to establish the feasibility of tracking the topographic profile of the skin surface, with a view to generating strain images. Part of the aim was to provide a preliminary understanding of the nature of the surface structures that may be tracked, the optimum window sizes for a simple correlation based 2D displacement estimator and a least-squares strain estimator, and the degree of variation in these properties over a number of different skin types. This was achieved by studying the variation with window size of the correlation coefficient after 2D tracking and the signal to noise ratio (SNR) of the displacement and strain estimates. The trade-off with spatial resolution was also considered. For this study, silicon rubber skin replicas were used as phantoms, to avoid the complicating effects of stress relaxation that occur in skin over the time scale (about 10 seconds) that it took to acquire 2D surface profile data in our experimental system. Replicas from various skin sites and age groups were analyzed in order to investigate the extent of variation in optimal window sizes for different skin types. Static linear tensile strains from zero to 10% were applied to the skin replicas and surface height images of the pre and post strained region, an area of 19 x 14 mm, were acquired using a Primos™ micro-profilometry system.

The skin surface is made up of skin lines running in various directions, forming peaks and troughs, which form the basis of the signal being tracked. Unlike ultrasound elastography, where optimum window size is determined by speckle, in this application it is determined by the skin line pattern. Experimental data have shown that the variation in skin line pattern between samples makes it worthwhile to estimate the optimal window size for each different sample. At small displacement tracking window sizes, the displacement SNR increases as the window size increases. However, at large window sizes the amount of unstrained signal and the amount of strained signal seen in the window become very different, leading to a decrease in SNR with increasing window size. Such behavior is expected from experience with ultrasound echo tracking, but in this application there may be even greater opportunity to compensate for the effect by predicting the change in the signal after straining i.e. by companding. The strain SNR increases as the strain estimation window size increases, so the choice of this window size depends on the desired compromise between good strain SNR and spatial resolution.

A wide range of optimal displacement tracking window sizes has been found for different samples. Nevertheless, good spatial resolutions may generally be achieved. For example, for strains of up to 2%, window sizes as small as 600 microns have consistently produced correlation coefficients higher than 0.93 after tracking. A procedure has now been developed which calculates the correlation coefficients over a range of strains and window sizes, allowing an optimal window size to be chosen for each separate skin sample being analyzed.

Skin replicas have shown that skin surface tracking is feasible, the next stage being to develop a tool that can acquire data fast enough to take into account the time-dependent properties of the skin response to an applied stress or strain. This will allow the feasibility of tracking skin itself to be determined.

* indicates Presenter

052   DESCRIPTION OF A NEW ITERATIVE ALGORITHM FOR SCALING FACTOR ESTIMATION.

J. Fromageau[1], H. Liebgott[1], E. Brusseau[1]* and P. Delachartre[1].
[1]CREATIS, CNRS Research Unit (UMR 5515), INSERM U 630, Lyon, FRANCE.

Because of its importance, time delay estimation has long been an active research topic with numerous developed techniques that have led to many applications. In previous works, the interest to estimate scaling factor instead of time delay was discussed. The purpose of this paper is to present an estimation of the scaling factor.

The scaling factor estimation algorithm is described; it is based on the search of the root of the imaginary part of the cross-correlation of signals before and after compression. The interest to study the imaginary part of the cross-correlation is that it is not necessary to consider the whole analytic signals, but only the imaginary part of reference signal and the real part of the scaled signal. The root-seeking is performed using an iterative algorithm. In this work, the analytic expression of the estimator and the algorithm are described. Due to the analytic expression of the estimator, a statistical study according the signal to noise ratio (SNR) can be performed, and theoretical mean and variance of the estimator are calculated. Then estimation performance is studied; the convergence and bias of the estimated mean scaling factor and the lower bound of the variance are compared to theoretical and true values.

The main results show that the estimation converges to the true value of the scaling factor for any SNR, but the number of iterations needed to reach the convergence increases with decreasing SNR. Finally, estimator performance is evaluated on numerical signals and experimental images; it shows a good agreement with the expected characteristics. A typical result is obtained for a signal scaled by 1% compared to the reference signal. For signals that have an SNR of 30dB, we find that the algorithm reaches the correct estimation of the scaling factor after 3 iterations.

055   GAUSSIAN MODELING OF DISPERSIVE MEDIA: APPLICATION TO CALCIFIED TISSUES.

D Hazony[1], JL Katz[2]*.
[1]Department of Electrical & Systems Engineering, Case School of Engineering, Case Western Reserve University, Cleveland, OH, USA; [2]UMKC–Center for Research on Interfacial Structure and Properties (UMKC–CRISP), Department of Oral Biology, School of Dentistry and Division of Civil & Mechanical Engineering, School of Computing & Engineering, University of Missouri–Kansas City, Kansas City, MO, USA.

Ample experimental evidence suggests that the impulse response of propagation media is intrinsically dispersive and that solutions based on distributed properties are often in error. Accordingly a cellular model is developed based on lumped physical properties (like those of resistors inductors and capacitors) and a strict analytical foundation. It is shown that the model becomes arbitrarily more efficient with increasing cell-density and that its impulse response evolves into the Gaussian shape. A boundary condition is set when the model cell-size matches a medium imperfection parameter (akin to the average grain-size in a polycrystalline material, or the heterogeniety in calcified tissues) to define the attenuation constant. In essence, the model provides the physical parameters associated with pulse propagation along the channel. Consequently, it may be used to describe dispersive media such as porous media, biological tissues, and composites. Applications are found in communication systems, non-destructive testing, and the study of wave propagation in dispersive media. An ultrasonic grain-size determination in cast iron plate is provided based on experimental data. The model also has been applied to ultrasonic measurements of both human haversian and bovine plexiform bone.

072 **EXTRACTION OF MODULUS FROM THE OSMOTIC SWELLING OF ARTICULAR CARTILAGE MEASURED USING ULTRASOUND.**

Haijun Niu[1], Qing Wang[1], Yongping Zheng[1]*.
[1]Rehabilitation Engineering Center, The Hong Kong Polytechnic University, Hong Kong, CHINA.

Earlier, we have used ultrasound to monitor the transient depth-dependent osmotic swelling behavior of cartilage [1]. The objective of this study was to use the triphasic theory to extract the aggregated modulus (Ha) of articular cartilage using the depth-dependent strain distribution obtained by the ultrasound measurement.

The ultrasonic swelling measurement system used in this study is showed in Figure 1. The container was filled with NaCl solution. A 50 MHz focused ultrasonic transducer was used to produce ultrasonic pulses and to receive the ultrasonic echoes. A 500 MHz A/D converter card was used to digitize the ultrasonic signals. The displacements of the bovine cartilage tissues at different depths were estimated from the ultrasonic echoes using a cross-correlation tracking algorithm [1]. Using this system, the sensitivity of displacement measurement was approximately 0.4 μm in articular cartilage.

The cartilage was modeled as a mixture of a linear, isotropic, incompressible collagen-proteoglycan solid matrix and an incompressible fluid consisting of water and NaCl ions [2]. The total stress equation in cartilage at equilibrium under free-swelling conditions was used to obtain its aggregated modulus (Ha). It was assumed that all swelling effects arose from the Donnan effect in this study. The key problem was to compute the Donnan osmotic pressure p. A linearity constitutive expression for p can be obtained from the boundary conditions (Equation1) for equivalent chemical potential of water and NaCl ions across the free surface [3].

$$p \approx RT\left(\left[(c_0^F)^2 + (2c^*)^2\right]^{1/2} - 2c^* - tr\varepsilon \cdot (c_0^F)^2 / (\phi_0^w[(c_0^F)^2 + (2c^*)^2]^{1/2})\right) \qquad \text{Equation (1)}$$

where R is gas constant, T is absolute temperature and c^* is the NaCl concentration. Fixed Charge Density (c_0^F) values and Water Volume Fraction (ϕ_0^w) values of the cartilage specimen could be measured using the biochemical method after equilibration in 0.15M NaCl. In this study, they were obtained from the literature. The Poisson's ratio was assume to be a constant = 0.21.

The distribution of strains of a typical cartilage specimen (approximately 1.057 mm in thickness) caused by changing the NaCl concentration from 2 M to 0.15 M is shown in Figure 2. The data were obtained at the equilibrium conditions. The theoretical prediction using the triphasic model together with the known parameters is shown as the solid line. The least square error between the predicted strain values and those measured experimentally was used as curve fitting criteria. The estimated aggregated modulus for this typical specimen was 0.46MPa. This study demonstrated that the ultrasonic measurement of swelling together with the triphasic modeling can be used to obtain the material property of the cartilage in a non-contact manner. More results will be reported.

References:
[1] Zheng YP, et al. Dynamic depth-dependent osmotic swelling and solute diffusion in articular cartilage monitored using real-time ultrasound. Ultrasound in Medicine and Biology. May 2004.
[2] Lai et al. J A triphasic theory for the swelling and deformation behaviors of articular cartilage. J. Biomech. Eng. 113: 245-258. 1991.
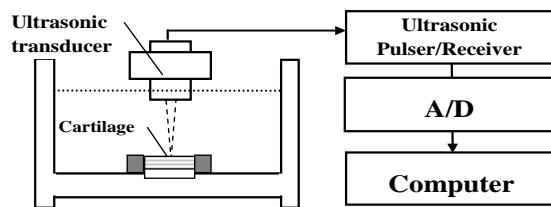

Figure 1: Diagram of the ultrasound swelling measurement system. The cartilage specimen was fixed on the bottom of the container filled with saline solution, surrounded by rubber gel to prevent the solution infiltrating from the sides.
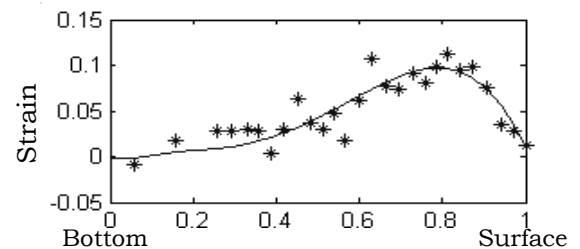

Figure 2: The strain of tissues at different depths of a typical bovine cartilage specimen. (concentration = 0.15M NaCl). (Star mark) Experiment data. (Solid line) Predicted curve.

073   **OSMOTICALLY–INDUCED SHRINKAGE AND SWELLING BEHAVIOR OF NORMAL BOVINE PATELLAR ARTICULAR CARTILAGE *IN SITU* MONITORED BY ULTRASOUND.**

Qing Wang[1], Yongping Zheng[1]*.
[1]Rehabilitation Engineering Center, The Hong Kong Polytechnic University, Hong Kong, CHINA.

Articular cartilage is the thin white layer of soft connective tissue that covers the articulating bony ends in diarthrodial joints. It has been discovered that the swelling of articular cartilage is attributed to the interactions between the fixed negative charges along proteoglycans and mobile ions. Few studies, however, had been reported on the internal transient changes of cartilage during the free swelling or shrinkage after the concentration of the bathing saline solution was altered. In this study, a 50 MHz ultrasound biomicroscopy system [1] was applied to investigate the transient osmotically-induced shrinkage and swelling of normal bovine patellar articular cartilage.

Cylindrical cartilage-bone plugs (20 for shrinkage-swelling test and 3 for repeatability test) approximately 3 mm thick were prepared from fresh normal mature bovine patellae by using a metal punch with a diameter of 6.35 mm [1]. The specimen was fixed on the bottom of a container, surrounded by rubber gel, submerged in the bathing saline solution, and then continuously monitored by ultrasound during the sequential alteration of the saline concentration from 0.15 M to 2 M and back to 0.15 M. The imbalance of the ion concentration between the cartilage and the bathing solution gave a positive or negative increment to the Donnan osmotic pressure inside cartilage. During the repeatability test, the shrinkage-swelling test was repeated three times for each sample. The echoes could be tracked by using the individual tracking windows (Figure 1).

The ultrasound measurement had a good repeatability (ICC > 0.94) for the investigation of the shrinkage and swelling behaviors of cartilage. The mean coefficients of variation (CV%) for the maximum displacement and duration were 7.3%, 6.4%, and 8.2% and 8.0%, respectively for the shrinkage and swelling measurement. The mean maximum amplitude of shrinkage (11.7±11.5 µm) and the mean shrinkage duration (223.4±258.2 s) were respectively significantly ($P < 0.05$, Paired t-test) larger than those of swelling (4.2±4.5 µm; 110.5±130.8 s) (Figure 2). Results indicated that cartilage behaved differently in shrinkage and swelling processes and there were large variations between these two behaviors among individual cartilage specimens. In addition, the study demonstrated that the deformation of cartilage did not keep in the equilibrium state after reaching the peak value. Instead, the surface moved back towards the original state. Moreover, the shift of the cartilage-bone interface was related to the change of sound speed in cartilage. The rates of sound speed change were related to the ion diffusion during the shrinkage and swelling phases, both showing a time-dependent exponential relationship $a(t) = Ae^{-Bt}$ (Figure 3). In summary, the reported ultrasound method could be potentially used for the *in situ* measurement of transient swelling-shrinkage responses of intact cartilage layer.

Reference: [1] Zheng YP, et al. Dynamic depth-dependent osmotic swelling and solute diffusion in articular cartilage monitored using real-time ultrasound. Ultrasound in Medicine and Biology. May 2004.
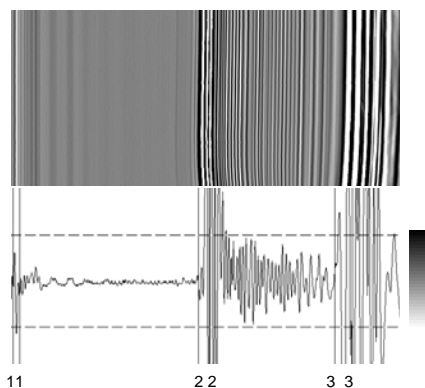
Figure 1: Results of ultrasonic monitoring of transient shrinkage induced by changing 0.15 M saline to 2 M saline. M-mode image (top); A-mode signals with tracking windows (bottom).
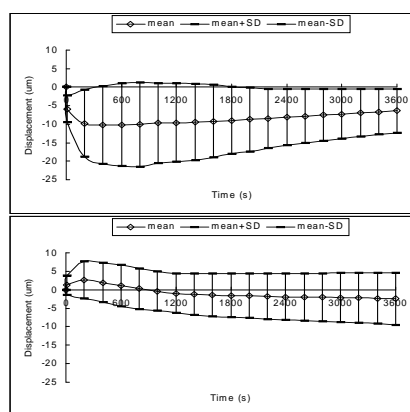
Figure 2: Mean & SD of displacement of cartilage surface versus time in the shrinkage (top) and swelling (bottom) phases (n = 20).
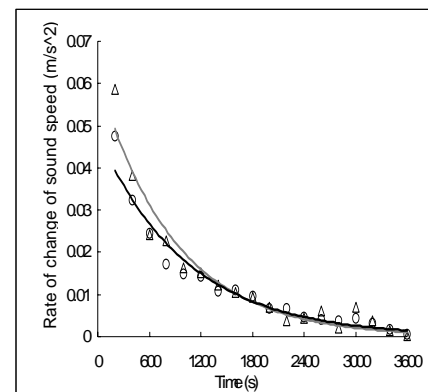
Figure 3: Rates of sound speed change in cartilage during the shrinkage (Δ) & swelling (○) phases. Exponential functions were used to fit the data.

074   **EFFECT OF SALINE CONCENTRATION ON SOUND SPEED OF ARTICULAR CARTILAGE.**
Sushil Patil[1], Yongping Zheng[1]*.
[1]Rehabilitation Engineering Center, The Hong Kong Polytechnic University, Hong Kong, CHINA.

Articular cartilage (AC) in its normal physiological state (0.15M NaCl) is in a swollen state. The swelling pressure balances with the tensile stress of the collagen matrix [1]. Any changes in the swelling state is considered as an imbalance in the normal cartilage composition and may lead to degeneration. The change in AC dimensions and decrease in thickness due to the change in bathing saline concentration have been previously reported [2, 3]. Ultrasound measurement of AC swelling has been used to determine its mechanical properties [3]. However, the propogation of ultrasound in AC with change in saline concentration is not yet documented. The objective of this study is to investigate the change in sound speed in AC with variation of saline concentration.

A total of 20 AC-bone plugs with a diameter of 6.35 mm were prepared from the top quadrant of the lateral side of bovine knee patellas. The plugs were thawed in 0.15 M saline for 30 min. These specimens were then excised from the bone layer to obtain full-thickness AC layers. The specimens were installed on the specimen holder and thawed again in 0.15 M saline for 30 min. The instrumentation and sound speed calculation method used in the study has been described in our previous study [4]. Eight concentrations of saline solution were used ranging from 0M (distilled water), 0.0075M, 0.082M, 0.15M, 0.3M, 0.75M, 1.25M, and 2.5M. At each concentration, the specimen was thawed for 30 min before the measurement. The ultrasound beam was scanned across the specimen with a resolution of 0.1 mm. The sound speed in each saline concentration was measured at the start and end of each scan by moving the ultrasound transducer vertically by a predetermined distance.

The ultrasound speeds in AC and saline changed from 1681 ± 50 m/s (Mean $\pm$ SD) to 1816 ± 53 m/s; 1521 ± 3 m/s to 1674 ± 3 m/s, respectively, when the saline concentration changed from 0 M to 2.5 M. The sound speed of full-thickness AC (1675 ± 51 m/s) in normal saline solution was similar to that reported in other studies and our previous study [4]. Significant differences in sound speed were observed in saline as well as AC with the change in the saline concentration (t–tests, $p<0.001$). The sound speeds in both AC and saline increased linearly with the increase of the concentration (Figure 1). The thickness of AC decreased linearly with increase of saline concentration, which agreed to results of previous studies [2, 3]. Figure 2 represents the shrinkage of cartilage thickness with the increase in molar of the saline solution. It has been reported that the sound speed in AC decreases with its degeneration. Swelling status of AC is also considered as an abnormality. The change in the biomechanical properties of AC with degeneration of AC is well known. The change in sound speed plays an important role in detecting AC degeneration and in the assessment of biomechanical properties of AC. The results suggested that the concentration of saline should be documented in reporting the sound speed in AC. In addition, the concentration-dependent sound speed should be taken into account when ultrasound is used to detect the swelling behavior of AC.

References:
[1] Maroudas A. Physicochemical properties of articular cartilage. Adult Articular Carilage, ed M.A.R. Freeman, Pitman Medical 1979, 215-.
[2] Mow VC and Schoonbeck JM. Contribution of Donnon Osmotic Pressure towards the biphasic compressive modulus of articular cartilage. Trans. Orthop. Res. Soc., 1984; 9: 262.
[3] Zheng YP, et al. Dynamic depth-dependent osmotic swelling and solute diffusion in articular cartilage monitored using real-time ultrasound. Ultrasound in Medicine and Biology, May 2004.
[4] Patil SG, et al. Measurement of depth-dependence and anisotropy of sound speed of bovine articular cartilage *in vitro*. Ultrasound in Medicine and Biology, May 2004.
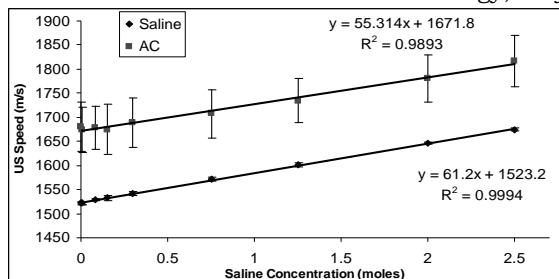
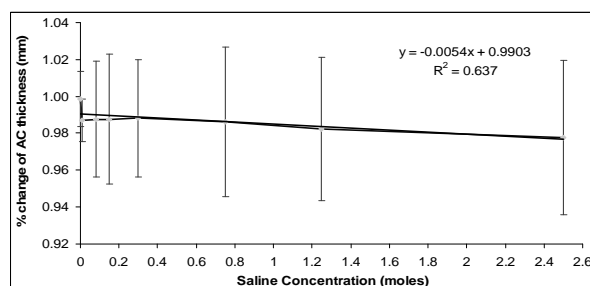Figure 1: US speed in saline and AC with increasing concentration of saline solution.

Figure 2: Change in AC thickness with increase in saline concentration.

075   **SKIN ELASTICITY MEASUREMENT BASED ON A 20 MHz ULTRASOUND BIOMICROSCOPE.**

Yanping Huang[1], Yongping Zheng[1]*.
[1]Rehabilitation Engineering Center, The Hong Kong Polytechnic University, Hong Kong, CHINA.

Research in elasticity imaging typically relies on 1 to 10 MHz ultrasound which is the frequency range used for most medical imaging applications. For the mapping of elasticity in very thin tissue, such as skin, high frequency ultrasound should be utilized to obtain a high enough resolution [1]. However, the application of high-resolution elastography to date is still limited to few fields such as in the detection of atherosclerotic plaque morphology. Skin is an important tissue covering the human body and many skin diseases such as sclerosis are associated with the change of elastic properties. Elasticity measurement using the combination of ultrasound biomicroscopy and suction has been reported earlier. In the present study, we measured the skin elasticity based on an ultrasound biomicroscope and compression.

We used a real-time ultrasound biomicroscopy system with a cylindrical probe in which there was a linear-scanning focused transducer with a central frequency of 20 MHz (Figure 1). The axial and lateral resolutions of this system were better than 100 µm and 200 µm, respectively. The transducer during working was immersed in a coupling medium (usually water) sealed by a cover at the tip of the probe. RF signals obtained through linear scanning of this transducer provided a real-time 2-D image of a cross-sectional area of tissues 6 mm in width and 8 mm in depth at a rate of 10 frames/s. The probe was modified by using a rigid film at its tip so that a more uniform stress could be applied on the tissues. During the test, the pressure was directly applied to the skin and monitored by a force sensor attached to the probe. Images could be obtained step by step in static loading or consequently as a sequence in dynamic loading. Through this system, applied pressure, skin deformation as well as strain information (via cross-correlation algorithm) can be obtained simultaneously after the mechanical loading on the skin.

To test the feasibility of this system, the probe was fixed in a standard mechanical testing machine for better control of the loading. The results of experiments on three kinds of phantoms will be reported including (1) two simple layers of different stiffness without scattering; (2) two homogeneous layers of different stiffness with scattering; (3) an irregular scattering inclusion in a softer or harder scattering background. *In vitro* experiments on porcine skins will also be reported. Preliminary experimental results showed that the designed system worked if proper phantoms were prepared. B-mode cross-sectional images as well as strain images could be obtained when the test was conducted on human skin tissues *in vivo*. Our ultimate aim is to provide an *in vivo* high-resolution elastomicroscopy system to noninvasively measure the effective stiffness of the skin, to differentiate skin layers with different elastic properties such as dermis and hypodermis, and to view the tumors surrounded by the normal skin.

References:
[1] Zheng YP, et al. Ultrasonic measurement for *in vitro* depth-dependent equilibrium strains of articular cartilage in compression. Physics in Medicine and Biology 47: 3165-3180, 2002.
[2] Zheng YP, et al. High resolution ultrasound elastomicroscopy imaging of soft tissues: System development and feasibility. Physics in Medicine and Biology. In review.
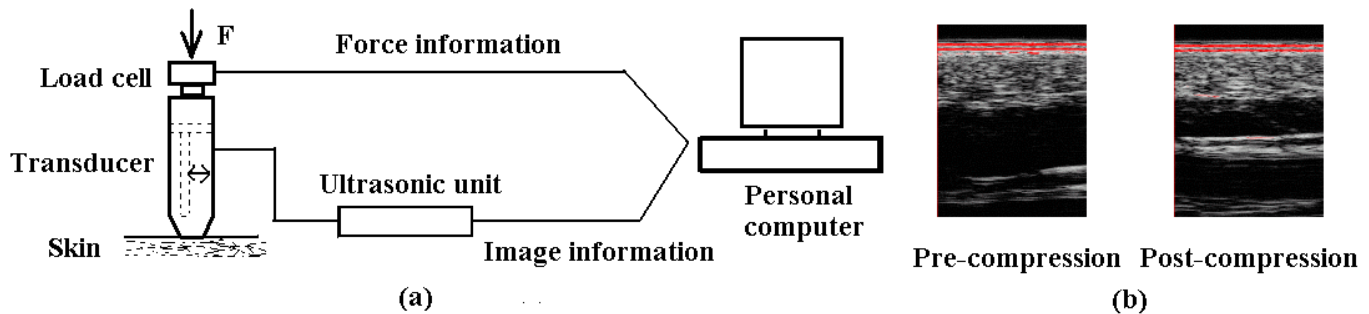

Figure 1: (a) Schematic diagram of the system for measuring skin elasticity;
(b) The B-mode images of the skin before and after the compression was applied.

082 **ULTRASONIC MEASUREMENT OF *IN–VIVO* STRAIN OF SURGICALLY REPAIRED ACHILLES TENDON UNDER ISOMETRIC CONTRACTION.**

Jolinna Chan[1,2], Yongping Zheng[1]*, Ka Ho Ng[3].
[1]Rehabilitation Engineering Center, The Hong Kong Polytechnic University, Hong Kong, CHINA;
[2]Physiotherapy Department, Maclehose Medical Rehabilitation Centre, Hong Kong, CHINA;
[3]Department of Orthopaedic and Traumatology, Queen Mary Hospital, Hong Kong, CHINA.

The mechanical properties of the Achilles tendon are of great interest especially after rupture because it is subject to large stresses during human locomotion. During rehabilitation, type and intensity of exercise are important and crucial to prevent any damage to the repaired tendon. Investigations on tendon biomechanics are usually limited by biomechanical testing equipment especially for *in-vivo* conditions. Therapists usually rely on clinical symptoms such as swelling, signs of inflammation to determine whether the given exercise is appropriate or not. Not much information on strain, stress under exercise condition is used to provide guidelines for the therapist to plan treatment. Recently, ultrasonic measurement of tissue elasticity *in-vivo* has been widely used for various tissues. In this study, ultrasound imaging was used to measure the strains of Achilles tendons under isometric contraction *in-vivo*. Our aim is to investigate the differences between the local strains of the healthy and repaired Achilles tendon (mean post-operation 12.8 weeks) to obtain useful information for providing a better physiotherapy scheme during the rehabilitation stage.

A portable ultrasound scanner (Sonosite 180 plus) with a linear-array probe (7.5MHz) was used to study strains of the Achilles tendon during isometric contractions (Figure 1). Six male subjects with age ranging from 28 to 51 were recruited, and their level of rupture range was 2cm to 7cm from the insertion of Achilles tendon. Their healthy legs were used as controls. In addition, three healthy male subjects were recruited to find any difference between the dominant and non-dominant leg. Ultrasound images (Figure 2) were obtained along the Achilles tendon at the level of rupture site *in-vivo* under isometric contraction using Cybex 6000 to record the torque of gastrocnemius muscle simultaneously. The displacement of the selected part of the tendon was extracted using a custom-made program for dynamic ultrasound signal and image analysis. Results were compared with the good side of the same subject. In addition, porcine Achilles tendons were measured *in-vitro* for the validation of the technique. Porcine tendon was stabilized by a modified caliper with a pin inserted as the marker for ultrasound measurement. Stain was placed on the same point for tracking displacement by digital video simultaneously.

Results demonstrated that the local strain of the repaired side was significantly smaller than that of the normal side under the same torque condition (p=0.017, paired t-test). The strain difference ranged from 0.8% to 35%. Results of normal subjects showed that dominance had no effect on the measured torque as well as the strain. In addition, the validation results showed a good correlation between the displacements measured by the ultrasound and optical methods (R^2=0.903±0.028). The results of the present study demonstrated that ultrasound imaging could be used to measure the strains of Achilles tendons under isometric contraction *in-vivo*. This method is useful for the functional assessment of Achilles tendons, particularly during the rehabilitation of rupture.

Figure 1: Experimental setup for the dynamic ultrasonic measurement of the Achilles tendon.

(a)   (b)
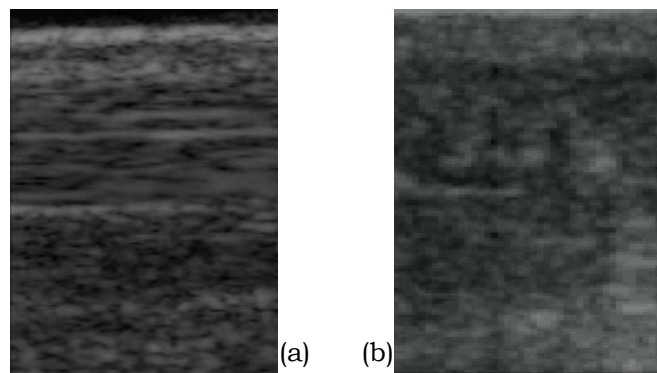
Figure 2: Typical ultrasound images of Achilles tendons. (a) Normal; (b) Healed.

* indicates Presenter

092   **EFFECTS OF INTERNAL DISCONTINUITIES ON STRAIN ELASTOGRAMS.**
T.A. Krouskop[1,2]*, R. Righetti[2,3], J. Ophir[2,3], H. Lim[1] and E.L. Madsen[4].
[1]Baylor College of Medicine, Department of Physical Medicine and Rehabilitation, Houston, TX, USA; [2]The University of Texas Medical School, Department of Radiology, Ultrasonics Laboratory, Houston, TX, USA; [3]University of Houston, Electrical and Computer Engineering Department, Houston, TX, USA; [4]University of Wisconsin–Madison, Madison, WI, USA.

Introduction: Inherent in current algorithms used to solve the inverse problem is the assumption that the material in the region of interest is continuous. Moreover, the inverse problem is often simplified further by assuming that the materials are incompressible and exhibit linear elastic behavior. While these assumptions may be justified under certain conditions, the effects of discontinuous boundaries within the material block may produce strain data that must be interpreted differently.

Methods: To study the effect of internal discontinuities on strain elastograms, two gelatin-based phantoms were constructed and immersed in oil. The first phantom was an oil-in-gelatin block 9cm x 9cm x 9cm with a 2cm diameter cylindrical inclusion that was bonded to the matrix. The second phantom was also a 9cm x 9cm x 9cm block of the same oil-in-gelatin material, but, instead of a bound inclusion, it had a 2cm diameter cylindrical hole corresponding to the location of the inclusion in the first phantom. For the second phantom either of two gelatin rods, one 1.95cm in diameter and one 1.98cm in diameter, could be placed in the void. Thus, neither of the rods was bound to the matrix. Each of the phantoms was used to create quasi-static strain elastograms.

Results: Figure 1a shows the axial strain elastogram associated with the area surrounding the inclusion in the phantom with the bound inclusion, and Figures 1b and 1c are the corresponding axial strain elastograms of the second phantom with the 1.95cm diameter rod in place and the 1.98cm diameter rod in place, respectively. The high strain areas shown as white regions just above and below the boundary between the matrix and inclusion (Figures 1b and 1c) are predicted by theory (1-2), and they should not be considered artifacts. They are indicative of a boundary that does not transfer shear stresses. Figures 2a, 2b and 2c show the corresponding strain ratio elastograms for the two phantoms. This last set of figures illustrates that because the materials in the second phantom were not bound to each other, the regions on the sides of the inclusion became compressible during the loading and the usually assumed value of 0.5 for Poisson's ratio is not appropriate. If this value is used in the inverse problem, it would lead to erroneous results in calculating the modulus of the materials.

Conclusion: The internal connectedness of various regions within a block of material produces significant changes in the corresponding axial strain elastograms. Poisson's ratio elastograms (strain ratio elastograms) convey information about the internal connectedness of the material. This information is necessary to properly interpret the axial strain elastograms. We believe that this information will be fundamental for proper modulus image reconstruction. Moreover, further work is needed to explore how varying degrees of internal connectedness are manifest in the strain elastograms.

References:
1. Knight, MG, de Lacerda, LA, Wrobel, LC, Henshall JL, Parametric study of the contact stresses around spherical and cylindrical inclusions, Computational Materials Science, 2002:(25)115-121.
2. Maciejko, E., Bertrand, M., Krouskop, T.A., "Characterization of the Mechanical Behavior of the Inclusion-Matrix Interface: Theory and Simulation of Breast Lesion Models," 2nd International Conference on the Ultrasonic Measurement and Imaging of Tissue Elasticity, Corpus Christi, TX, Oct. 2003, p 91.
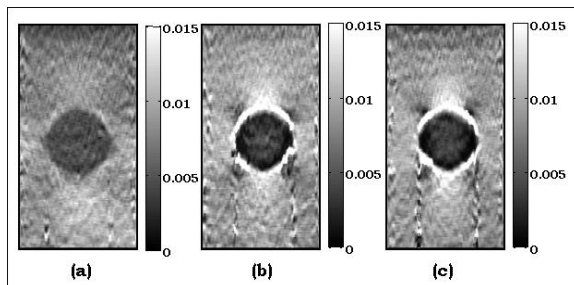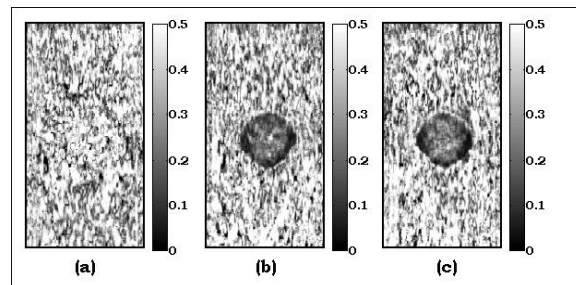
Figure 1

Figure 2

093 **BIOMECHANICAL PROPERTIES OF CORNEAL TISSUE DETERMINED BY APPLANATION AND THIN SHELL MODEL.**

J Liu[1]*, C Roberts[1].
[1]The Ohio State University, Columbus, OH, USA.

Intraocular pressure is a critical parameter for diagnosis and treatment of multiple ocular diseases. The current gold standard for measuring intraocular pressure (IOP) is Goldmann applanation tonometry, which applies a certain amount of force on corneal surface to flatten a predefined area. This measurement was developed based on Imbert-Fick law that assumes human corneas as infinitely thin, perfectly elastic and dry materials. When these criteria were met, the applanation force/pressure will be equal to the internal pressure acting on the thin membrane. Nevertheless, the variations across subjects in corneal thickness, radius of curvature and biomechanical properties may introduce substantial errors to tonometry readings. In this study, we conducted a quantitative analysis of these intrinsic errors through a thin-shell model. The effects of different corneal variables were computer simulated to study their influences on applanation tonometry measurement of intraocular pressure. In combination with the experimental data obtained on normal subjects from an Ocular Response Analyzer (Reichert Ophthalmic Instruments), the model yielded prediction on the distribution of corneal biomechanical properties, i.e., Young's modulus in normal subjects. It was found that corneal biomechanical properties could cause significant yet unrecognized inaccuracies in IOP measurement within normal subjects, and more so for patients with chronic ocular diseases. We concluded that an independent measurement of corneal biomechanical properties is essential for correcting IOP measurement errors, and perhaps guiding management and treatment of IOP-related ocular diseases.

095 IMPOSING PHYSICAL CONSTRAINTS TO YIELD ACCURATE AND UNBIASED DISPLACEMENT ESTIMATES.

NH Gokhale[1], MS Richards[1], MM Doyley[2], AA Oberai[1], PE Barbone[1]*.
[1]Boston University, Boston, MA, USA; [2]Dartmouth College, Hanover, NH, USA.

In two dimensional cross correlation methods, displacement estimates of adjacent pixels are typically determined independently of each other. This can result in noisy displacement estimates which have some obviously non-physical outliers. Here we address the problem of imposing physical constraints on the displacement estimation. We consider both regularization and elastic constraints. In regularization, a "smoothness" penalty is added to the image matching criterion (say SSD). While this method can provide smooth displacement fields, it also biases the result by pulling the solution off the minimizer of the image matching criterion. Imposing instead an elastic smoothness constraint can avoid the bias of the regularization method. The constraint formulation still optimizes the image matching criterion, but now within a constrained space of "smooth" displacement fields. The key to success of this method is our choice of "smooth displacement fields": solutions of the incompressible linear elastic equations with undetermined modulus. We iteratively search for the modulus distribution that provides the best match between our images. Doing so requires known boundary conditions for a single deformation sequence. In this poster, we show how both boundary conditions and elastic modulus distribution can be recovered by using two deformation sequences.

103 **ANALYSIS OF 3D LEFT VENTRICULAR WALL MOTION USING TISSUE DOPPLER IMAGING.**

AF Kolen[1]*, T Delhaas[1,2], T Arts[2].
[1]University Hospital Maastricht, Maastricht, The NETHERLANDS; [2]Maastricht University, Maastricht, The NETHERLANDS.

Introduction: Measurements of left ventricular local and global deformations were successfully implemented using magnetic resonance imaging (MRI) tagging techniques. Information about cardiac deformation helps to understand and to predict cardiac dysfunction. For example: an increase in the left ventricular torsion during the ejection phase is an indication of cardiac dysfunction.

Objective: Clinical application of the measure of increased ventricular torsion would be greatly enhanced if it could be estimated by an easily available, economic imaging modality capable of capturing tissue motion reliably. Therefore, the objective of this study is to assess the feasibility of ultrasound tissue Doppler to measure ventricular torsion during the ejection phase in similarity with magnetic resonance tagging techniques.

Method: For this study a 2.5 MHz phased array transducer (Vingmed™) was used to obtain tissue Doppler echo data (frame rate ≈160Hz) in two left ventricular short axis views during breath hold. A magnetic space tracker (Ascension™, flock of birds) was used to measure the distance and angulations between both image planes. Off–line, the contour of the left ventricular wall was manually drawn. Within this contour, the component of motion along the ultrasound beam was measured using the scanner's internal tissue Doppler algorithms. Rotation and radial shortening of the cardiac wall were estimated by using a 3D–model of cardiac motion. Torsion (T) was calculated using data on rotation (rot) and cavity radius (r) from 2 adjacent slices according to: T = (rotu-rotl)/d * (ru+rl)/2 in which u and l refer to the upper and lower scan plane, respectively, and d denotes the distance between the two scan planes.

Results: The magnetic space tracker could accurately establish the image plane position and orientation, and, hence, the average distance between the two scan planes. Rotation, change of cavity area, torsion and radial contraction components of the left ventricular wall could be estimated on a frame–to–frame base by fitting many local tissue Doppler measurements to a global cardiac motion model. When expressing torsion as a function of radial shortening an almost linear relation was found. This validated against equivalent measurements using magnetic resonance tagging techniques.

Conclusion: Therefore, we concluded that the global planar rotation and contraction of left ventricular wall motion could be determined by fitting many local tissue Doppler measurements to a global cardiac motion model. These promising findings make tissue Doppler potentially suitable to replace magnetic resonance tagging in order to measure cardiac motion.
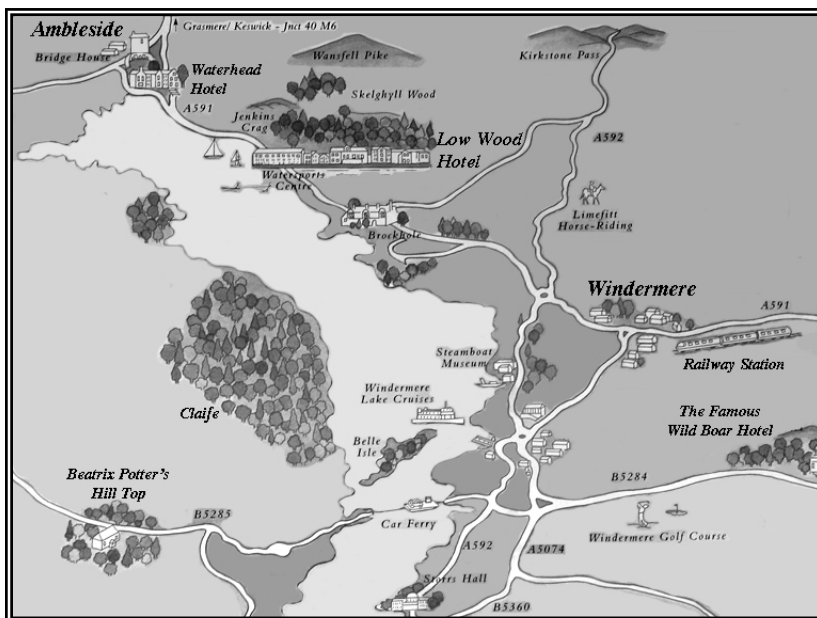
Map to Zeffirellis
Compston Road, Ambleside, Cumbria LA22 9AD
Telephone 015394 33845   Fax 015394 32986   info@zeffirellis.co.uk
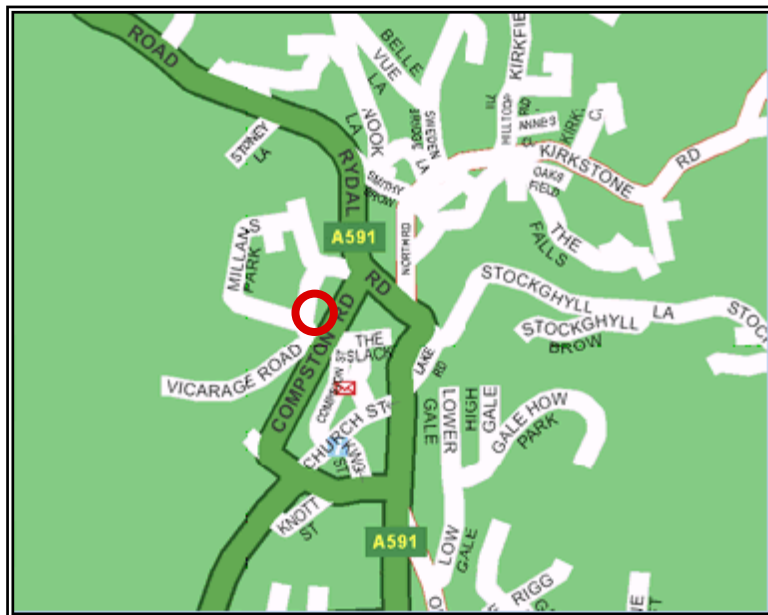
Zeffirellis is situated in the centre of Ambleside on the left hand side of COMPSTON Road (coming in from the south, on the one way system) at the junction with Millans Park.
First bus to Zeffirellis departs the Low Wood Hotel at 7:00P.
First bus to the Low Wood Hotel departs Zeffirellis at 11:00P.

Zeffirellis Restaurant
Wine and Dine in this award-winning restaurant recommended by many good food guides.
The specialties include our home-baked wheat meal pizzas, pasta dishes, imaginative salads, desserts and ices. A good choice of wines and other drinks completes the menu.
The restaurant is **NO SMOKING**.
Children are welcome in the restaurant. We serve children's pizzas and pastas. High chairs are available.
Zeffirellis Cafe
The recently renovated Cafe serves a variety of freshly ground coffees, home made soup, scones, filled baguettes , ciabatas, ice creams and much more.
Cafe Bar
We now have an upstairs bar where you may be served a variety of beers, wines, soft drinks and snacks. The cafe bar will be host to some of the finest live contemporary bands.
The Lake District's Premier Cinema
Presenting the latest films on national release as well as hosting Film Premieres for the Film Industry. 4 theaters are available seating from 180, Screen No 1, to 60, Screen No 4.
We have a kiosk open until the main feature commences.
All four cinemas are **NO SMOKING**.
The Box Office opens approx 20 minutes before programme starts.

Ground floor plan:

CONISTON ROOM · ULLSWATER ROOM · THIRLEMERE ROOM · WASTWATER ROOM

TOILETS

GALLERY LOUNGE

WINDERMERE RESTAURANT (GROUND FLOOR)

DERWENT ROOM

GRASMERE ROOM

BUTTERMERE ROOM

RYDAL ROOM

ELTERWATER ROOM

LIFT

GARDENS

← HOTEL and RECEPTION

BUCKLEY ROOM

Ground Floor - Rooms 306 to 323
1st Floor - Rooms 400 to 418
2nd Floor - Rooms 500 to 511

Japanese Garden

Alternative access to rooms

To Main Car Park

FIRE ASSEMBLY POINT

Main access to Club and Brasserie

Leisure Club

Stair access to Club and Brasserie

Rear entrance to Hotel Reception

Bedrooms 300 to 303

Room 305

Room 304

LIFT

Lift access to Conference Centre

Conference Centre and Gallery Lounge

Low Wood
Lake Windermere
AA ★★★★ RAC

Denotes higher level

Cocktail Bar

Reception

Stairs to 300's 400's 500's

Stairs to all rooms

LIFT

Snooker Room

Toilets

Windermere Restaurant

1st Floor - Rooms 161 to 169
2nd Floor - Rooms 271 to 279

Stairs to 100's/200's Leisure Club and Café del Lago

Access from 1st Floor

Room 4 to Room 18

Room 36 to Room 38

1st Floor

2nd Floor

Room 19 to Room 30

Room 39 to Room 54

Ground Floor corridor

Langdale Lounge

Café del Lago

Sullivan's Bar

Conference Evaluation and Questionnaire

SCORING:	Very Poor		Mid		Excellent
	1	2	3	4	5

OVERALL CONFERENCE:

Overall	1	2	3	4	5
Additional comments:					

SCIENTIFIC PROGRAM

Quality of the Presentations	1	2	3	4	5
Relevance of Presentations to the Conference's Theme	1	2	3	4	5
Time Allotted for Presentations	1	2	3	4	5
Time Allotted for Discussion	1	2	3	4	5
Poster Session	1	2	3	4	5
Guest Lecture	1	2	3	4	5
Tutorials and Panel Discussions	1	2	3	4	5
Equipment Exhibit	1	2	3	4	5
Student Participation	1	2	3	4	5
Additional comments:					

CONFERENCE MATERIALS:

Printed Proceedings Book	1	2	3	4	5
CD Proceedings	1	2	3	4	5
Other Registration Materials	1	2	3	4	5
Additional comments:					

CONFERENCE FACILITIES

Lecture Hall	1	2	3	4	5
Registration Desk and Conference Office	1	2	3	4	5
Meals: Overall	1	2	3	4	5
Conference Breakfasts and Lunches	1	2	3	4	5
Conference Dinner	1	2	3	4	5
Coffee Breaks	1	2	3	4	5
Audio-Visual	1	2	3	4	5
Additional comments:					

Conference Evaluation and Questionnaire

VENUE AND HOTEL

Venue – Lake Windermere, Cumbria, UK and Environs	1	2	3	4	5
Area Attractions	1	2	3	4	5
Hotel: Overall	1	2	3	4	5
Reservations	1	2	3	4	5
Transportation and Accessibility	1	2	3	4	5
Reception and Check – In	1	2	3	4	5
Accommodations	1	2	3	4	5
Facilities	1	2	3	4	5
Parking	1	2	3	4	5
Additional comments:					

ADMINISTRATION

Website	1	2	3	4	5
Registration off-site	1	2	3	4	5
Registration on-site	1	2	3	4	5
Administrative staff	1	2	3	4	5
Correspondence	1	2	3	4	5
Additional comments:					

GENERAL INFORMATION

I am a Returning Delegate	Yes		No
I plan to attend the next conference	Yes	Perhaps	No
and present a paper(s) / poster(s)	Yes	Perhaps	No
Other(s) from my lab would attend the next conference	Yes	Perhaps	No
and he/she / they would present a paper(s) / poster(s)	Yes	Perhaps	No
How did you learn of this conference? (Check all that apply)	☐ Email Announcement		
☐ Meetings Calendar in Journal of Ultrasound in Medicine and Biology	☐ Web Site		
☐ Other	☐ Colleague		
Tutorial Topic Suggestions:			
Additional Comments, Improvements or Suggestions:			

If you would be willing to host the Conference in your city, please give your name to the Conference Staff.
Questions or comments are welcome at any time at <elasticity.conference@uth.tmc.edu>